INTERACTION BETWEEN MOLTEN BLISTER COPPER AND 316L STAINLESS STEEL

Odilon Kasongo Ilunga

A dissertation submitted to the Faculty of Engineering and the Built Environment, University of the Witwatersrand for the qualification of Masters of Science in Metallurgy and Materials Engineering

JOHANNESBURG, AUGUST 2013

DECLARATION

I, Odilon Kasongo Ilunga, hereby declare that this dissertation is a result of my own research, except where otherwise acknowledged. It was conceived and is submitted to the University of the Witwatersrand in order to qualify for a Masters of Science Degree in Metallurgical and Materials Engineering. It has not been submitted for a degree at this, or any other, University.

Odilon Kasongo Ilunga

August 2013

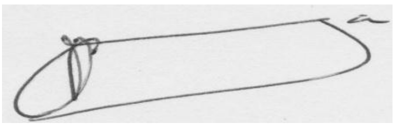

31st day of August 2013

ABSTRACT

Blister copper is cast and usually processed further. At the Tsumeb Custom Smelter, Namibia, it is blown with nitrogen from mild steel lances, but these lances do not last long, causing down-time and reduced copper throughput. Additionally, the blister copper purity should be at least 98.5 wt% Cu, else the price is compromised. Thus, keeping contamination to a minimum and reducing down-time are very important.

It was thought that stainless steel lances might last longer than those of mild steel, and since this could not be attempted at the smelter, a simple experiment was undertaken to identify any reactions between the molten copper and the stainless steel. The action of the lance was simulated by using agitation by nitrogen, and the molten copper was poured into stainless steel crucibles, rather than manufacturing lances.

XRF measurements were done on a wave length dispersive Philips PW2404.

Blister copper was melted at 1200°C in 316L stainless steel crucibles held at different times under the following conditions: in inert conditions without agitation, in inert conditions with agitation by nitrogen (600kPa pressure and 10 $L.min^{-1}$ flow-rate), and in oxidizing conditions (500kPa and 21 min^{-1}) with nitrogen agitation. Coke was placed on top of the melt to prevent oxidation. After the specified times, the copper was poured out. Sections were cut through the crucibles and copper remnants, prepared metallographically, and studied using SEM with EDX. Spot analyses were taken across the interface from the blister copper matrix to the steel. X-ray maps were also undertaken across the interface.

For 40 minutes in inert conditions without agitation, the interface was up to ~80μm wide. It comprised different discrete phases in the copper-rich matrix. Further from the steel was a very light two-phase mixture: overall: ~86 Cu, ~2 Fe, ~10 C with less than 1 Cr and Ni (wt%), deduced as (Cu) + graphite. Nearer the steel was a darker phase, ~67 Cu, ~20 Fe, ~7 C, ~3 Cr and less that 1 Ni (wt%), deduced as (Fe). The matrix had only ~85 wt% Cu.

After 80 minutes in the same conditions, some of the copper had diffused along the grain boundaries of the steel, and the interface was ~150μm. The very light phase mixture had nearly disappeared and there was much more porosity.

Under oxygen, there was much slag, of composition: ~10 Cu, ~44 Fe, ~12 Ni, ~2 Cr and ~27 O (wt%), with the copper only having ~96 wt%, purity, i.e. below the accepted limit. This copper could not be poured freely from the crucible because of the high slag content.

There is a liquid miscibility gap across most of the C-Cu-Fe system, which gave the two different regions in the interface. There is also a miscibility gap in the fcc solid solution, which gives the two different phases, (Fe) and (Cu) near the steel.

The 316L stainless steel crucibles contaminated the copper. Under industrial conditions, and longer times, the effects would be worse, and any 316L lances would deteriorate fast. Since the liquid miscibility gap occurs very near 100% Cu, it would be better to avoid any ferrous material, and instead use refractory linings, which are used for the larger vessels, which would also reduce diffusion.

DEDICATION

To my late brother, “Ingénieur Civil des Mines ” Sylvin Ilunga Senga Mwine Matanda, my first role model whom the destiny has taken from humanity, exactly the time I needed him the most. His legacy continues to inspire me so that every day of life I reflect the person he always dreamed me to be.

ACKNOWLEDGEMENTS

As any other academic qualification, a masters degree in Metallurgy and Material Engineering requires both physical, intellectual as well as moral efforts. As an individual, this could be impossible to achieve alone. This is why the following persons and institutions are acknowledged in a very special way for their contributions:

AMSEN for granting me the bursary at a time when it was the most needed.

Prof. L.A. Cornish and Prof. F.P.L. Kavishe for their supervision, their patience and intellectual determination that led this work to its final conclusion.

The University of Namibia, through the Faculty of Engineering and Information Technology, for the opportunity to complete higher education, and all assistance during practical experiments.

Mr Craig Thomas, the Managing Director of Weatherly Mining Namibia, who, by granting permission to study, recognised the positive impact of studies on the day to day operation.

Mr Borrie Burman from the Tsumeb Custom Smelter for assisting in sampling and other information related to the smelter operation.

Marina Labuschagne, Moira Messenger, as well as Elisabeth Shigwedha, for having contributed with professionalism to the AMSEN administration. This allowed all students to be all the time in any country where they were invited.

My wife, Nella Ngoie Muloko, for her endurance and continuous encouragements, Baba Christophe Ilunga Mazembe, Petronie Nkulu Butombe, Berenice Kyungu Ilunga, Elise Djese Ilunga, Ivon Banza Ilunga and Jonas Lufimbo Ngoie Tenkenya for their sacrifices and to whom this achievement is set as an example for their future.

TABLE OF CONTENTS

LIST OF TABLES

LIST OF FIGURES

LIST OF ABREVIATIONS

EDX	-	Energy Dispersive X-ray Spectrography
SEM	-	Scanning Electron Microscope
BSE	-	Backscattered electrons
SEI	-	Secondary electron image
Wppm	-	Weight part per million
XRD	-	X-ray diffraction
XRF	-	X-ray fluorenscence

CHAPTER 1: INTRODUCTION

1.1. Motivation

The need for reducing lost time in the matte converting process, improved life-time of steel lances, reduction of production cost of melting operations based on the above-mentioned experimental results and conclusions were the determining factors of the choice of the topic of this work.

1.2. Research Problems: atomic movement between liquid copper and solid 316L stainless steel

1.2.1 Statement of the problem

The Fe-Cu binary system consists of three condensed phases, namely liquid, face-centred cubic (fcc), and body-centred cubic (bcc). In common practice, the Fe-rich fcc phase is designated as γ, the Cu-rich fcc as ε, the high temperature Fe-rich bcc as δ, and the low temperature Fe-rich bcc as α [1995Qin]. Although intermetallic phases were not reported, Presnyakov *et al*. [2002Pre] suggested that such intermetallic compounds seemed to exist at high temperatures because of the high reactivity of iron. Many other researchers have treated the Fe-Cu system as being relatively simple, consisting of a mixture of iron and copper phases with transformations caused by the manifestation of iron polymorphism [2002Pre]. Vincent *et al.* observed that copper segregates into copper-rich precipitates within the ferrite matrix under irradiation [2008Vin].

Presnyakov *et al*. [2002Pre] first fabricated a specimen by inserting copper in a low–carbon steel crucible, maintained at different temperatures (1100°C to 1200°C) and different times from 5 to 90 minutes. Secondly, a steel rod was introduced into molten copper in the same temperature ranges. In the first experiment, liquid copper overflowing the outside the crucible was observed, and in the second experiment, liquid copper rose along the steel rod. The copper overflow outside the crucible and the copper rising along the steel rod was described as the superfluidity of copper.

According to Sil'man [2009Sil], despite iron-copper being much studied, there are contradictory data concerning the full or partial miscibility of Cu and Fe in the liquid state, which was found to depend on impurities. Austin *et al.* Recommended a Fe-Cu phase diagram showing the miscibility gap [1977Aus]. [2012Liu] found that there was a separation into two liquids of different composition, which then solidified with different microstructures, agreeing with Lin and Ho [2000Lin]. Fe-Cu alloy system is well known to have a metastable liquid miscibility gap below the liquidus [2006Tak] because of the mixing component of the Fe-Cu atom pair, but other authors did not find stratification.

The interaction between steel and liquid copper is common and particularly important for industrial metallurgists. Davenport *et al*. [1976Dav, 2004Dav] noted the use of mild steel lances in hearth furnaces and the converters, as well as water-cooled steel bands in the Hazelett continuous casting system. The development of durable, long lasting steel lances for submerged operations has proven to be difficult, and more work was still needed to solve this problem [2004Dav]. Industrial practice at the Tsumeb Custom Smelter in Namibia confirms this statement, as mild steel lances have to be replaced more frequently (three to four days) because of the corrosion.

This work intended to examine the reactivity of liquid copper with iron (which would be the cause of the postulated intermetallic formation in liquid copper [2002Pre]) by analytical chemical methods. It was thought that 316L stainless steel would perform better in this environment. The behaviour of two major components of stainless steel (Ni and Cr) were investigated.

1.2.2 Research questions

1. Are copper atoms transferred from blister copper to stainless steel at the blister copper melting temperature in different environments:

a. Inert melting environment,

b. Inert environment with agitation, and

c. Oxidising environment with agitation?

2. Are iron, chromium and nickel atoms, or any other components of the 316L stainless steel, transferred to blister copper?

3. Is the interaction between steel and copper able to compromise the overall behaviour of the two metals during melting in pyrometallurgy?
4. Could stainless steel be an alternative material for manufacturing tuyeres and lances for blowing air in the blister copper converter or at the fire refining stage?

1.3 Aim

This research aimed at the identification of various physical and metallurgical aspects to be considered while deciding to use 316L stainless steel as an alternative material for tuyere manufacturing in converting or fire refining of copper. Through these studies, Fe, Cu, Ni and Cr behaviour during melting was identified with, in some cases sulphur, oxygen and carbon, which are usual components of blister copper and/or stainless steel.

1.4 Objectives

To determine quantitatively and qualitatively the amount of metal involved during interaction between liquid blister copper and 316L stainless steel, by analysing the chemical composition of blister copper and the interface resulting from remelting.

The specific objectives are to:

i) quantify blister copper contamination by Fe, Cr, Ni from 316L stainless steel, and
ii) evaluate the interface between the crucible and the liquid copper by scanning electron microscopy (SEM).

1.5 Hypothesis

The hypothesis is that there is an interaction between blister copper and 316L stainless steel resulting in molten copper contamination which changes the chemical characteristics of the copper.

1.6. Scope of research

This research will cover two different aspects of metallurgy.
Firstly, pyrometallurgy, where studies were done on blister copper with the objective to determine the contamination level resulting from migration of stainless steel components (Fe, Cr, Ni), as this led to the deterioration of the copper properties.

Secondly, physical metallurgy, where the new phases formed at the interface between molten blister copper and 316L stainless steel were identified.

CHAPTER 2: LITERATURE REVIEW

2.1 Background

Copper-iron sulphide and copper sulphides are the most common copper minerals found in the earth's crust. Copper production from sulphide minerals is achieved by hydro or pyro-metallurgical processes; the latter involves smelting copper sulphide concentrate in oxidizing conditions which leads to a sulphide phase called matte and an oxide phase called slag which is a solution of molten oxides.

The use of oxygen-enriched air instead of air improves reactions kinetics and makes the process more autothermal, because less nitrogen is fed to the furnace, less heat is removed in the off gas of the furnace. The slag oxides contents includes FeO from iron oxidation, SiO_2 from the concentrate and from flux, Al_2O_3, Fe_2O_3, Fe_3O_3, CaO and MgO from the concentrate.

The temperature as well as the composition determine the viscosity of the slag. Matte is then converted to mainly remove sulphur and iron, and from the conversion, a metallic product containing an average of 99 wt% copper and less than 0.3 wt% iron, called blister copper, is made. Impurities (Fe, Zn, S, O_2, As, Se, Te, Bi, etc.) in blister copper prohibit its industrial use, as they interfere with mechanical, electrical and other properties of the copper [2004Dav].

In order to remove residual sulphur, blister copper is melted at 1200°C and oxidized through a process of fire refining. In fire refining, oxidation is always followed by deoxidation, aiming at the removal of additional oxygen; and this process uses hydrocarbons as reducers. The removal of sulphur and oxygen from blister copper through fire refining is done by:

a) Air oxidation removal of sulphur as SO_2

$$\text{S (in molten copper)} + O_2\text{(gas)} \rightarrow SO_2\text{(gas)}$$

While sulphur is removed, oxygen dissolved through the following reaction:

$$O_2\text{(gas)} \rightarrow 2O \text{ (in molten copper)}$$

Oxidation of molten copper was investigated, using different compositions of oxygen and nitrogen between 5 and 100 % volume. The rate of oxidation of liquid copper [2005Mar] at a given partial pressure was reported to be linear function of blowing time, and independent of the oxygen concentration of the molten copper. The same observation was done by Barton and Brimacombe [1977Bar] on the oxidation stage of fire refining. Pure oxygen was blown 1 mm over the liquid copper surface at gas flow rates between 500 and $2000\mathrm{cm}^3/\mathrm{minute}$ at 1200°C.

b) Hydrocarbon-reduction removal of oxygen as CO and H_2O

This processs takes place though the following equations:

C(solid) + [O] → CO (gas)

$\mathrm{CO(gas)} + [\mathrm{O}] \rightarrow \mathrm{CO_2(gas)}$

$\mathrm{H_2(gas)} + [\mathrm{O}] \rightarrow \mathrm{H_2O\ (gas)}.$

There are many different types of furnaces used for this purpose; the hearth furnace uses steel lances for the injection of air in the molten metal [2004Dav]. After being deoxidized, blister copper is cast into anodes for electrorefining, where the mould consists of water-cooled low carbon steel. When iron reactivity is high with respect to liquid copper, this leads to both contamination of the liquid copper and corrosion of the furnaces and mould sides or lances. Consequently, the process is technically and economically compromised.

The phase diagram of Fe-Cu is shown in Figure 1.1. It shows a calculated metastable miscibility gap in the supercooled (Cu,Fe) solid + liquid phase. The solidification of Cu-Fe alloys in the miscibility gap has yet to be investigated quantitatively as the kinetic evolution of the microstructure during cooling in the above mentioned metastable miscibility gap is very complex [2004Rag]. The very flat shape of the liquidus indicates that the pre-stratification of the melt is caused by a change in the nature of the melt, i.e. is connected with its transformation from an iron-based solution to a copper-based one. This factor is primarily responsible for the retrograde behaviour of the solidus line [2009Sil]. Numerous investigations on liquid immiscible alloys were done on materials due to the results of researches by Nakgawa in 1958 [1958Nak]. The systems Cu-Co and Cu-Fe have nearly flat liquidus boundaries and positive deviation from the Raoult's law. They exhibit a thermodynamic tendency for liquid immiscibility when undercooling or cooling rates exceed a critical value. A homogenous liquid decomposes into two liquids if undercooled into the metastable immiscibility gap: Co or Fe-rich liquid and Cu-rich liquid [2012Liu].

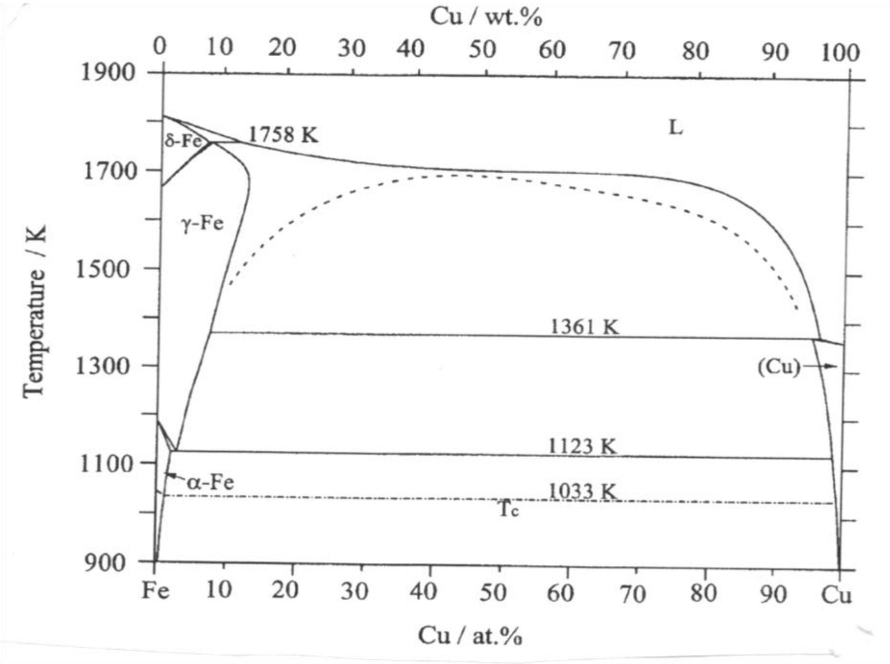

Figure 2.1. Fe-Cu phase diagram [1993Oka].

In a study of the Fe-Cu phase diagram by Presnyakov *et al*. [2002Pre] using thermodiffusion, a phenomenon qualified as superfluidity of copper was observed. Fluid superfluidity is characterized by zero viscosity, allowing frictionless flow and the ability to climb out of open-topped containers by symphonic action [2006Cha]. At the lambda transition temperature ($T_{\lambda} = 2.17K$) under saturated vapour pressure, helium undergoes a transformation from a classical fluid of low density and viscosity to a superfluid [2002Pre]. In order to link the observed phenomenon to superfluidity, Presnyakov *et al*. gave the following explanation: despite the fact that no intermetallic compounds have been discovered in the Fe-Cu diagram [2002Pre], he thought that the liquid separation would encourage the formation on intermetallic phases. Although the studies were limited to the establishment of higher reactivity of the two metals as a cause of superfluidity of the copper.

Lin and Ho [2000Lin] have examined the interaction between steel and copper through SK3 steel-copper cast welding and they established the existence of three different layers at the interface. SK3 steel is a carbon tool steel in the Japanese industrial standard, which is equivalent to TC105 of the International Standardization Organisation (I.S.O.). The first layer or the layer closest to SK3 was the casting layer; the layer formation was mainly due to iron diffusion into copper matrix. Four phases were found in the interface by XRD analysis: $CuFeO_2$, Fe, Cu, C with the first due to inter-diffusion of iron and copper atoms, and the last due to decarbonisation of SK3 steel. The microstructure of air-cooled cast welds consisted of medium pearlite.

The interaction between liquid copper and iron becomes particularly important for extractive metallurgists because if there are intermetallic compounds formed, two possibilities have to be considered:

- The intermetallic compound adhesion to stainless steel could form a coating which later behaves like a protecting layer for stainless against corrosion, or
- The intermetallic does not adhere to stainless steel and migrates through liquid mass, this means that chemical reactions, resulting in formation of intermetallic compounds could speed up corrosion and increase melted copper contamination.

This work assessed the reactivity of blister copper with 316L stainless steel, which means liquid copper contamination and stainless steel corrosion. Miedema [1973Mie, 1992Mie] and Chen [1976Che] successfully used two atomic parameters, electronegativity and valence electron density, to study the possibility of formation of binary compounds. The results and recommendations could contribute to a better understanding of the phenomenon occurring between liquid copper and the components of 316L stainless steel, and at the same time enlighten metallurgists on the behaviour of copper during the melting and casting processes.

After numerous visits to the Tsumeb Custom Smelter, and discussions with operators and the plant foreman, it was established that operations were negatively affected by the use of steel lances for air injection in the furnace at the conversion stage.

Lances are repaired every 60 days [2004Dav] (Norddeutsche Affinerie, Hamburg, Germany) or 100 days (Onahama Smelting and Refining Onahama, Japan), this representing a total of 50000 tons of copper of metal copper for the first and 21600 tons of copper for the second. The repairing time was not clearly stated. These companies use carbon steel pipes fitted in refractory bricks or stainless steel lances, However, at the Tsumeb Custom Smelter, the repair is done after 80 charges of the furnaces (each charge representing 8.4 tons of copper). The furnace is taking four charges per day, which means the repair is done every 20 days or 672 copper metal tons produced. The maintenance takes two to three weeks. For two to three weeks without operation, the company looses 470.4 to 705.6 copper metal tons production although the cost of one lance does not exceed 2.6 US$.

The life-time of lances in the furnace was becoming a matter of concern, as more frequent replacement was necessary because of fast corrosion. Permanent contact of copper with steel during operations was responsible of this unfortunate behaviour of steel. The study and design of an alternative type of material for fabrication of the lance and furnace sides was then necessary to withstand high temperatures and chemical reactions as those encountered in furnaces.

2.2. Blister Copper

Blister copper is a semi-finished product in the copper pyrometallurgy process. The different steps which lead to blister copper are given below [2004Dav].

Concentration of copper sulphide ore which comprises smelting at 1220°C and oxidation of the concentrate to form the matte (matte smelting) as shown in Equation 2.1.

$$2\mathrm{CuFeS_2} + \frac{13}{4}\mathrm{O_2} \rightarrow \mathrm{Cu_2S}.\frac{1}{2}\mathrm{FeS} + \frac{3}{2}\mathrm{FeO} + \frac{5}{2}\mathrm{SO_2}\ \Delta \mathrm{H_{25}} = -450\mathrm{MJ/kgmol\ \ CuFeS_2} \quad 2.1.$$

Matte conversion to blister copper at 1200°C. Equations 2.2 and 2.3 show the two steps of slag and blister copper formation.

$$2\mathrm{FeS} + 3\mathrm{O_2} + \mathrm{SiO_2} \rightarrow 2\mathrm{FeO.SiO_2} + 2\mathrm{SO_2} + \text{heat [kcal/mol]} \quad 2.2$$

$$\mathrm{Cu_2S} + \mathrm{O_2} \rightarrow 2\mathrm{Cu} + \mathrm{SO_2} + \text{heat [kcal/mol]} \quad 2.3$$

The blister copper production flow sheet of the Tsumeb Custom Smelter is presented in Figure 2.1. This is the original design obtained from Tsumeb Custom Smelter management.

The tuyere analysed in this work was drawn from the converter air feed after four days operation and blister copper came from the converter itself.

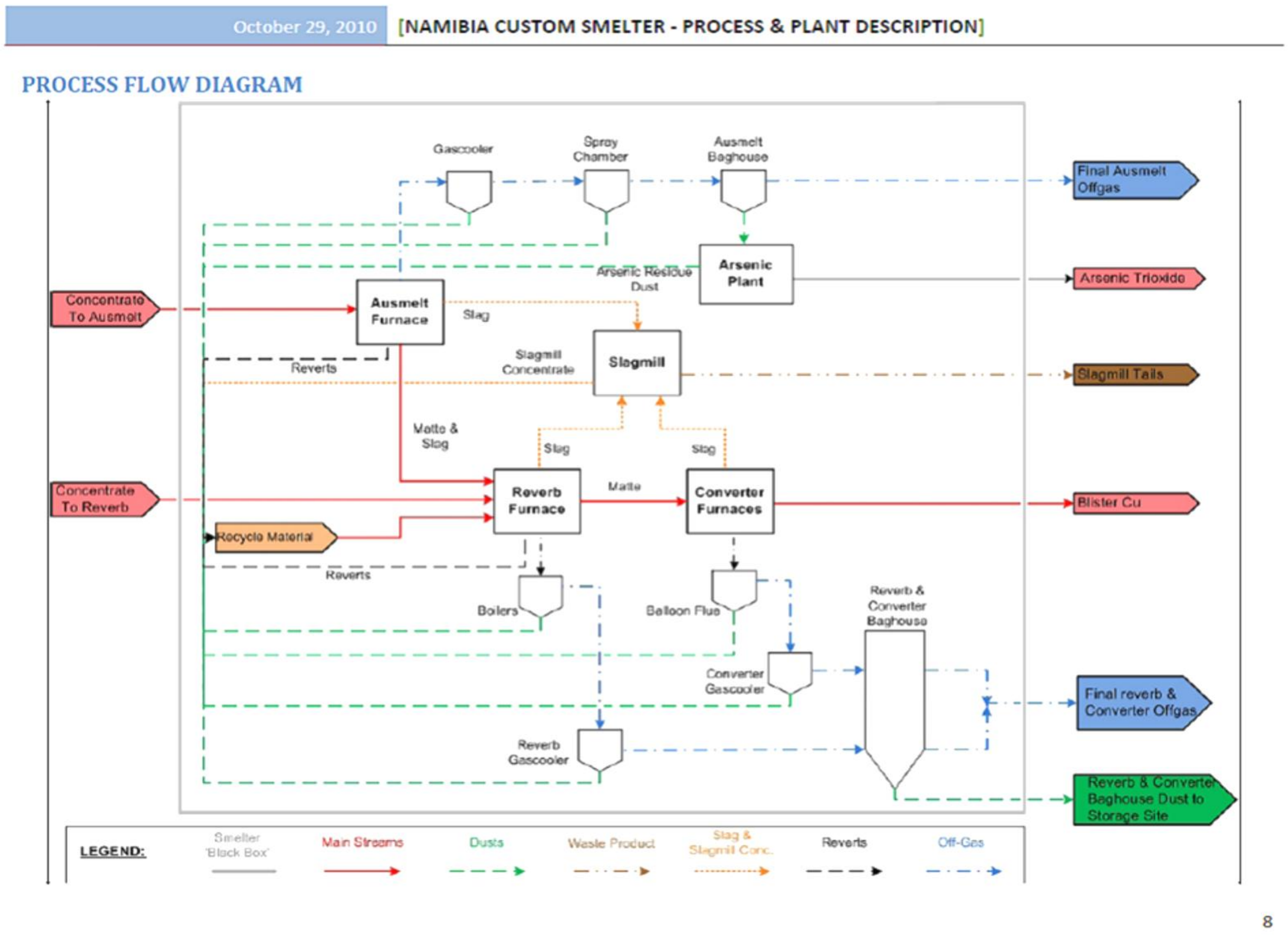

Figure 2.2. Flow sheet of the Tsumeb smelter.

2.3. Interaction of copper with iron, nickel and chromium

In any system, proportions of the components of metallic compounds or phases are chemically and thermodynamically defined. Any excess amount of one of the component in the system will remain unreacted [1990Atk]. This should be considered when studying the system consisting of blister copper and other components of stainless steel.

The major components of 316L stainless steel are iron, chromium and nickel. At 1200°C, copper can dissolve a maximum of 5.5 Fe, 20 Ni and 3.8 Cr wt% to form a single liquid phase [2004Rag]. Figures 2.2, 2.3 and 2.5 show the Cu-Ni, Cu-Cr and Cu-Fe phase diagrams respectively. Any additional amount of these metals to molten copper will result in precipitation of solid phases (austenite γ in the case of Fe, and austenite α in the case of nickel). Table 2.2 shows different compositions of copper, iron and nickel that were used to derive the miscibility gap shown in Figure 2.4.

Table 2.1 Alloy compositions in wt% and at.% for $\mathbf{Cu_x(Fe_{0.5}Ni_{0.5})_{1-x}}$ [2008Gal].

X	Cu:Fe:Ni, (wt%)	Cu:Fe:Ni, (at.%)
0.1	10:45:45	9.1:46.6:44.3
0.2	20:40:40	18.4:41.8:39.8
0.3	30:35:35	27.8:37:35.2
0.4	40:30:30	37.5:32:30.5
0.6	60:20:20	57.5:21.8:20.7
0.7	70:15:15	67.8:16.5:15.7

2.4. Phase diagrams

The copper-nickel binary phase diagram (Figure. 2.2) [1991Nas] is a simple isomorphous system, with a spinodal decomposition of the face–centred cubic (fcc) phase below the critical point 354.5°C at the composition of 67.3 at % Ni. It depicts complete solid solubility between Cu and Ni over a wide range of temperature [2004Rag].

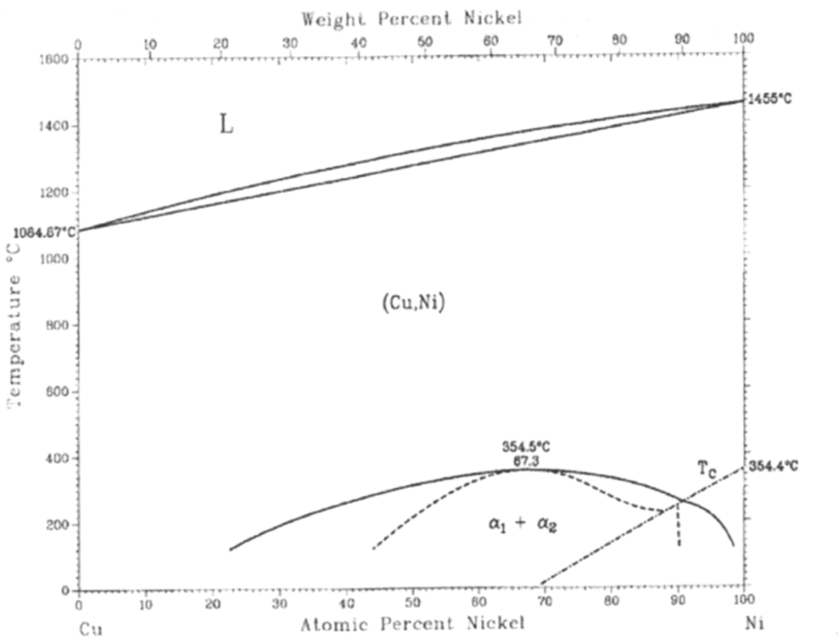

Figure 2.3. Cu-Ni Phase diagram [1991Nas].

The Cu-Cr phase diagram (Figure 2.3) [1997Oka]), reviewed by Okamoto, (solid line) was reported by Zeng [1995Zan] and preferred to that of Chakrabarti [1984Cha] because the former was based on more recent and abundant phase boundary and the thermodynamic data.

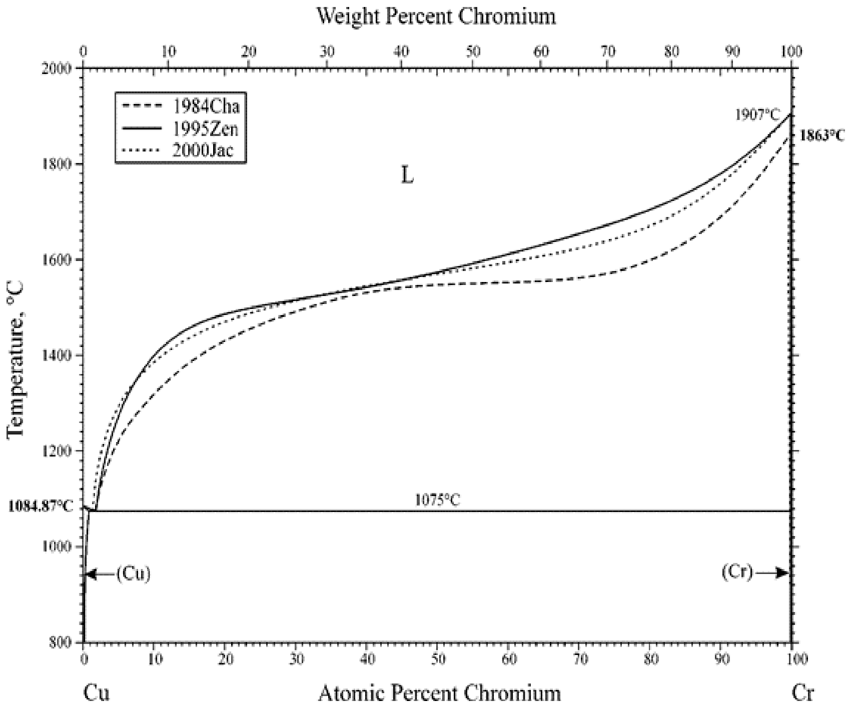

Figure 2.4. Cu-Cr phase diagram [1997Oka].

The phase relationship at high temperatures (600-1200°C) are not completely assessed, and some experimental results differed from the thermodynamic calculations.

The new thermodynamic modelling still failed to correctly predict the phase equilibria within the temperature ranges 527°C to 1127°C [2008Gal]. There is experimental evidence of a smaller miscibility gap and of a window of temperatures, in which Cu-Fe-Ni alloys can be unexpectedly homogeneized into a single face-centered cubic (fcc) phase. Figure 2.4 shows the miscibility gap for Cu-Fe-Ni at temperatures ranging from 527°C to 1127°C.

In 2003 Turrchanin *et al*. [2001Tur] re-examined all published thermodynamic data for the phases of the Cu-Fe system. A thermodynamic model of the liquid phase, which accounted for the temperature variation of the enthalpy of mixing, yielded highly accurate descriptions of the stable $(\mathrm{L} + \delta \leftrightarrow \gamma, \mathrm{L} + \gamma \leftrightarrow \varepsilon + \alpha)$ and metastable phase transformations $(\mathrm{L}_1 \leftrightarrow \mathrm{L}_2, \mathrm{L}_1 + \mathrm{L}_2 \leftrightarrow \varepsilon)$ involving melts as shown in Figure 2.5.

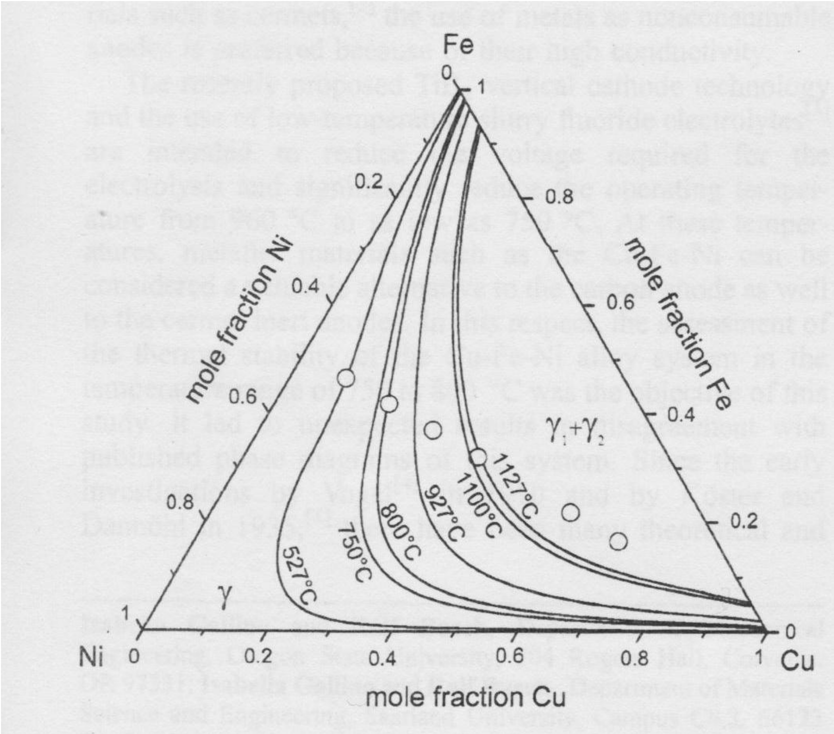

Figure 2.5. Projections of the calculated gap for Cu-Fe-Ni [2008Gal].

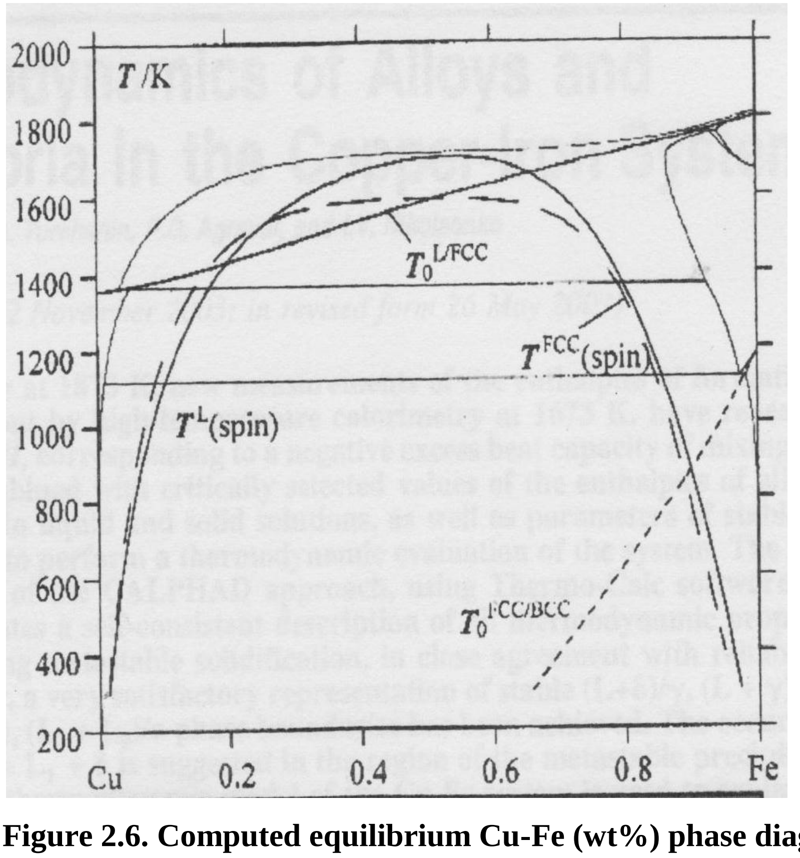

Figure 2.6. Computed equilibrium Cu-Fe (wt%) phase diagram [2001Tur].

2.5. 316 L Stainless steel

Type 316L stainless steel is an austenitic chromium-nickel steel with the composition shown in Table 2.2. Austenitic stainless steels are specified for more severe corrosion conditions, such as those encountered in the process industry and where contamination is undesirable. The addition of chromium to ordinary steel imparts corrosion resistance to the steel in many environments and generally more than 12% chromium is needed to make steel stainless in oxidizing environment [1987Fon].

Table 2.2. Composition of 316L stainless steel [1987Fon].

Element	Composition (wt%)
Fe	Balance
Cr	16 – 18
Ni	10 – 14
Mo	2 – 3
Mn	2 (max)
Si	0.75 (max)
P	0.045 (max)
C	0.03 (max)
S	0.03 (max)
N	0.1 (max)

If carbon content is about 0.02% or higher, in the temperature range of 510°C-787°C, $Cr_{23}C_6$ precipitates out of the solid solution, and some chromium is thereby removed from the austenite solid solution. The result is metal with lowered chromium content i the region adjacent to the grain boundaries, where the carbides mostly form.

If the chromium content is effectively lowered, the corrosion resistance is reduced near the grain boundaries. The $Cr_{23}C_6$ in the boundary is not attacked, but the chromium-depleted zone near the grain boundary is corroded (intergranular corrosion), because it does not exhibit sufficient corrosion resistance. High-temperature oxidation of stainless steels showed selective oxidation of chromium when exposed to low-oxygen atmospheres at 982°C [1987Fon]. In addition to chromium in stainless steels, nickel is added to these steels to stabilize austenite [2006Ash]. A minimum of 8% Ni is needed for a fully austenitic microstructure at room temperature.

2.6. Solid-liquid metal interaction

Liquid metals can cause different types of corrosive attack on solids, but the interaction that occurs is not electrochemical in nature [1963Eva]. Liquid-metal corrosion is primarily a physical, rather than a chemical effect. It is the result of direct solution or solid-state interactions. The types of liquid-metal corrosion that have been observed with respect to liquid metal and solid interaction are:

- Solution of the structural metal,
- Diffusion of liquid into solid metal, and
- Intermetallic compound formation.

In addition, a combined mechanism of agitation and chemical reaction may lead to erosion-corrosion which is the acceleration of deterioration on a metal, because of relative movement between a corrosive fluid and the metal surface [1973Uhi]. Generally, this movement is quite rapid, and mechanical wear effects or abrasion are involved. Metal is removed from the surface as dissolved ions, or it forms solid corrosion products that are mechanically swept from the metal surface.

The interaction between liquid copper and stainless steel might result in continuous corrosion through an electrochemical phenomenon [1973Uhl]. One way of protecting metal is chemical conversion in which coatings are sometimes produced by corroding the metal surface to form a protective corrosion product such as metal oxide.

2.7. Fe–Cu reaction through welding

Cast welding is another form of liquid and solid metal interaction. It is a bonding of copper and iron (SK3 component), resulting from casting liquid copper on solid tool steel. An experiment has shown that bonding tool steel type SK3 (hyper-eutectoid steel) to copper resulted in the formation of three layers between the two metals [2000Lin]. The closest layer to the SK3 steel was described as the cast welding layer. Different microstructures were identified on the interface, depending on the type of heat treatment that the material was subjected to, as shown in Figure 2.6. In a first trial, liquid copper was cast on solid steel and the microstructure is shown in Figure 2.6a [2000Lin]. The interaction between liquid copper and solid steel yielded a third phase in the interface which grew through the steel side. In a second trial, after liquid copper was cast on SK3 steel, the two metals were quenched in water, as shown in Figure 2.6b. In the third trial, the quenching medium was oil and is shown in 2.6c. In the fourth trial the two metal were cooled in air (Figure 2.6.d). In the last trial, the two metals were cooled in the furnace (Figure 2.6e) and different microstructures were obtained.

The effect of cooling rates on the microstructures of Fe-Cu alloys was investigated. A variety of solidification techniques was employed [1987Mun], in order to obtain a wide range of cooling rates. At high cooling rates (about $10^4 \mathrm{K/sec}$), and in the composition range 30 - 80 wt% Cu, the microstructure showed clear evidence of metastable liquid separation. This indicated a melt supercooling of about 50 to 100K. Liquid separation, coupled with high interfacial velocities, resulted in solute trapping, and in a spherical morphology for one of the solids. At cooling rates lower than $10^4 \mathrm{K/sec}$ no liquid separation was observed, and the alloys solidified in a conventional manner, i.e. with a polycrystalline or a dendritic microstructure, depending on the copper content in the γ-Fe phase. At medium cooling rates, the transformation was martensitic, while at low or high cooling rates, a polycrystalline transformed structure was obtained [1987Mun]. All the above mentioned microstructures (Figure 2.6) showed new phases with different morphologies laying on copper rich matrix, at the copper rich side. At the steel side copper penetration into steel was observed.

Zang *et al.* [2007Zha], using selective laser sintering, showed that in Fe-Cu-C alloys there were eutectoid structures of (Fe)-C and (Fe)-Cu at room temperature. Copper was used to infiltrate Fe-Cu-C green powder metallurgy compacts.

After Nakagawa's research on Cu-Co and Cu-Fe alloys in 1958, numerous studies were done on liquid immiscible solid. Huang *et al.* [1984Chu, 1987Hua] indicated that binary alloy systems with large positive heat of mixing are hard to be homogeneously mixed. Amorphization was achieved by ion beam mixing in Fe-Cu because of its very high positive heat of formation [1987Hua].

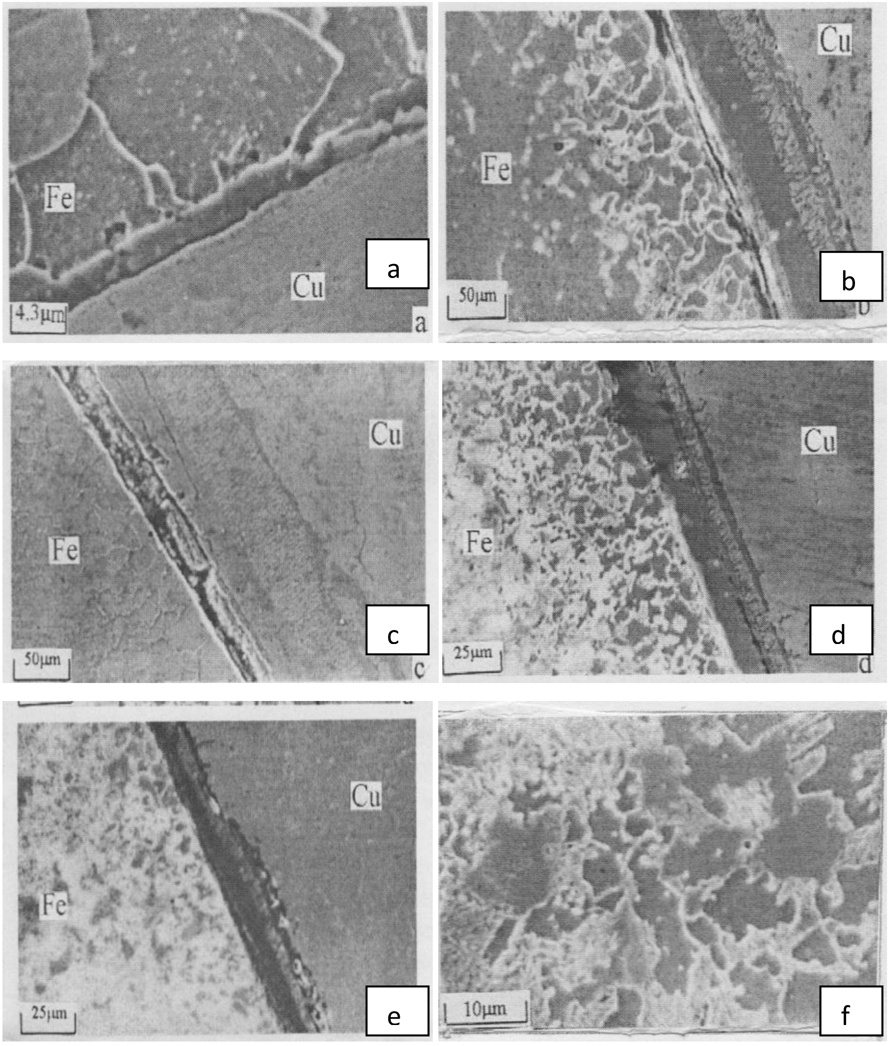

Figure 2.7. SEM photograph showing microstructures of welded SK3 steel-copper, after different heat treatment [2000Lin].

a) Without heat treatment
b) Quenched in water
c) Quenched in oil
d) Air cooled
e) Furnace cooled
f) Fe-rich side of furnace cooled sample.

2.8. Diffusion

The diffusion between copper and iron is substitutional since the atoms have similar sizes:

Cu=0.3615nm and γFe=0.3590nm.

The driving force for diffusion to occur is the activity difference between the parts. Ideal solutions activities are described by Raoult's law, while real or non-ideal solution activities are described by Henry's law. Activities of components of liquid copper and iron alloys were investigated by Batalin and Sudavtsova [1980Bat] and Park and Gastell [1989Par]. Turchanisn and Agravl [2001Tur] stated that copper activity increased as a function of temperature, and activities of different compounds of the alloys deviated negatively from ideality. This is particularly important to the current work, as it focus on the interaction between liquid copper and stainless steel which is an iron alloy.

Diffusion of iron in copper was described by regression as in Equation 2.4:

$$\mathbf{D_{Fe-Cu} = 0.504\exp(-49740/RT)\ \ cm^2/s} \qquad \text{..........} 2.4$$

where R is the gas constant, T is the absolute temperature [2012Sal].

The solubility was described by regression as Equation 2.5:

$$\mathbf{\log C = 2.951 - 3357(1/T)} \qquad \text{..........} 2.5$$

where C is the concentration of iron in copper at temperature T in Kelvin.

2.9. Oxide film formation on metal

In the current studies, blister copper was oxidized in a 316L stainless steel crucible for the sulphur removal. Therefore, it was important to examine stainless steel behaviour with respect to copper in an oxidizing environment. Chromium, silicon, aluminium and other metal oxide coatings are produced on low carbon steels by heating in air, or by exposing to hot liquid [1986Fon]. When there is competition for oxygen, the element with the lowest free energy for oxide formation (higher affinity for oxygen) is oxidized to a greater degree. In the case of stainless steel, this resulted in a more protective scale [1987Fon]. Without such oxide layers, metals would adhere to and react with each other, as well as with other materials. The rate of oxide growth is dependent on a pre-exponential factor and an activation term.

The activation energy in the exponential is reduced by the electric field across the oxide. While oxidizing copper in steel-sided furnaces, a copper oxide film might form and create a protective layer for the liquid metal. The rate of oxide growth according to the Cabrera-Mott expression can be described in Equation 2.6.

$$\frac{dx}{dt} = N\Omega\nu\exp\left(\frac{W-qaE}{kT}\right) \qquad \text{2.6}$$

where:

x: oxide film thickness at time t

a: distance between the energy barrier maximum and adjacent minimum

q: charges passed in growing the film

k: Boltzman constant

T: absolute temperature

E: activation energy

W: energy barrier

υ: vibrational frequency

N: number of mobile ions

Ω: potential across the interface.

When an iron-based alloy is exposed to an atmosphere containing oxygen at room or higher temperatures, an oxide layer and/or oxide particles are, to a greater extent, formed on the surface of the alloy. The characteristic features of the oxides formed on the surface of the iron-based alloy strongly depend on temperature, constituent elements in the alloy, chemical species in the atmospheric gas, etc. [Was2006]. The Elligham diagram (Figure 2.8) shows several elements by which the formation of oxides of elements may be predicted.

In the case of copper-based alloys containing various kinds of alloying elements, of which the chemical characters are different from those of copper. Therefore some alloying elements are likely to selectively react with gas species during annealing. In 2004 Shigeru *et al.* [2004Shi] characterized thin surface layers formed in different copper-based alloys by annealing under low oxygen partial pressure. Their studies included Copper-chromium, copper-iron and copper-nickel-silicon alloys. They established that chromium in the copper-chromium alloy and silicon in the copper-nickel-silicon alloys were enriched to a surface after forming oxides layers. This phenomenon was likely to be based on reactivity of alloying elements with oxygen leading to the formation compounds as shown in Figure 2.8.

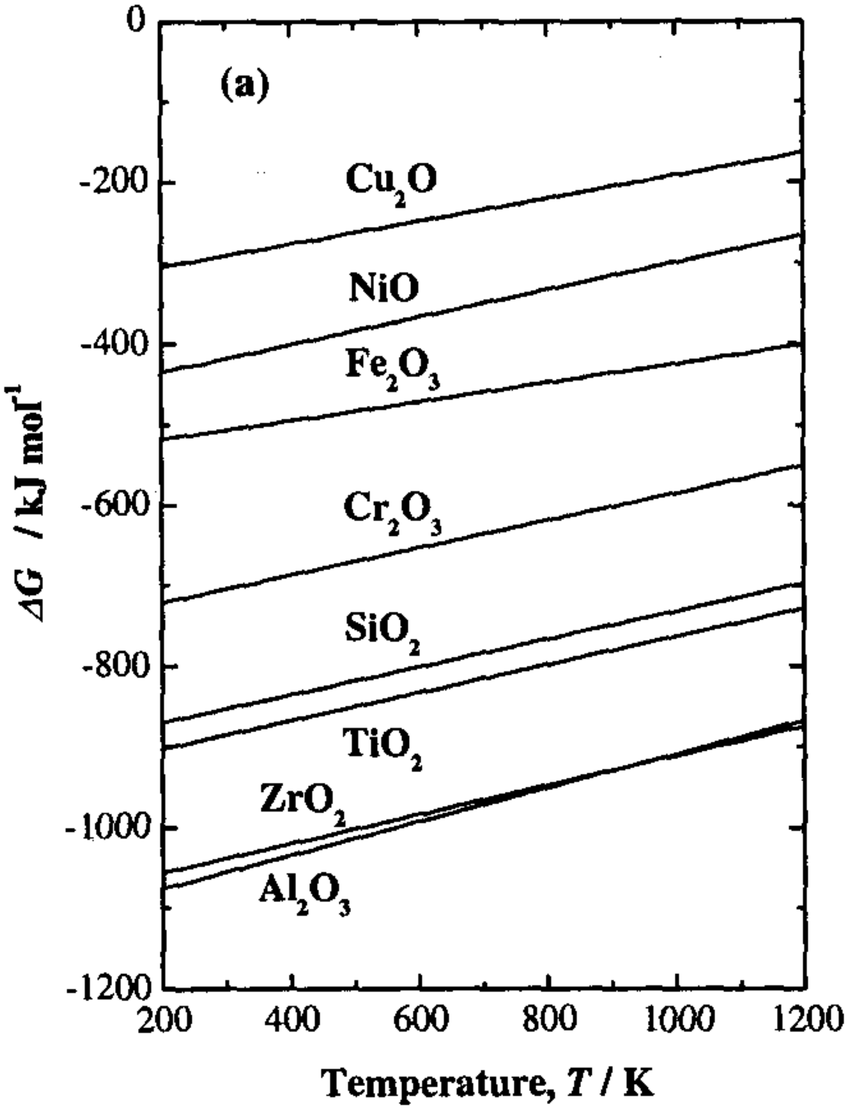

Figure 2.8. Ellingham Digram for oxides [2004Shi].

2.10. Factors which influence the formation of solid solutions

A solid solution is formed when more than one element is present in another element without changing the structure. Most solid solutions are terminal, i.e based on one element.

The greater the difference in size between the atoms of the two metals involved, the smaller will be the range over which they are soluble. If atom diameter differs by more than 15% of that of the solvent metal, then solid solubility is generally extremely small. However, if diameters differ by less than 7% [1953Hum], then other things being equal, they will be likely to form solid solutions in all proportions. Additionally, the structure needs to be the same, and the valencies and electronegativities similar.

Most molten metals dissolve in each other in all concentrations, but when the liquid mixture begins to cool down and a low potential lattice begins to form, not all the impurities will be accepted in the lattice, and several solid phases may form [1990Mic]. A metal of low valency is more likely to dissolve in one of higher valency than vice versa [1994Hig].

2.11. Factors which affect the formation of intermetallic compounds

The ions of all metals are electropositive, but some are more electropositive than others. The greater the difference of electropositivity, the greater will be the chemical affinity of one ion for another, so that they will tend to form a compound rather than a solid solution [1994Hig]. If their electropositivities are similar, other things being equal, they will very probably form solid solutions.

2.12. Viscosity

Liquid metal viscosity is a very important thermo-physical property in many industries especially melting and casting. Any phases resulting from the interaction between liquid Cu and solid 316L stainless steel would modify the physical properties, such as viscosity of the melt. Viscosity denotes opposition to flow, or resistance to movement of neighbouring portions relative to one another. It is constant for a given fluid at a fixed temperature, and controls liquid flow in surface coating [2003Tru]. The viscosity of metallic melts is of great importance in metallurgical processes. Mi *et al*. [2010Mi] measured the kinetic viscosity of molten aluminium, and from a calculation model found that the viscosity and the size of atomic clusters in the melt were directly dependent on the temperature.

Oleksiak *et al.* studied the effect of iron concentration and temperature on the surface tension of liquid copper [2010Ole]. It was established that the higher Fe content in copper increased the surface tension and higher temperature decreased it. Early studies by Schonhorn established a relationship [1967Har] between surface tension and viscosity.

CHAPTER 3: EXPERIMENTAL PROCEDURE

3.1. Sample manufacturing and initial conditions

In commercial practice, blister copper is melted at 1200°C in an inert atmosphere, comprising a flow of nitrogen. Crucibles and a lance made from 316L stainless steel were used for melting. Nitrogen and oxygen were supplied through pressure gauges and flow meters.

3.2 Sample preparation and experimental runs

Blister copper samples were received from the smelter in a square shape (100x100x15mm). A 10 mm drill bit was used to produce chippings from the samples.
These chippings were cast in stainless crucibles, and the liquid metal was poured into copper moulds. The stainless steel crucibles were then cross-sectioned for interface studies on a scanning electron microscope. The blister copper in the copper mould was weighed and analyzed separately. The experimental runs are summarised in Table 3.1.

The crucibles were of square cross-sections of 40 mm side and 60 mm high. They were placed in a 316L stainless steel box inside a chamber furnace. Lances were 700 mm long and 10mm wide square cross-sections, The gas was blown directly from the supply to a stainless steel chamber (100mm x 100mm x 45 mm) to which the 700mm long lances were welded. This chamber was situated on the exhaust of the furnace to allow the gas to heat it up before leaving the furnace. About 90 % of the lances length was inside the furnace to allow gas preheating. On the portion of the lances located on top of the furnace, a bolt and nut mechanism allowed the lowering and lifting of the lances into or out of the melt.

Table 3.1: Sample specification and experimental runs: all samples were chippings, the reducer used was coke, the melting temperature was 1200°C, the nitrogen pressure was 600 KPa and all were air cooled.

Sample No	**O pressure (kPa)**	**O flow (l/minute)**	**Melting time (minutes)**	**Melting environment**	**Lance position**
N01092010	-	-	20	Inert	Top blown
N02092010	-	-	40	Inert	Top blown
N03092010	-	-	60	Inert	Top blown
N04102010	-	-	80	Inert	Top blown
N05122011	-	-	100	Inert	Top blown
06/12/2010	-	-	20	Inert	Submerged
N07/10/12/2010	-	-	40	Inert	Submerged
N08/10/12/2010	-	-	60	Inert	Submerged
N09/13/12/2010	-	-	80	Inert	Submerged
N10/13/12/2011	-	-	100	Inert	Submerged
N1113/1210	500	21	20	Oxidizing	Submerged
1213/1210	500	21	40	Oxidizing	Submerged
1313/1210	500	21	60	Oxidizing	Submerged
1413/1210	500	21	80	Oxidizing	Submerged
1513/1210	500	21	100	Oxidizing	Submerged

In the cases where agitation was needed, the lances were directly lowered in the liquid metal before the gas was introduced. At their lowest points, lances had five holes of than 1 mm, that allowed the flow of gas from the lances into the liquid metal. After furnace was started, the temperature was set at 1200°C and the furnace allowed to heat up. The temperature took 3 hours and 20 minutes to reach 1200°C. The temperature in the crucibles was assumed to be the same as that of the chamber furnace, as the gas was preheated before its introduction into the melt. The gas used was made of 33.34 (wt%) nitrogen and 66.66 (wt%) oxygen, and fell into the category of oxygen-enriched air. This allowed the reduction of energy loss through exhausted inert nitrogen and speed up oxidation.

A set of five samples was maintained at 20, 40, 60, 80, 100 minutes at 1200°C, without any agitation. A second set of five samples was maintained at the same times, with nitrogen agitation. The last set of molten copper samples was maintained in the same conditions, but agitation by mixture of nitrogen and oxygen was used. Copper, iron, chromium, and nickel contents of the resulting samples were analysed. The iron–copper reactivity was identified through the blister copper chemical composition after melting.

3.3. Preliminary analysis

3.3.1. Electrolytic analysis

This study used blister copper (98.6% Cu) that was produced at the Namibia Custom Smelter in Tsumeb Namibia. The material was available as small ingots of 1 kg, from which chippings were made by drilling.

Electrolytic analysis was done in Tsumeb on the original blister copper to determine copper concentration.

The conditions used were:

Electrodes types: platinum

Current: 2.2 A

Voltage: 3 Volts

Temperature and agitation: The process took place at room temperature, and agitation was pneumatic.

3.3.2. Atomic absorption

A spectrophotometric atomic absorption analysis was done in Tsumeb to identify the other elements in the original blister copper such as zinc, iron, lead, cobalt, manganese, arsenic, selenium, gold, silver, titanium and antimony.

3.4. Process for manufacturing the copper-iron interaction samples

The design of the system for the flow of gas into the liquid metal was done and the flow sheet shown in Figure 3.1 was finally adopted.

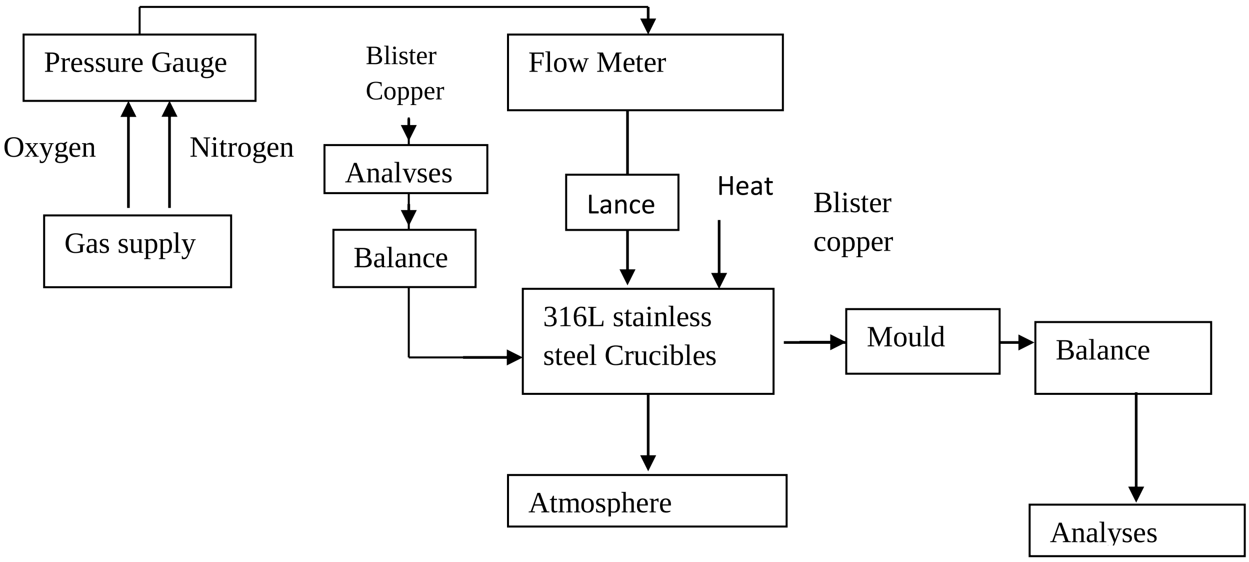

Figure 3.1. Flow sheet of the experimental process.

A small chamber (100x100x45 mm) with a lifting mechanism was designed using 316L stainless steel. The gas flow rate and pressure was measured by pressure gauges and flow meters, and nitrogen was introduced through a lance that was also made from 316L stainless steel.

The copper was melted and immediately poured out into crucibles made of 316L stainless steel.

3.5 XRF spectroscopy

This method was used at the Ministry of Mines and Energy in Windhoek, Namibia. It was done in order to determine Ni, Fe, Cu, Cr in the cast blister copper. Atoms in the sample were excited by X-rays emitted from a X-ray tube.

Specific X-rays Fluorescent signals emitted by atoms after photoelectric ionisation were collected and measured simultaneously in a fixed mounted semiconductor detector. The radiation intensity of each element's signal was converted into concentrations of the element in the specimen. Through this method, Ni, Cr, Fe, Cu concentrations of the sample were determined. The weight was determined before and after melting.

3.6. Sample preparation for Scanning Electron Microscope (SEM/EDX) analysis

An original tuyere from the Tsumeb converter was cross-sectioned at the most corroded region. Number N1513/12/2010 stainless steel tuyere from the lab was also sectioned. In each set of the copper-iron interaction experiments, two crucibles were cross-sectioned and analysed in the SEM, and the results were compared to those obtained by XRF on the cast blister copper.

Nitrogen was used to make the furnace atmosphere inert and agitate blister copper. The flow of nitrogen and oxygen was measured by pressure gauges and flow meters, and adjusted without any pre-heating. Nitrogen was used for agitation and oxygen for oxidation.

Oxygen was used in the last five samples in order to simulate practical conditions where impurities were oxidized and removed from blister copper. Where applicable, the agitation time was varied from 10 minutes to 50 minutes. The melting time varied from 20 to 100 minutes in each of the five sets of experiments.

All samples were melted, cast in ceramic crucibles and cooled. Initially samples and empty crucibles were weighed on the balance. The weight of the sample after melting was determined by deducting the weight of the crucible from total weight of the crucible and the samples. The weight was determined before and after melting. The load of the crucible was prepared by drilling original smelter samples with a 10 mm high speed drilling bit.

The copper was melted at 1200°C in crucibles made of 316L stainless steel and was immediately pored out into the refractory moulds (45x20x5mm) and air cooled to ambient temperature (31°C). The top of the molten metal was immediately covered with industrial coke to avoid re-oxidation; the cooling rate (1-10 K/s) was kept constant during all experiments.

The following experiment crucibles were sectioned for SEM:

- Sample N0209/12/10 (Sample 2, 40 minutes) and N0410/12/10 (Sample 4, 80 minutes) from the first set of experiments, treated in inert condition without agitation;
- Sample N0810/12/10 (Sample 8, 60 minutes) and N1013/12/10 (Sample 10, 100 minutes) in the second set of experiments treated in inert conditions with agitation;
- N1113/12/10 (Sample 11, 20 minutes) and N1213/12/10 (Sample 12, 40 minutes) in the third set of experiments, treated in oxidizing conditions with agitation.

The samples were cut on a Struers Labotom-3 cutting machine, at 2850 rpm.

Struers waterproof papers of silicon carbide with different grit sizes 320, 500 and 800 were used to grind the samples.

Sample polishing was done on a Struers Labo Pol 21 Specimen Mover at 2 to 3 Amps and 10 bars maximum water pressure. The paste consisted of monocrystaline diamonds particles of ¼ microns size, commonly known as Struers DP-Paste M.

A lance was made from 316L stainless steel, 10 mm x10mm section and 65 mm long with five holes and was used to blow the gas into the copper. Lances were top blowing in the first series of experiments, but submerged in the liquid blister copper through the second and the last series.

3.7. SEM/EDX analyses

A Field Emission (LEO 1525) scanning electron microscope was used, and the EDX were done on an Oxford Inca Analyser. This work was done at the National Metrology Institute of South Africa (NMISA), Pretoria, South Africa.

Scanning electron microscopy analyses are presented for comparison and confirmation of tests for N0209/12/10; N0410/12/10; N0810/12/10; 1013/12/10; N1113/12/10; N1213/12/10. The thickness of the interfaces were also measured.

3.8. Consolidation of results

The MATLAB programme was used for plotting all the data.

CHAPTER 4: RESULTS

4.1 Analyses of the original blister copper

The blister copper had a composition of 98.6 wt% as shown by electrolysis and atomic absorption spectrophotometric results in Table 4.1.

Table 4.1. Blister copper composition.

Element	Concentration (wt%)
Cu	98.5 - 99.5
O	0.5 - 0.8
Sb	0 - 0.3
Fe	0.1
Au	10^{-4} - 0.1
Ag	0 - 0.1
S	0.02 - 0.1
Pb	0 - 0.1
As	0 - 0.03
Bi	0 - 0.01
Zn	0.005

4.2. Results on cast blister copper

The results of the first series of experiments, done in inert conditions without agitation are presented in Table 4.2. The results of the second series of experiments, done in inert conditions with agitation are presented in Table 4.3. Results of the third series of experiments, done in oxidizing conditions with agitation are presented in Table 4.4. The results consist of the weight of crucibles before and after melting, the weight of blister copper before and after melting, the melting times, as well as the concentration of iron, nickel, and chromium in blister copper after melting.

Iron, nickel and chromium were not detected in the cast blister copper by XRF for all tests (N01092010, N0209201, N03092010, N04102010, N05122011) done without any agitation.

Table 4.2. XRF results for specimens, weight and percentage of blister copper recovered from the crucible after melting, for the samples treated in inert conditions without agitation, with top blown nitrogen at 1200°C.

Sample number	N0109/12/10	N0209/12/10	N0309/12/10	N0410/12/10	N0510/12/10
Melting time (minutes)	20	40	60	80	100
Cu (wt%)	99.46	99.46	99.47	99.22	99.43
Weight of blister copper before melting (g)	220	183	173	200	202
Weight of blister copper after melting (g)	184	96	45	85	93
Weight of crucible before melting (g)	266	283	266	281	278
Weight of crucible after melting (g)	302	370	396	398	381
Proportion of Blister copper after melting (%)	83.64	52.46	26.01	45.5	46.04

Table 4.3. XRF result for specimens, weight and percentage of metal recovered from the crucible for the sample treated in inert conditions with agitation, with submerged lance at 1200°C.

Sample number	N0610/12/10	N0710/12/10	N0810/1210	N0913/12/10	N1013/12/10
Agitation time (minutes)	10	20	30	40	50
Melting time (minutes)	20	40	60	80	100
Ni (wt%)	0.05	0.1	0.26	0	0.05
Fe (wt%)	0	0	0.34	0.07	0.03
Cr (wt%)	0	0	0	0	0
Cu (wt%)	99.47	99.21	98.82	99.37	99.54
Weight of blister copper before melting (g)	195	195	198	166	169
Weight of blister copper after melting (g)	133	108	92	106	144
Weight of crucible before melting (g)	276	272	272	263	288
Weight of crucible after melting (g)	398	351	386	324	313
Proportion of blister copper recovered from crucible after melting (%)	68.21	55.39	46.47	63.86	85.21

Table 4.4. XRF results, weight and percentage of blister copper recovered from the crucible after melting for the sample treated in oxidized conditions with agitation, with submerged lance at 1200°C.

Sample number	N1113/1210	1213/1210	1313/1210	1413/1210	1513/1210
Agitation time (minutes)	10	20	30	40	50
Melting time (minutes)	20	40	60	80	100
Ni (wt%)	0.2	0.16	2.13	3.77	3.88
Fe (wt%)	0.04	0.06	13.63	13.56	15.43
Cr (wt%)	0	0	3.1	4.24	4.43
Cu (wt%)	99.35	99.35	80.37	77.61	75.39
Weight of blister copper before melting (g)	163	169	201	183	105
Weight of blister copper after melting (g)	57	32	0	0	0
Weight of crucible before melting (g)	269	284	286	296	277
Weight of crucible after melting (g)	382	438	487	479	382
Proportion of blister copper recovered from crucible after melting (%)	34.97	18.94	0	0	0

The same was observed for the samples treated in inert conditions with agitation. The chromium content did not change in the five tests (06/12/2010, N07/10/12/2010, N08/10/12/2010, N09/13/12/2010, N10/13/12/2011) done with nitrogen agitation. Nickel increased in blister copper from the first 20 minutes of melting while iron, appeared only 60 minutes later with a maximum concentration before dropping again.

After 60 minutes of melting and 30 minutes agitation in oxidizing condition, some chromium was transferred from stainless steel to blister copper. The blister copper nickel concentration increased after 20 minutes melting with agitation. No oxidation took place at this stage.

Iron started to show a difference after 60 minutes in the inert conditions with agitation as shown in Table 4.3 and continued to change in the oxidizing conditions.

4.2.1. Residual amounts of blister copper in crucible

Figures 4.1–4.7 show the crucibles after melting. The amounts of blister copper remaining in the crucibles after casting and its distribution along the sides of the crucible were variable.

Figure 4.1. Photograph showing the interior of crucible treated for 60 minutes in inert conditions without agitation.

Figure 4.2. Photograph showing the interior of crucible treated for 40 minutes ininertl conditions without agitation.

Figure 4.3. Photograph showing the interior of crucible treated for 20 minutes in inert conditions without agitation.

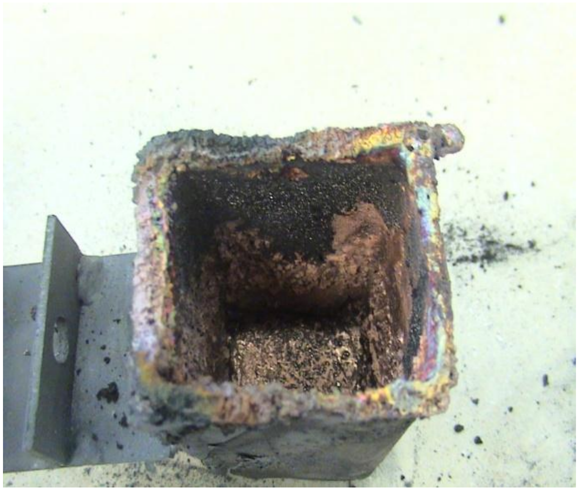

Figure 4.4. Photograph showing the interior of crucible treated for 80 minutes in inert conditions without agitation.

The amount of blister copper recovered after melting in inert conditions with agitation after 20 minutes of melting was higher than that recovered in inert conditions without agitation. Although the other conditions were kept constant, the amount of cast blister copper recovered was a minimum at 26.01 wt% copper. There was also a minimum amount of copper recovered at 60 minutes for the melt done in inert conditions without agitation. For the samples melted under oxidizing conditions, there was more slag with increased time, and after 60 minutes, the slag was stopping the copper from being poured out of the crucible. In industry, silica is added to make the slag flow better [2004Dav].

During melting, copper had risen up the steel crucible sides. The height reached inside differed between crucibles and depended upon the melting time. Figure 4.3. shows copper up to the top of the crucible, while all the other figures show lower levels. The top part of the crucible appearing yellow was covered by sulphur from the copper by distillation and condensation.

Figure 4.5. Photograph showing the interior of crucible treated for 20 minutes in inert conditions with agitation.

Figure 4.6. Photograph showing the of crucible treated for 80 minutes in inert conditions with agitation.

Figure 4.7. Photograph showing the interior of crucible treated 100 minutes in inert conditions without agitation.

4.2. 2 Analyses using SEM/EDX

Studies of the microstructures using scanning electron microscopy was done, as well as EDX, on two samples from each of the three categories of the experiments.

The sections comprised three zones characterized by:

- the copper that remained in the crucible, which is the copper-rich zone,
- the inside of the crucible, which is the iron-rich zone, and

- the interface between the copper-rich and the iron-rich zones.

In general, throughout the SEM analyses five phases were identified (through all the samples studied) and compositions determined as shown in Table 4.5. In this table compositions were determined by taking the average of compositions of each phase from samples. The carbon concentration was higher in the samples than in the typical composition shown in Table 2.2. This was caused by the metallurgical coke used to create a reducing environment around the samples during the cooling.

Carbon contributed to the final microstructures by forming $Cr_{23}C_6$. Its contribution was minimised, as the samples were not maintained between 510°C and 787°C where thermodynamically stable chromium precipitates as $Cr_{23}C_6$.

Table 4.5. Compositions of different phases, identified after tests, wt%.

Phase No.	Fe	Cu	Cr	Ni	C	O	S	Mn
1	2.3	86.6	0.2	0.2	10	0.8	0.1	0
2	51.1	19.1	3.9	8.6	2.5	1.4	1.7	0
3	3.6	87.2	0.4	2.1	3.4	0.9	0	0
4	67.8	0.5	17.5	10.2	1.8	0.6	0.6	1.1
5	23.8	27.3	4.8	5.2	4.6	23.4	0.3	0.3

Although the test was conducted in an inert environment, oxygen was found in different samples. This oxygen mainly came from the original blister which had 0.8 wt% copper. Immediately after melting, the poured metal was covered with coke and the crucible was filled with coke.

The gas composition around the crucible during cooling might had influenced the general oxygen composition of samples. However, this influence could not affect the final results interpretation for the following reasons:

1. Air cooling was fast
2. Although oxygen could be in the gas, the environment was highly reducing because of carbon combustion.

4.2.2.1 Sample treated for 40 minutes in inert conditions without agitation

Figures 4.8 and Figure 4.9 show X-ray maps at two different magnifications, where elements are represented by different colours. The first, at 2000X magnification shows a clear demarcation between the copper-rich side (left) and the iron-rich side (right), while the second, at 300X magnification shows the interface as well. Figures 4.8a and 4.9a show all elements in the same maps, while Figures 8b-h and 9b-j show individual elements. They clearly show the distribution of elements through interface.

Iron was mostly concentrated in stainless steel and was also seen in the interface with very little in the copper-rich side. Copper was completely distributed between copper-rich side and the interface. Chromium was found in the steel, some in the copper-rich side; it was almost non-existent in the interface. Nickel was almost completely in the steel.

EDX done on the interface between stainless steel and blister copper (Figure 4.10.) and Table 4.1 showed the presence of these metals as far as 1.75 mm from the interface. Carbon and silicon were evenly distributed between copper-rich and steel. Sulphur was found mostly in the interface, while major amounts of oxygen were found at the copper-rich side.

In addition to the X-ray maps, line scans showing concentration variation across the interface were carried out on a total length of 66 microns. Figures 4.10b-i. must be read in conjunction with Figure 4.10a. In addition to line scans, they show four different phases.

The overall elements concentrations of the analysed area of the sample, as well as the different phases compositions, were determined by EDX as shown in Table 4.5.

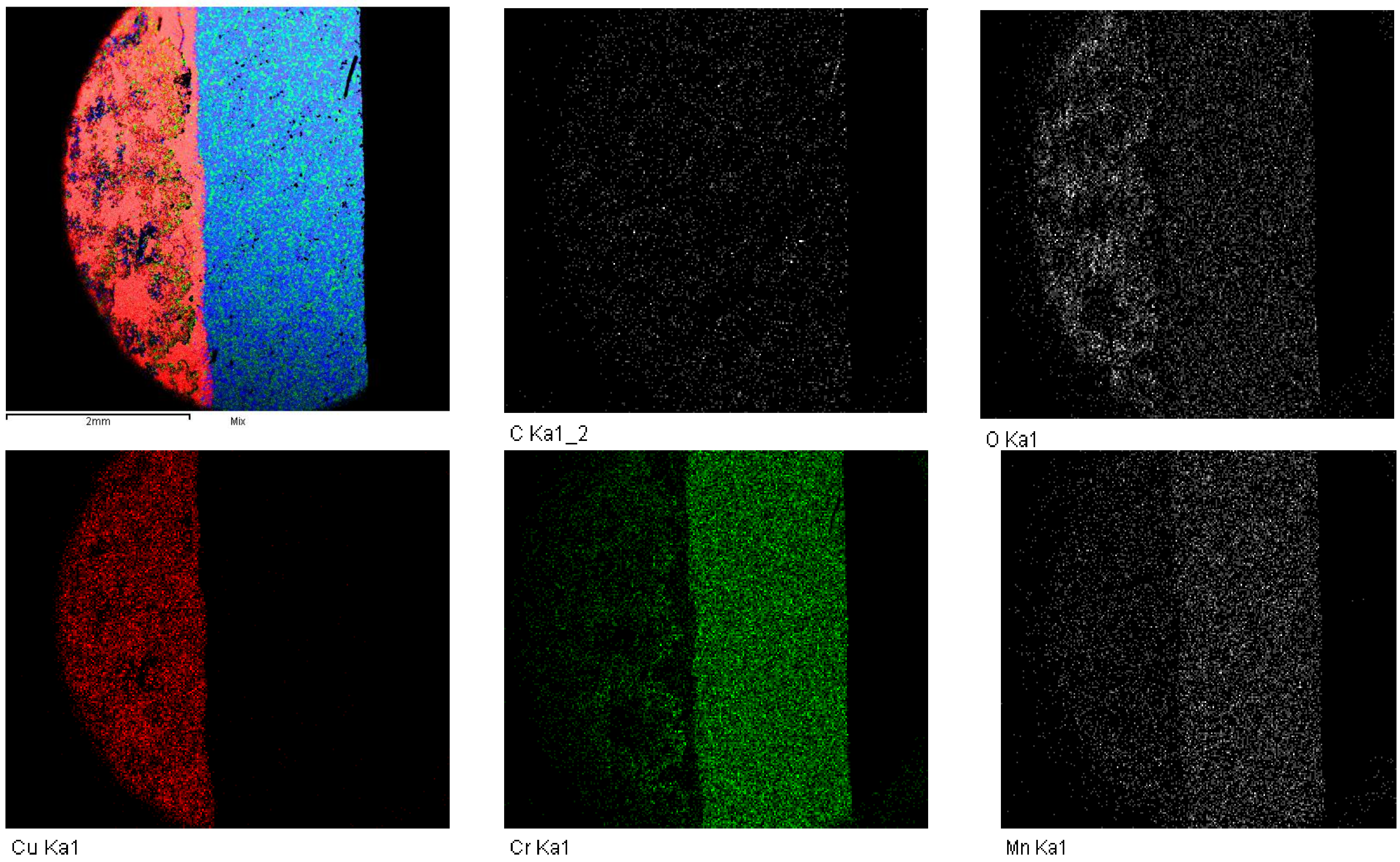

Figure 4.8. **X-ray maps showing different components of the interface of the sample treated for 40 minutes in inert conditions without agitation. C: white, O: white, Cu: red, Cr: green, Mn: grey, Ni: white, Fe: green.**

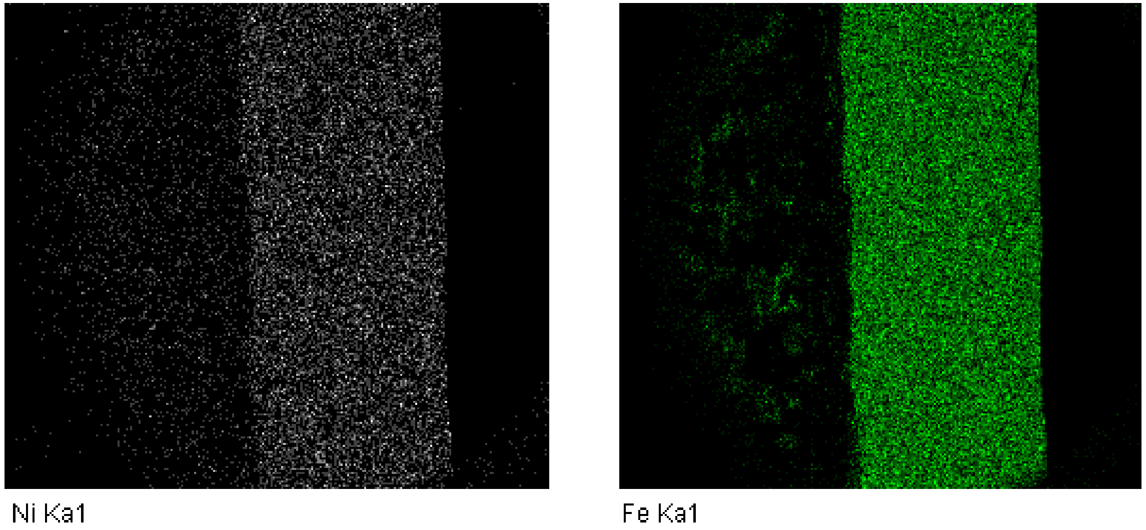

Figure 4.8. **X-ray maps showing different components of the interface of the sample treated for 40 minutes in inert conditions without agitation (continued). C: white, O: white, Cu: red, Cr: green, Mn: grey, Ni: white, Fe: green.**

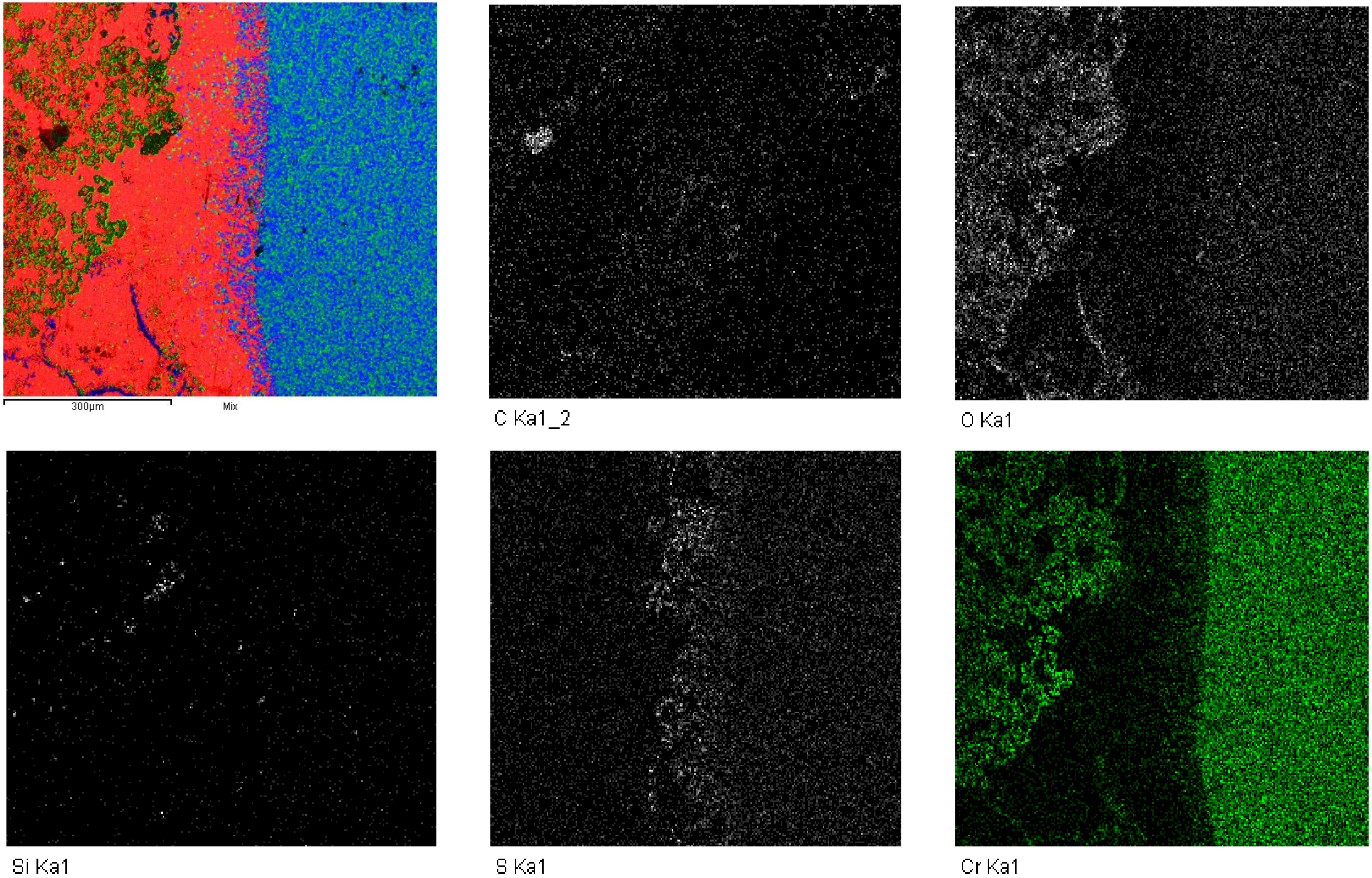

Figure 4.9. X-ray maps showing different components of the interface of the sample treated 40 minutes in inert conditions. C: white, O: white, Si: white, S: white, Cr: green, Mn: white, Fe: blue, Ni: white, Cu: red.

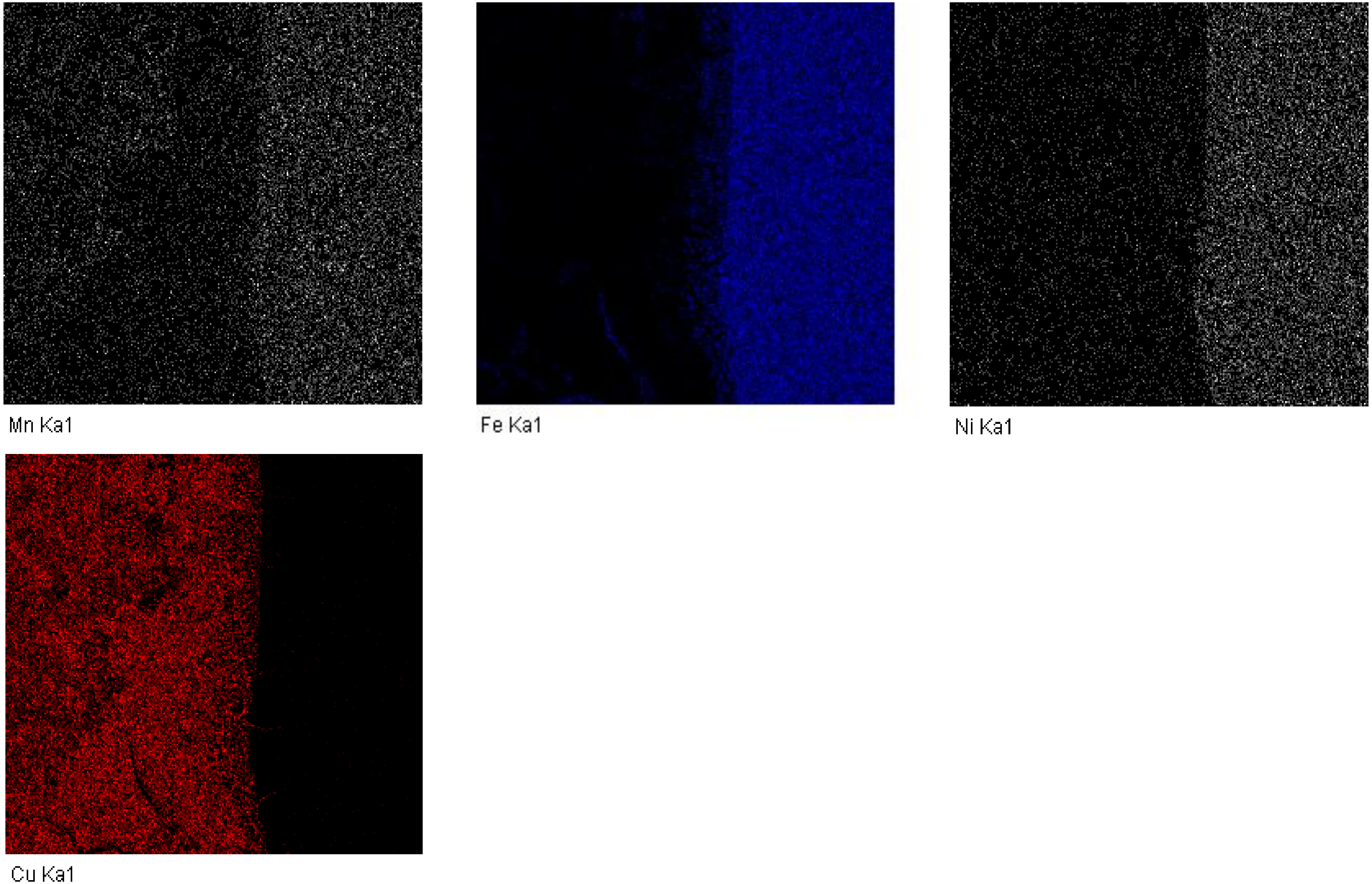

Figure 4.9. **X-ray maps showing different components of the interface of the sample treated 40 minutes in inert conditions (continued). C: white, O: white, Si: white, S: white, Cr: green, Mn: white, Fe: blue, Ni: white, Cu: red. (continued).**

Table 4.6. EDX analyses of the different phases (wt%) of the sample treated 40 minutes in inert conditions without agitation.

Phase	Fe	Cu	Cr	Ni	C	O	S	Mn	Phase Description
Phase 1	2.3	85.5	0.2	0.2	10	0.8	0.1	0	White of the interface
Phase 2	18.4	52.8	3.4	0.4	20.8	3.7	0.5	0	Dark of the ineterface
Phase 3	8.7	79.3	3.8	0.4	8.2	0.8	1.2	0	Light grey of the interface
Phase 4	66.9	1.7	17.1	9.9	2.8	0	0.7	1.1	Dark grey of the steel side
Overall	21	57.6	7.7	2.3	7.2	3.2	0.8	0.3	

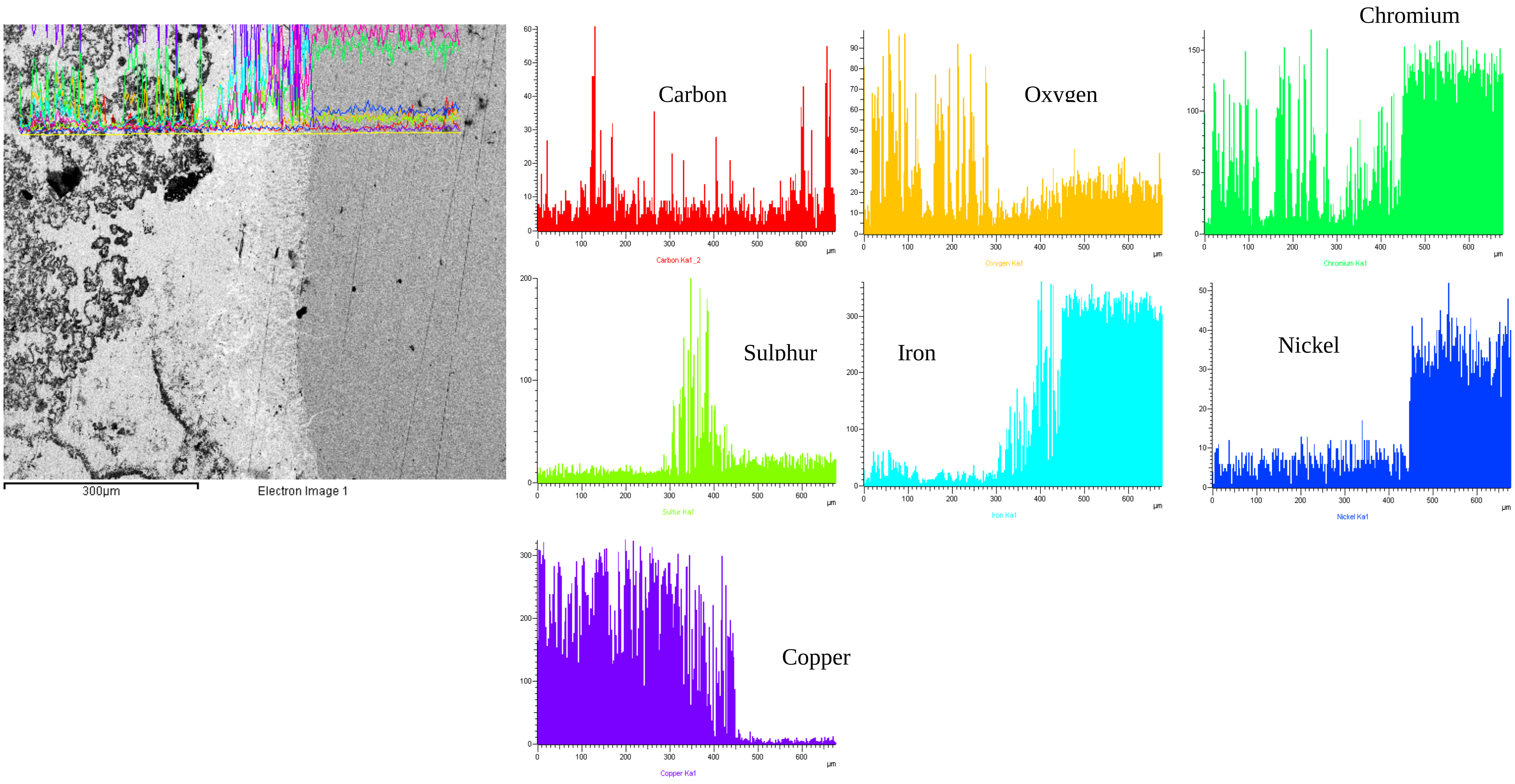

Figure 4.10. SEM-BSE image and spectra showing element distribution across the interface of the sample treated for 40 minutes in inert conditions without agitation.

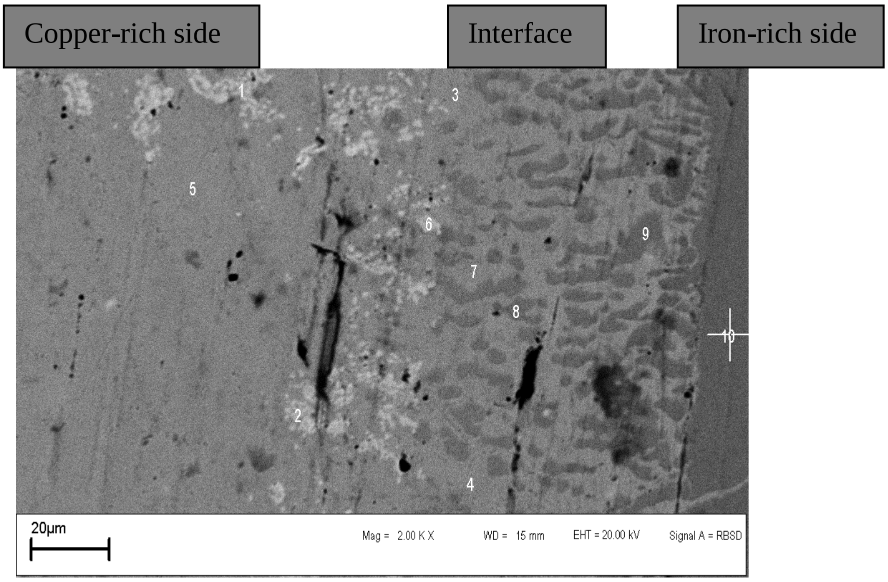

Figure 4.11. SEM-BSE image showing copper-rich and iron-rich sides for the sample treated 40 minutes in inert conditions without agitation.

In each place marked on the micrograph (Figure 4.11), spot analysis was done and is given in Table 4.7. The EDX spectra are shown in Appendix B, Figures B.1-B.21.
The analyses of the different spots helped to determine the composition of the different phases appearing on the micrograph.

Spot analyses were done across a line as shown in Figure 4.12. Iron, copper, chromium, Nickel as well as carbon, oxygen, sulphur and manganese compositions in each spot of the line were determined as shown in Table 4.8. This table shows the composition variation across the interface.

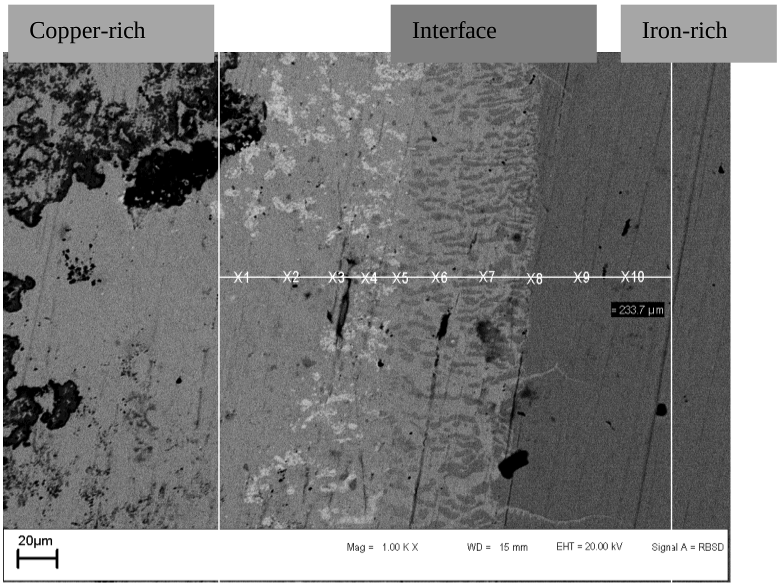

Figure 4.12. SEM-BSE image with line scan showing copper-rich and iron-rich sides of the sample treated 40 minutes in inert conditions without agitation.

Table 4.7. EDX spot analyses (wt%) of the sample treated for 40 minutes in inert conditions without agitation.

Spot	Fe	Cu	Cr	Ni	C	O	S	Mn
1	2	85.9	0.2	0	11.1	0.8	0	0
2	2.6	87.2	0.2	0.4	8.9	0.7	0.1	0
3	72.3	4.3	12.5	1.1	4.7	0.7	4.4	0
4	4.1	84.2	0.3	0.3	10.4	0.7	0	0
5	2.3	86.5	0.2	0.4	9.6	0.9	0	0
6	42.7	30.1	7.7	0.8	14.9	0.9	3	0
7	63.3	15.9	11	0.8	4.7	0.7	3.7	0
8	19.7	67.2	3.4	0.5	7.4	0.7	1.1	0
9	18.4	52.8	3.4	0.4	20.8	3.7	0.5	0
10	66.9	1.7	17.1	9.9	2.8	0	0.7	1.1

Table 4.8. Compositions of different points (wt%) on the line scan of sample treated 40 minutes in inert conditions without agitation.

Position	Fe	Cu	Cr	Ni	C	0	S	Mn
1	1.4	78.2	0.16	0	19.2	0.9	0	0
2	2.4	73.8	0.3	0.4	21.2	1.8	0.1	0
3	1.7	70.2	0.2	0.3	26.5	1.1	0	0
4	3	63.6	0.3	0.2	31.4	1.2	0.2	0
5	4	82.4	0.4	0.3	12.4	0.5	0	0
6	4	85.4	0.42	0.3	9.4	0.4	0	0
7	32.8	48.6	5.2	1	9.6	1.6	1.3	0
8	64.5	1.1	16.2	9.6	6.2	0.8	0.6	1
9	60.2	0	15.3	9	13.1	1	0.6	0.9
10	66.7	0	17	9.5	4.6	0.4	0.7	1.1
Overall	21	57.6	7.7	2.3	7.1	3.2	0.8	0.3

Apart from blister copper and 316L stainless steel, there were three different phases in the interface for the sample treated for 40 minutes in inert conditions without agitation. The stainless steel component's composition through the interface was decreasing from the iron-rich side to the copper-rich side. Copper decreased from the copper-rich side to the iron-rich side.

4.2.2.2. Samples treated for 80 minutes in inert conditions without agitation

Sample 4 was treated in inert conditions without agitation as well, but was melted for 80 minutes. Figure 4.13 shows the X-ray maps with the three main zones: iron-rich, copper-rich and the interface between. Figure 4.14 a shows all elements together, while Figure 4.14b-g shows the individual elements.

Most of iron was at the iron-rich side, with some at the interface and the copper-rich side. Copper was found on the copper-rich side and was regularly distributed in the interface. Chromium was abundant at the iron-rich side and irregularly distributed in small amounts in the copper-rich zone. Its amount in the interface was too small to see clearly. Nickel and sulphur were evenly distributed at both sides, but the amounts were higher at the steel side than at the copper-rich side. Carbon, oxygen and silicon were more concentrated at the copper-rich side, with small amounts regularly distributed at the steel side.

For the same sample, line scans and individual spectra were taken as shown in Figure 4.14. From iron-rich side to the copper-rich side the scanned distance was approximatively 2.7 mm, and the interface was approximatively 0.26 mm wide.

In addition to the line scans, individual spectra were taken as shown Figure 4.14. The copper-rich side was seriously affected by blisters, due to gas imprisonment as shown in the secondary electron image, Figure 4.15.

Spot analyses were also done as shown in Figure 4.16 and Table 4.10. The interface between the copper-rich and iron-rich sides had iron-rich and copper-rich phases, with a small amount of small very light phases. Copper had infiltrated between the stainless steel grains. Four phases were identified in this micrograph but white phase was too small to be analysed accurately. The compositions of the phases are shown in Table 4.9.

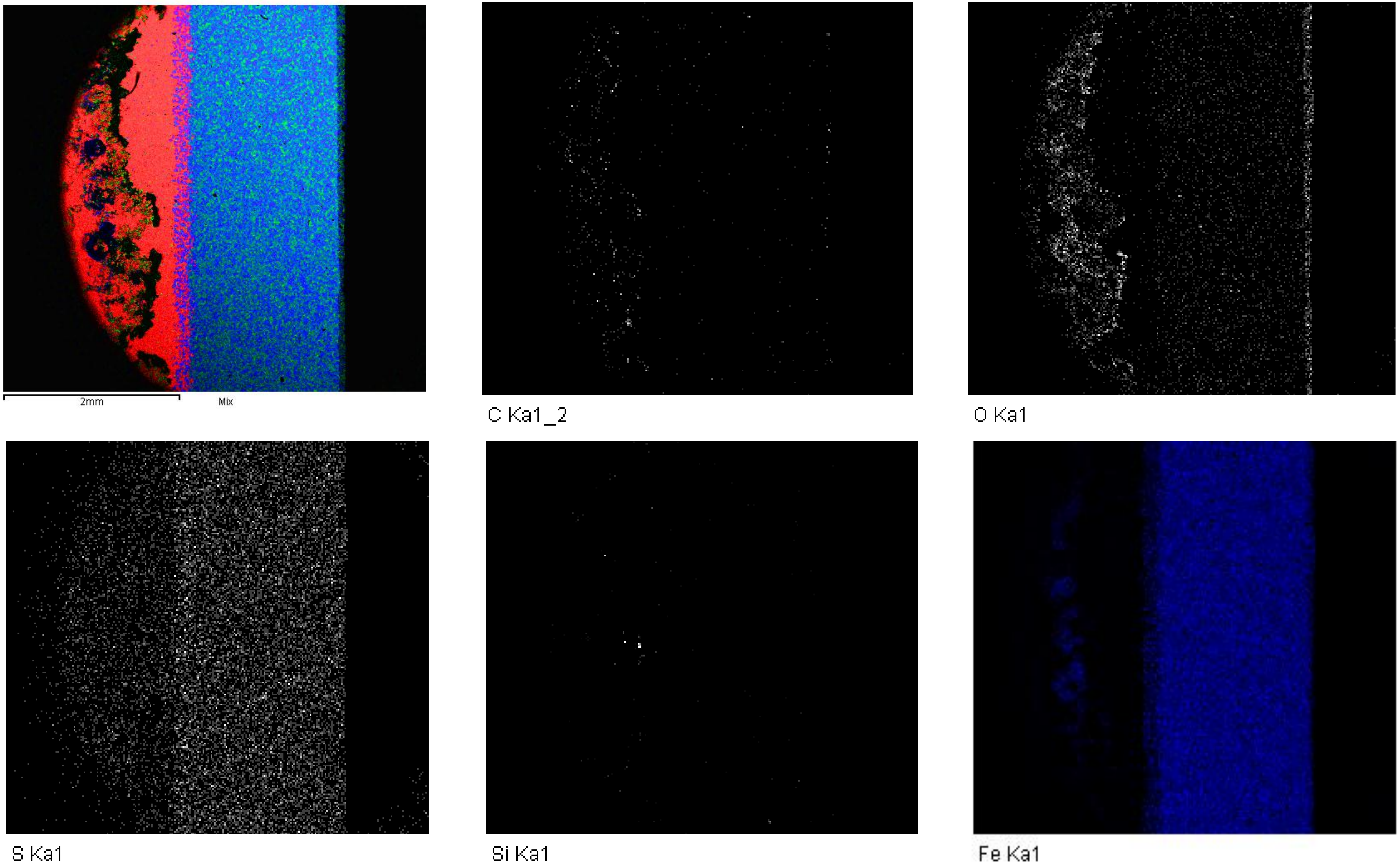

Figure 4.13. X-ray map showing element distribution through the interface of the sample treated for 80 minutes in inert conditions without agitation. C: white, O: white, S: white, Si: white, Fe: blue, Cu: red, Cr: green, Ni: white.

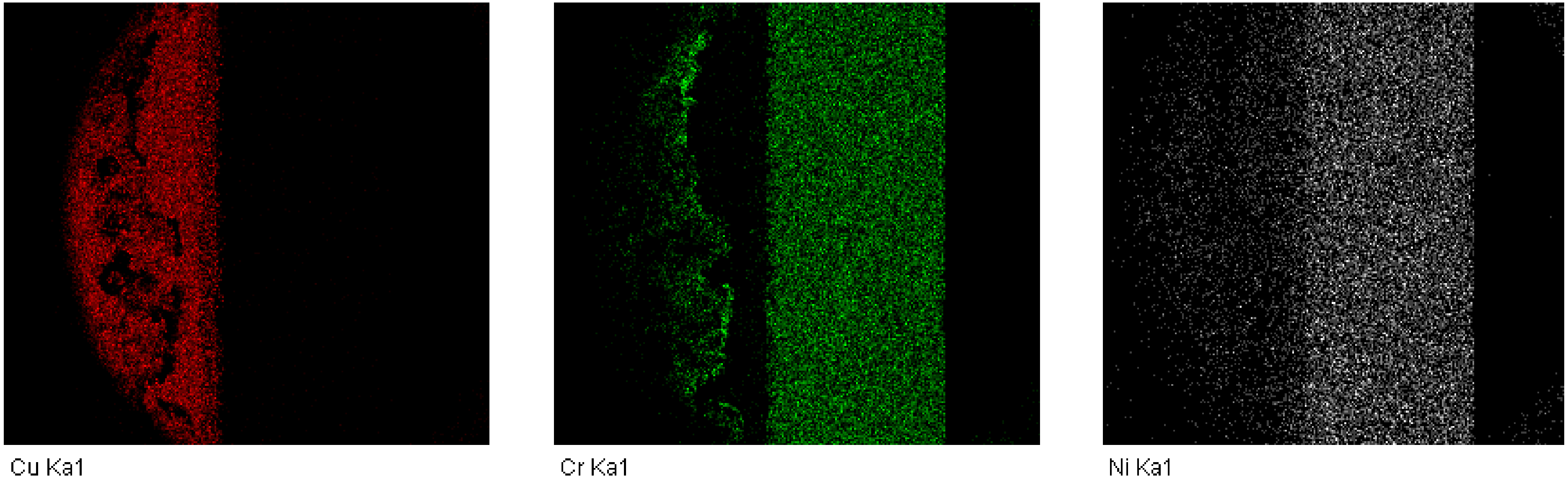

Figure 4.13. X-ray map showing element distribution through the interface of the sample treated for 80 minutes in inert conditions without agitation. (continued) C: white, O: white, S: white, Si: white, Fe: blue, Cu: red, Cr: green, Ni: white.

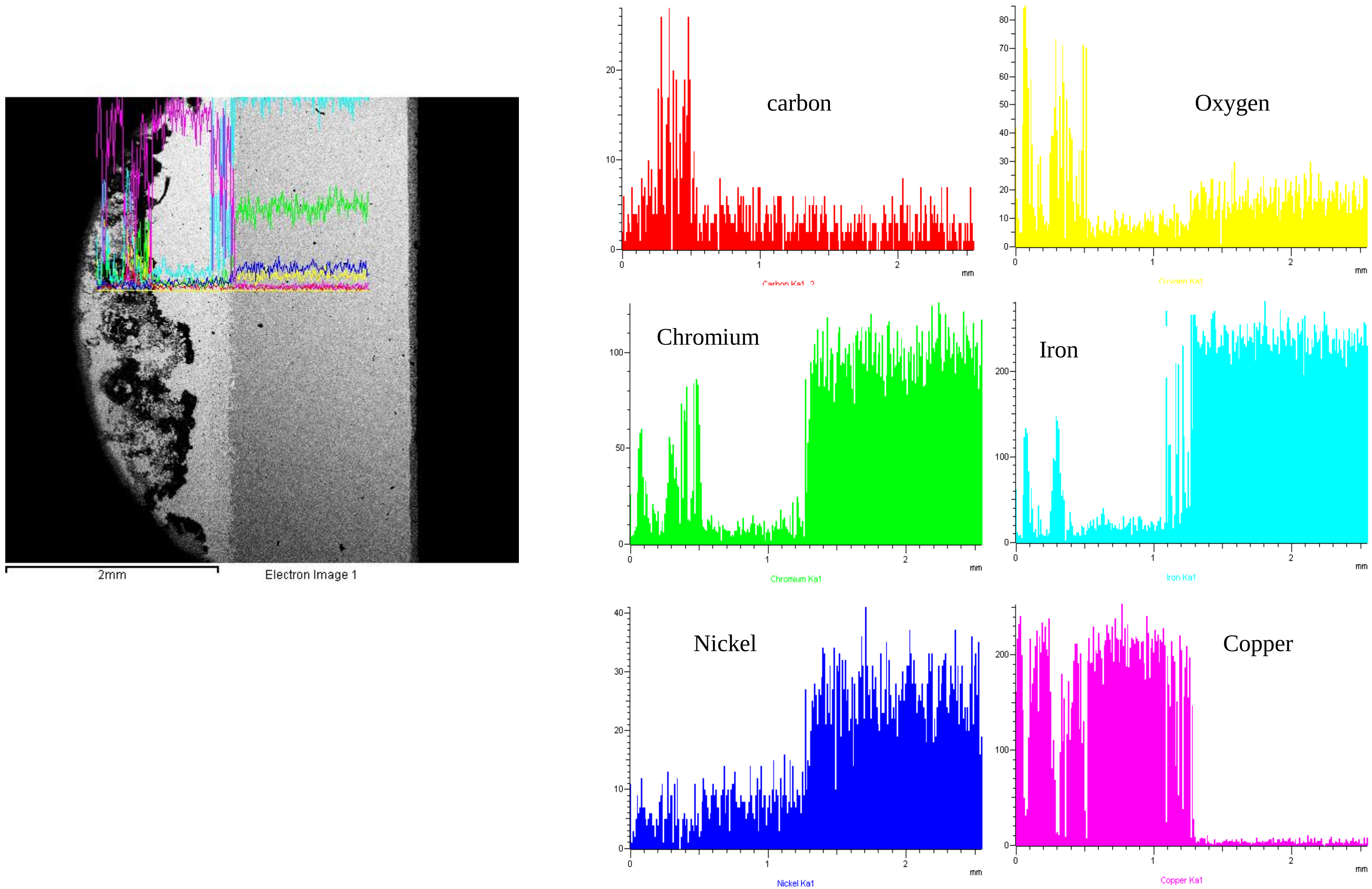

Figure 4.14. SEM-BSE image and spectra of the interface of the sample treated for 80 minutes in inert conditions without agitation.

Table 4.9. Phase compositions (wt%) of the sample treated for 80 minutes in inert conditions without agitation.

Phase	Fe	Cu	Cr	Ni	C	O	S	Mn	Phase description
1	Too small to be analysed								White in the interface
2	5.6	89.3	0.1	1.6	3.3	0.2	0.1	0	Grey at the copper-rich side
3	8.5	85.5	0.3	1.9	1.8	0	0.2	0	Dark grey in the interface
4	68.4	0	17.6	10.5	1.4	0.4	0.7	1.2	Dark grey at the steel side

The different phases described in Table 4.9 correspond to the micrograph Figure 4.16.

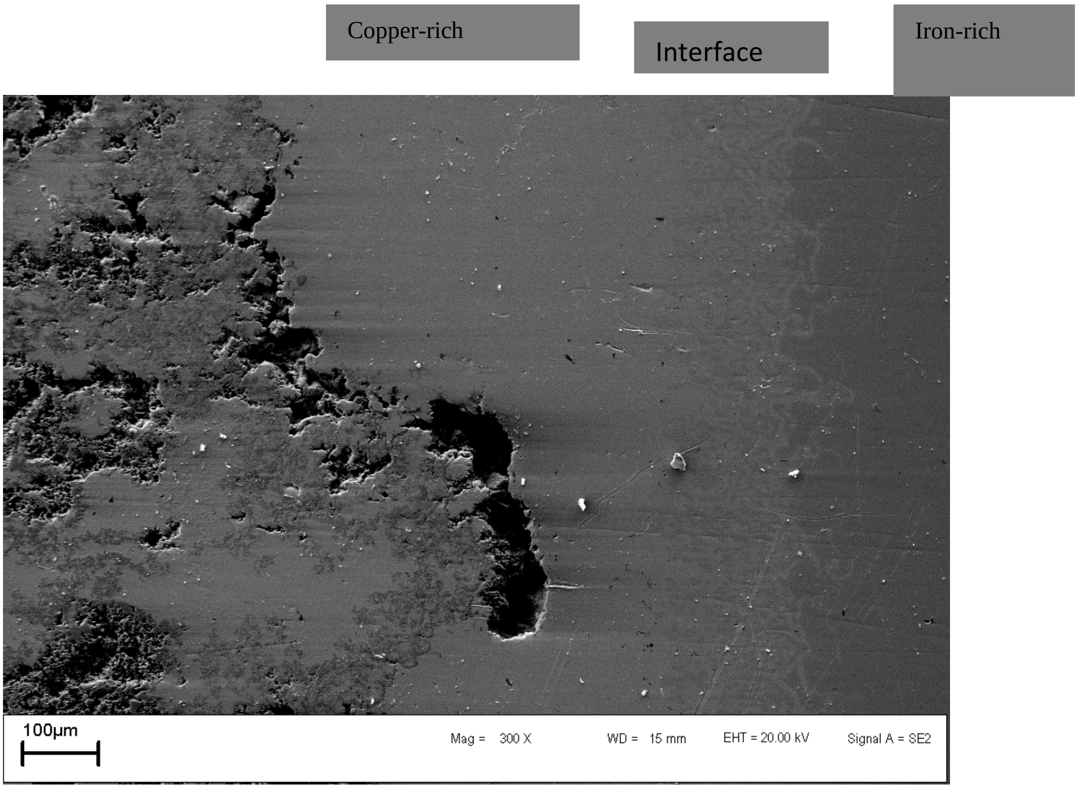

Figure 4.15. SEM-BSE image in secondary mode showing copper-rich and iron-rich sides for the sample treated 80 minutes in inert conditions without agitation.

The secondary electron image in Figure 4.15 shows a clear interface between the copper-rich and iron-rich sides. The copper-rich solution penetrated the steel grain boundaries up to ~70 µm.

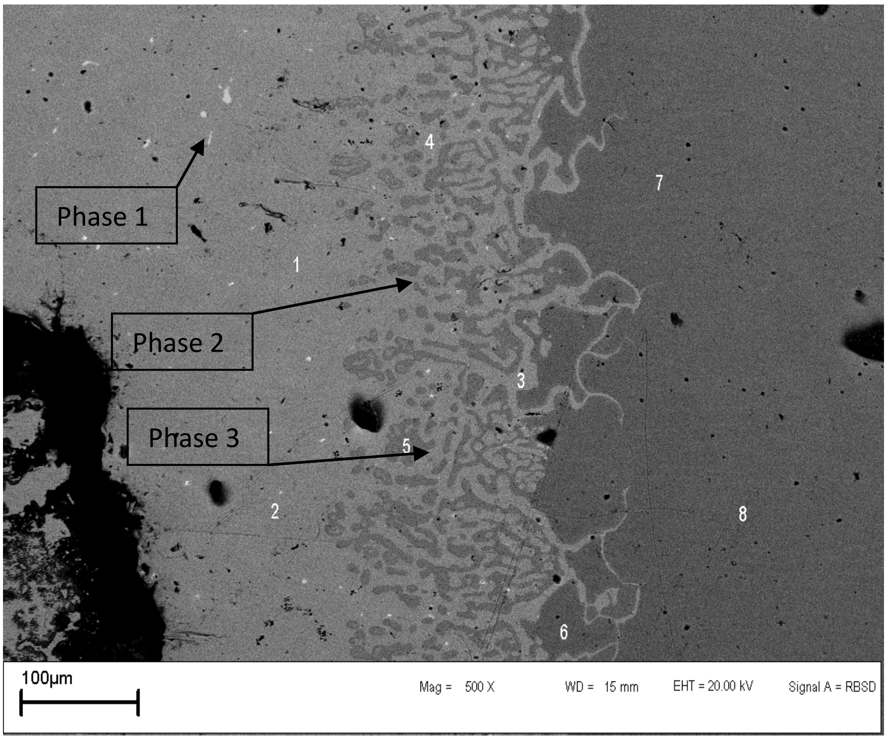

Figure 4.16. SEM-BSE image showing positions of spot analyses done on the sample treated for 80 minutes in inert conditions without agitation.

The composition of each spot of Figure 4.16 was determined and shown in Table 4.10.

Table 4.10. EDX analyses (wt%) of the sample treated 80 minutes in inert conditions without agitation.

Spot No.	Fe	Cu	Cr	Ni	C	O	S	Mn
1	3.0	92.4	0.0	1.0	3.6	0.0	0.0	0.0
2	5.2	90.0	0.0	1.8	2.6	0.5	0.0	0.0
3	68.2	1.5	15.8	10.1	2.0	0.5	0.9	1.0
4	8.5	85.5	0.3	1.9	3.6	0.0	0.2	0.0
5	74.8	11.6	3.3	5.7	1.8	0.0	2.9	0.0
6	73.3	8.2	7.1	7.6	1.9	0.6	1.2	0.2
7	68.8	0.0	17.7	10.4	1.3	0.0	0.6	1.2
8	68.0	0.0	17.5	10.5	1.5	0.8	0.7	1.2

Spots were analysed across a line of the second sample in the first set of experiments as well. The concentration gradient was established from the copper-rich to the iron-rich side as shown in the micrograph, Figure 4.17 and Table 4.11.

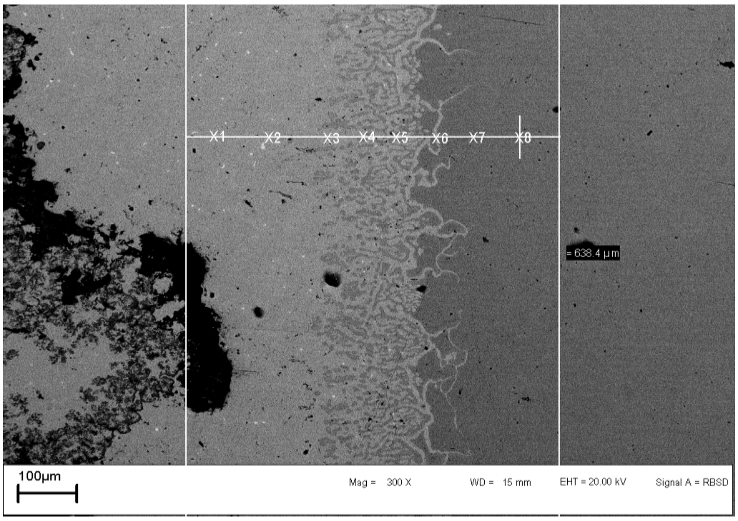

Figure 4.17. SEM-BSE image showing different spot positions in the line scan for the sample treated 80 minutes in inert conditions without agitation.

Table 4.11. Compositions of different spots (wt%) across a line for the sample treated for 40 minutes in inert conditions without agitation.

Position	Fe	Cu	Cr	Ni	C	O	S	Mn
1	2.9	92.6	0.1	1	2.9	0.5	0	0
2	2.92	91.4	0.2	1	4.1	0.4	0	0
3	3.9	92.4	0.2	0.8	2.2	0.5	0	0
4	26.8	66.7	1.3	2.3	1.5	0.4	0.9	0
5	6.1	89	0.3	1.1	2.8	0.6	0.2	0
6	67.3	1	17.4	10.2	1.8	0.4	0.7	1.2
7	68.4	0	17.6	9.9	1.7	0.7	0.7	1.1
8	67.5	1	17.3	9.9	1.9	0.7	0.7	1.1

The complete EDX spectra are in Appendix B, Figures C.1-C.17.

4.2.2.3. Samples treated for 60 minutes in inert conditions with agitation

The X-ray maps of the sample treated 60 minutes are shown in Figure 4.18. Three zones are clearly identified on the X-ray maps: copper-rich side, interface and iron-rich side. Figure 4.18a shows all elements together, while Figure 4.18b-g shows the individual elements.

Copper was mainly distributed between the copper-rich side and the interface. Iron was mainly distributed at the iron-rich and the interface, with only small concentrations identified at the copper-rich side. Chromium showed higher concentrations at the iron-rich side, while nickel was in the iron-rich side.

Figure 4.19 shows a different area in the same sample but. In both Figures 4.18 and 4.19, the interface was clearly identified and oval patterns of higher chromium concentration appeared in the copper-rich side.

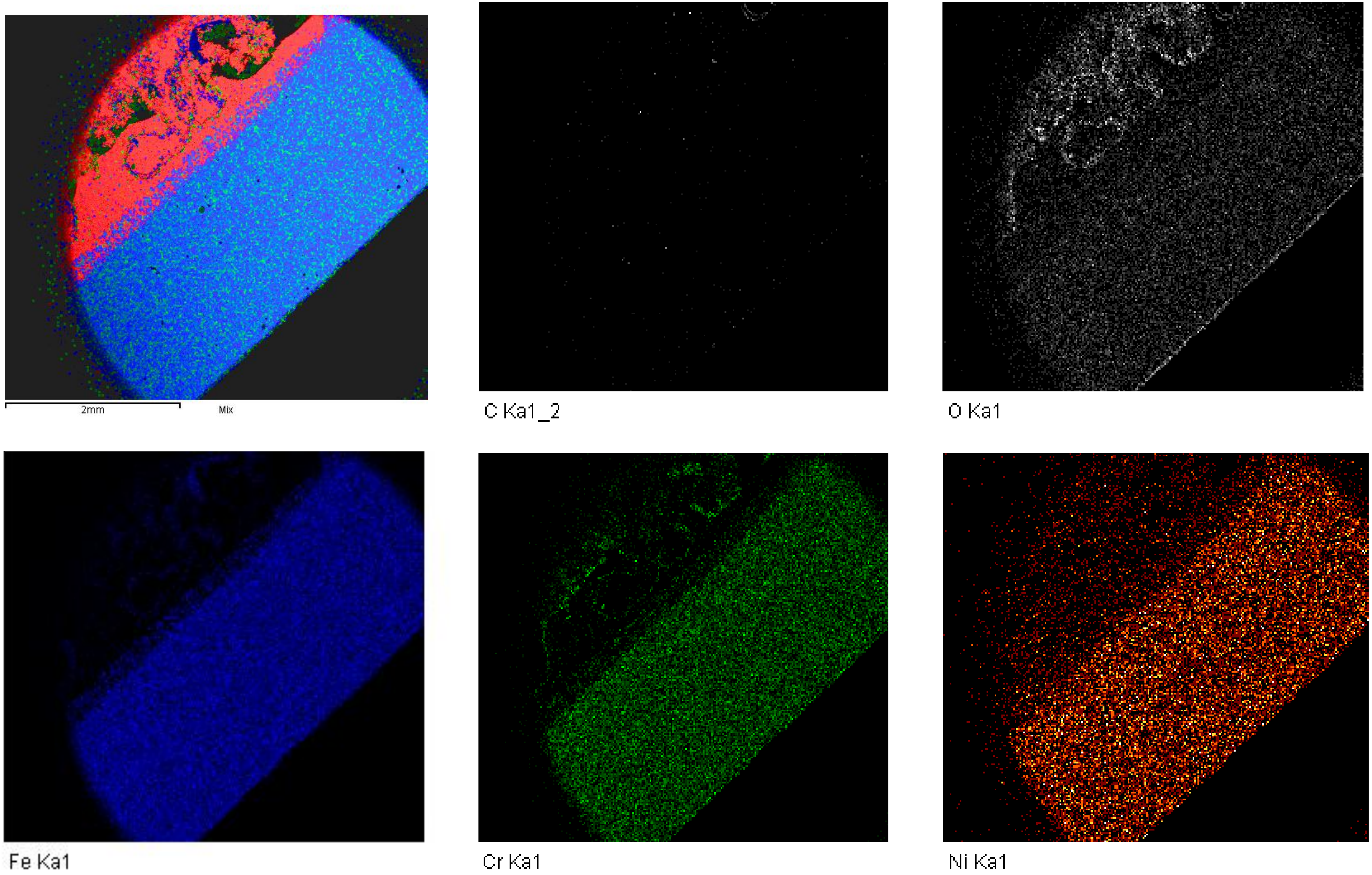

Figure 4.18. **X-ray map showing element distribution through the interface of the sample treated for 60 minutes in inert conditions with agitation. C: white, O: white, Fe: blue, Cr: green, Ni: yellow, Cu: red.**

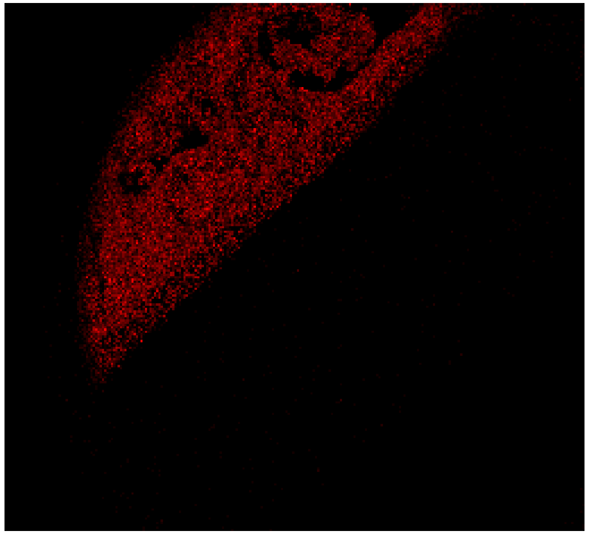

Figure 4.18. X-ray map showing element distribution through the interface of the sample treated for 60 minutes in inert conditions with agitation (continued). C: white, O: white, Fe: blue, Cr: green, Ni: yellow, Cu: red.

In order to characterize the different phases in the microstructure, an SEM-BSE image was taken as shown in Figure 4.19. Eleven positions are shown in Figure 4.19: Five positions at the copper-rich side, four positions in the interface and two positions at the iron-rich side. Four positions are shown in Figure 4.19a: one position at the copper-rich side, 2 positions in the interface and one position at the iron-rich side. Four positions were also analysed in Figure 4.19b: three in the interface and one at the copper-rich side. Both positions analysed in Figure 4.19c were located at the iron-rich side. The composition of each phase is presented in Table 4.12, in which phase No1 (white) was too small to be analysed. The EDX spectra are given in Appendix B, Figures D1-D19. In each spot of micrograph Figure 4.19, analyses was done as shown in Tables 4.13.

Table 4.12. EDX analyses (wt%) of the different phases of sample treated 60 minutes in inert conditions with agitation.

Phase No	Fe	Cu	Cr	Ni	C	O	S	Mn	Description
2	5.7	83.7	1.8	2.6	3.9	1.2	0.4	0.3	Light grey
3	65.6	2.7	16.5	9.2	1.7	0.9	0.6	1.1	Dark grey at steel
4	30.2	50.1	7.9	2.3	2.2	1.3	3.4	0	Dark grey in the interface

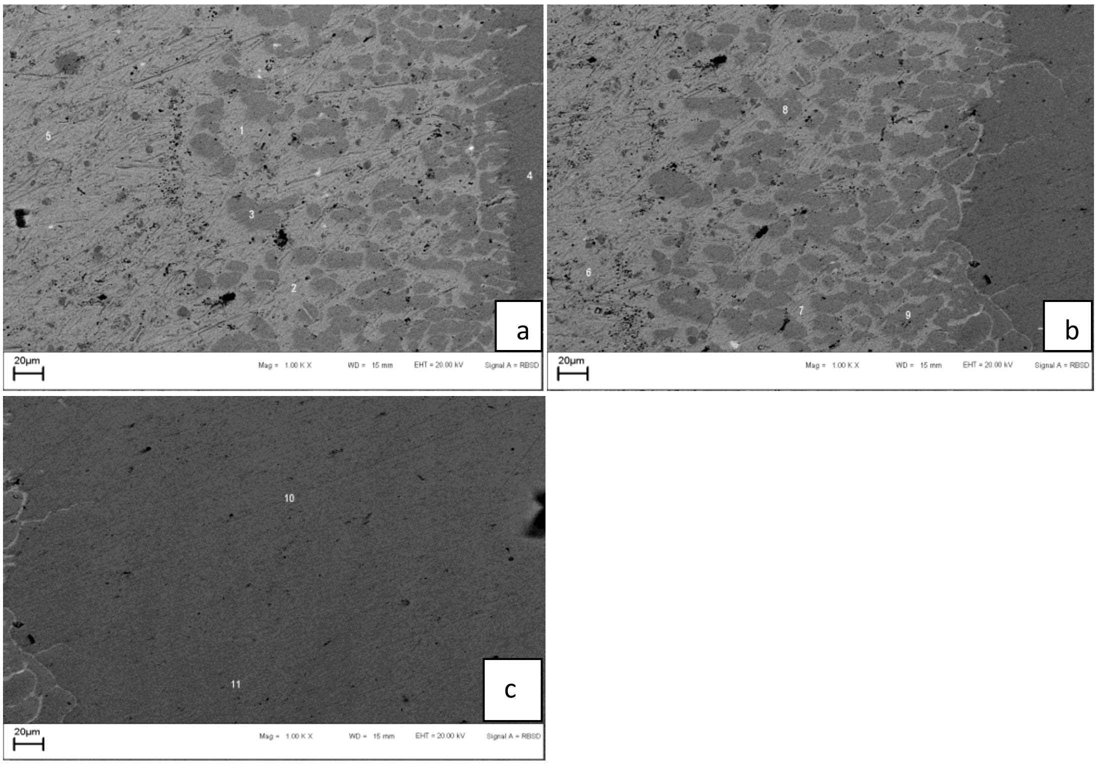

Figure 4.19. SEM-BSE images showing spot analysis positions for the sample treated 60 minutes in inert conditions with agitation.

Table 4.13. Compositions of different spots (wt%) across a line for the sample treated for 60 minutes in inert conditions with agitation.

Spot No.	Fe	Cu	Cr	Ni	C	O	S	Mn
1	4.3	88.8	0.5	1.6	3.4	1.4	0.0	0.0
2	24.3	63.9	4.0	1.8	3.2	1.6	1.3	0.0
3	72.7	4.5	11.9	4.6	2.0	0.8	3.5	0.0
4	60.6	4.8	16.0	8.9	2.1	5.9	0.6	1.0
5	3.0	92.6	0.4	0.8	2.7	0.5	0.0	0.0
6	3.2	91.6	0.3	1.5	2.8	0.6	0.0	0.0
7	49.0	25.1	12.1	3.1	3.6	0.8	5.0	1.1
8	59.0	20.2	10.5	2.9	2.3	1.7	3.3	0.0
10	66.5	1.5	16.8	10.4	2.0	1.1	0.6	1.1
11	66.9	1.4	17.1	10.3	1.7	0.9	0.6	1.1

In agitated conditions, the concentration trend was determined by analysing the composition of eight spots across a line as shown in Figure 4.20. The values are recorded in Table 4.14.

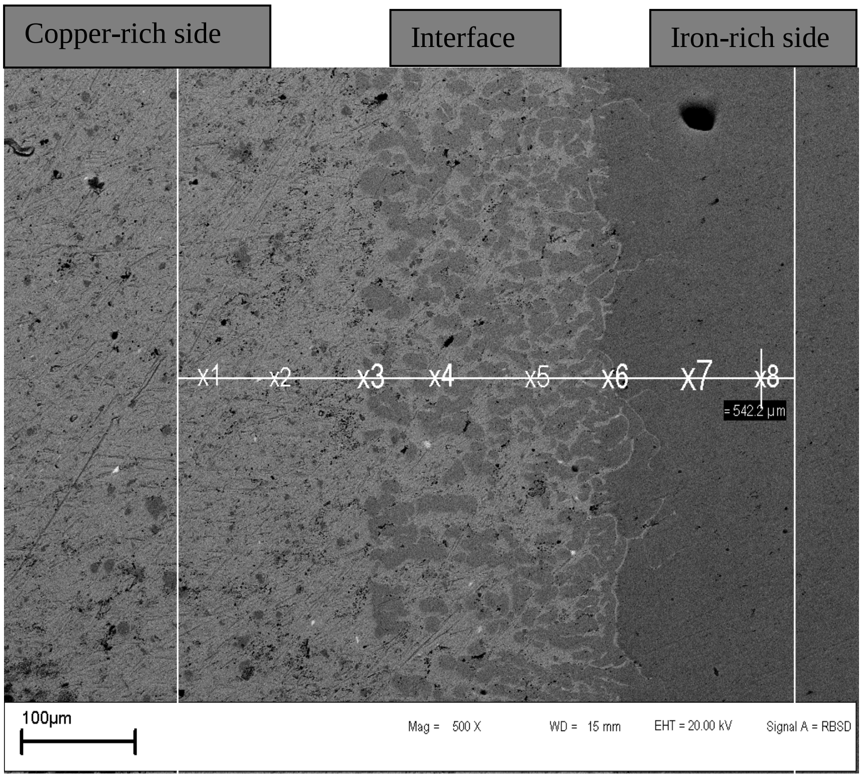

Figure 4.20. SEM-BSE micrograph showing the copper-rich and iron-rich sides for the sample treated 60 minutes in inert conditions with agitation.

Spots x1 and x2 are located at the copper-rich side. Spots x3, x4, x5, x6 are located in the interface while x7 and x8 are at the iron rich side. The interface was approximatively 190 microns wide. The concentration of the components of stainless steel decreased from the iron to the copper rich side. The point where curves changed the trend was inside the interface, ≈158 microns from the stainless steel.

EDX graphs for each spot across the line are in Appendix D, Figures D.1 to Figure D.19.

Table 4.14. EDX analyses (wt%) of different spots across a line of the sample treated for 60 minutes in inert conditions with agitation.

Spot	Fe	Cu	Cr	Ni	C	O	S	Mn
1	2.6	92.2	0.4	0.9	3.4	0.5	0.0	0.0
2	4.3	89.5	0.5	1.8	2.8	1.2	0.0	0.0
3	69	9.2	11.1	4.3	2.4	1.0	3.2	0.0
4	64.8	13.7	10.7	3.4	2.7	0.9	3.8	0.0
5	66.4	11.2	11.1	3.9	2.2	1.7	3.6	0.0
6	66.2	1.3	17.2	9.6	2.6	1.4	0.7	1.1
7	67.0	1.3	17.1	9.9	1.9	0.9	0.7	1.1
8	66.6	1.6	17.1	10	2.0	1.0	0.6	1.1

Line scans showing the element concentrations are presented in Figure 4.21. Iron was in the steel and irregularly distributed in the interface. Copper was in the copper-rich side, and almost non-existent at the iron-rich side. Chromium and nickel had similar distributions to iron but to a lesser extent. High concentration of sulphur was found in the interface than any side of the sample. Although regularly distributed both side, Sulphur was higher at the steel side than the copper-rich side. Carbon was almost constant throughout the line, while oxygen decreased continuously from the iron-rich to the copper-rich side.

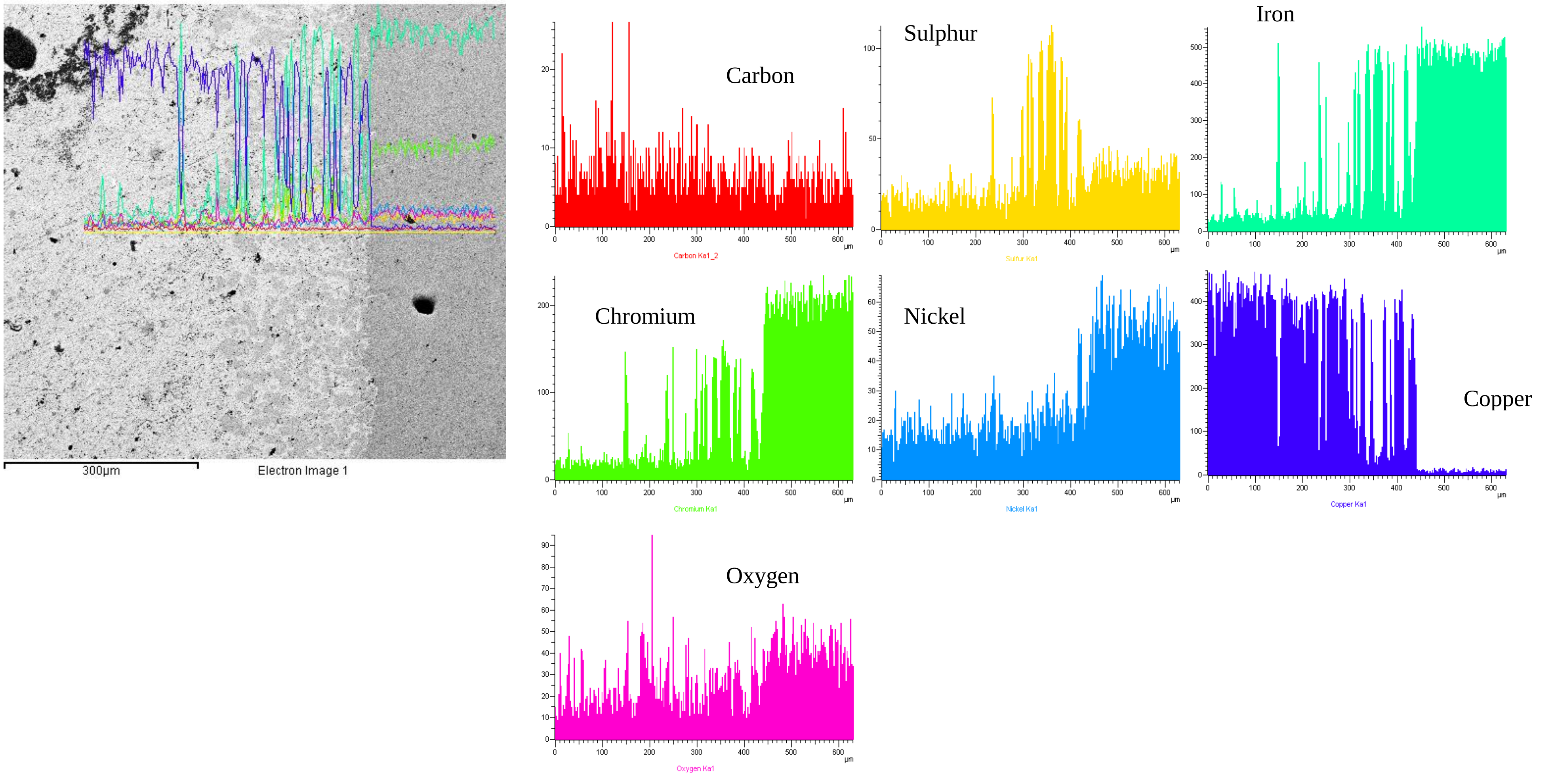

Figure 4.21. SEM image and spectra taken across the interface the sample treated for 60 minutes in inert conditions with agitation.

4.2.2.4. Sample treated for 100 minutes in inert conditions with agitation

The sample treated 100 minutes in inert conditions with agitation comprised three different zones: copper-rich, interface and iron-rich, as shown in Figure 4.22.

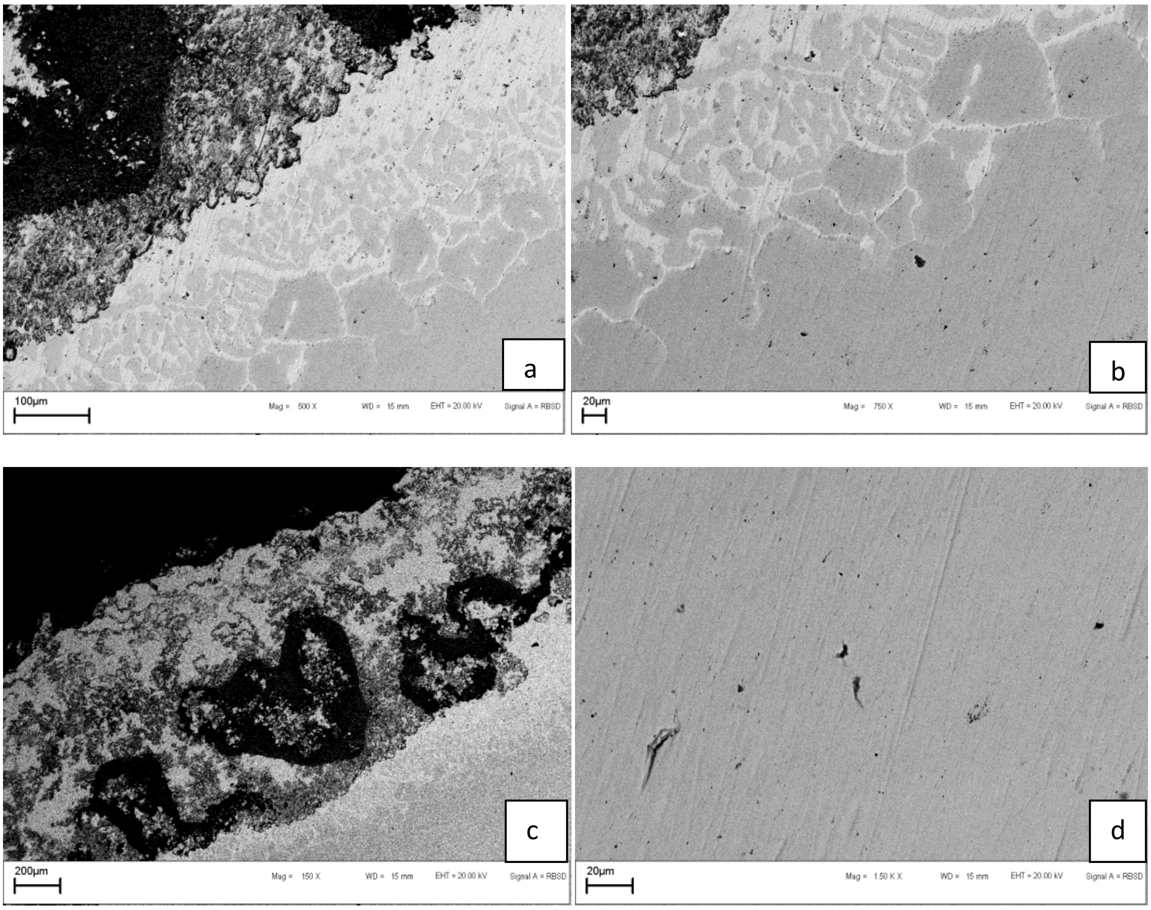

Figure 4.22. SEM-BSE images showing different portions of the sample treated for 100 minutes in inert conditions with agitation at different magnifications.

The overall area of Figure 4.23 was analysed and the EDX spectra are given in Appendix B. Figures E.1-E18.

In order to identify irregularly distributed phases at the copper-rich side and the iron-rich sides, secondary electron images were taken as shown in Figures 4.23b. The composition of outer portion of the sample (Figure 4.22b) is shown Table 4.15. Apart from the expected components of stainless steel, this table shows a quite high percentage of copper and carbon.

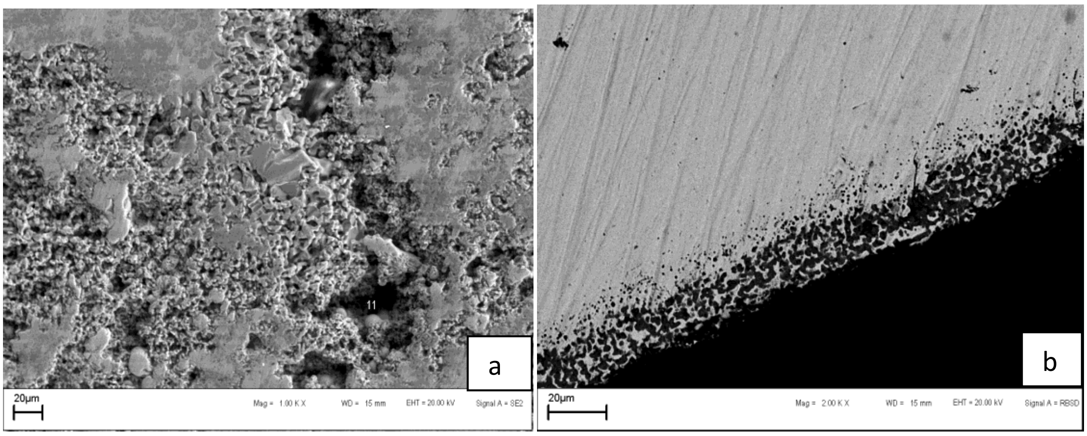

Figure 4.23. SEM-SE images showing: a) the copper-rich part, and b) the steel crucible of the sample treated for 100 minutes in inert conditions with agitation.

Table 4.15. EDX analyses showing average metal distribution through the outer portion of the sample treated 100 minutes in inert conditions with agitation, at the iron rich side.

Elements	Composition (wt%)
C	2.4
O	1.4
S	0.6
Cr	17.2
Mn	1.0
Fe	66.8
Ni	9.5
Cu	1.2

The X-ray maps are shown in Figures 4.24 and 4.25. The three regions of the sample were clearly identified. At the copper-rich side, a mixture of irregularly distributed phases and blisters left by the gas agitation were within the copper-rich matrix.

The majority of the iron was uniformly distributed in the steel, while a small amount was in the copper-rich matrix. Copper was uniformly distributed in the copper-rich side, and decreased through the interface. Chromium was not found at the interface, although it was uniformly distributed in different proportions in both the iron-rich and the copper-rich sides.

Nickel was distributed uniformly at the copper-rich side and the iron-rich side, but in different amounts at each side.

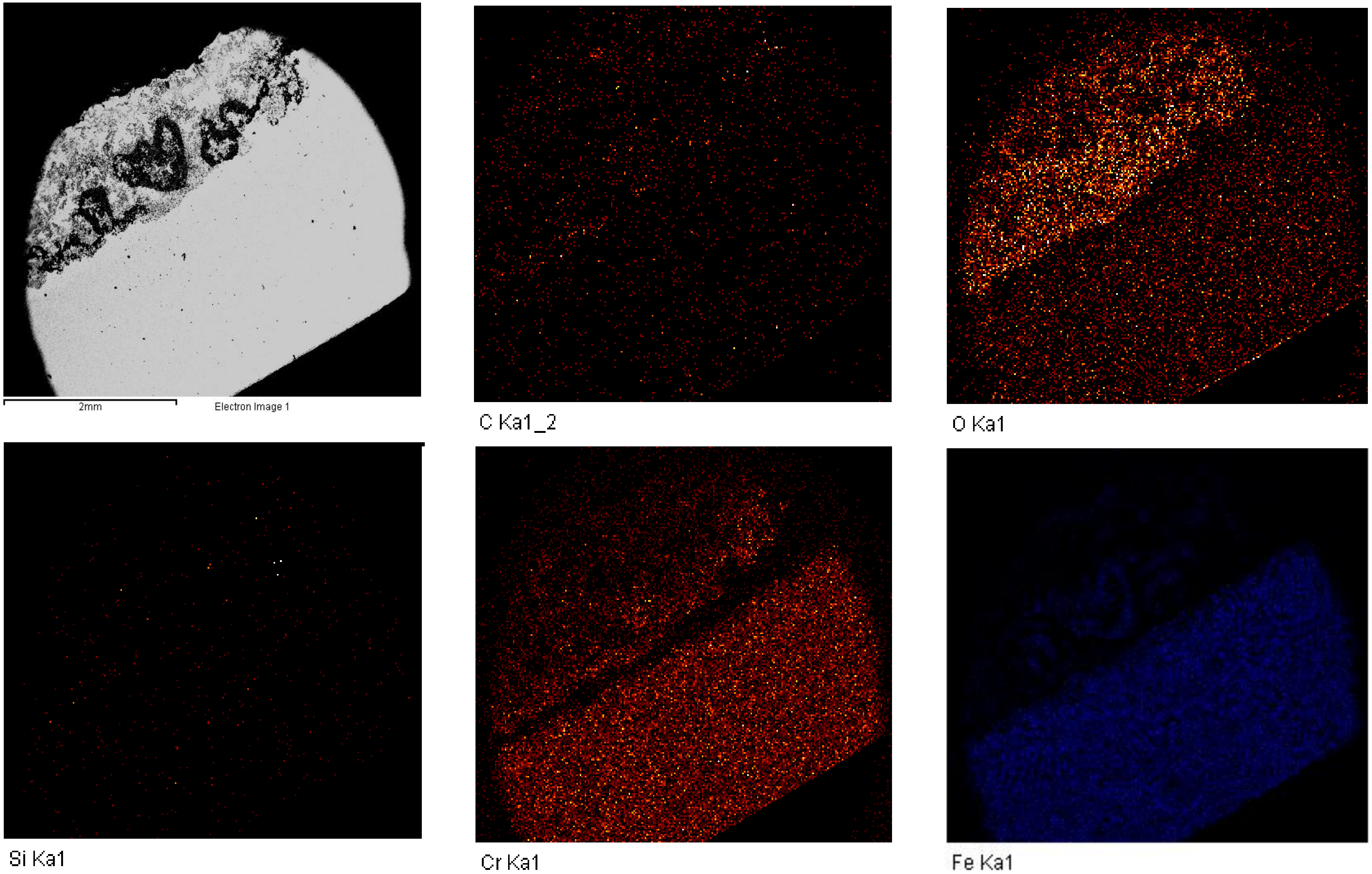

Figure 4.24. SEM image in BSE and X-ray maps showing element distributions through the interface of the sample treated for 100 minutes in inert conditions with agitation. C: red, O: red, Si: red, Cr: red, Fe: blue, Cu: red, Ni: green.

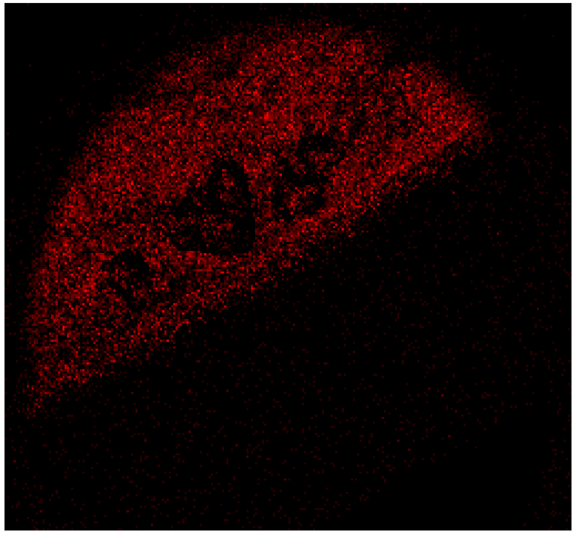

Cu Ka1

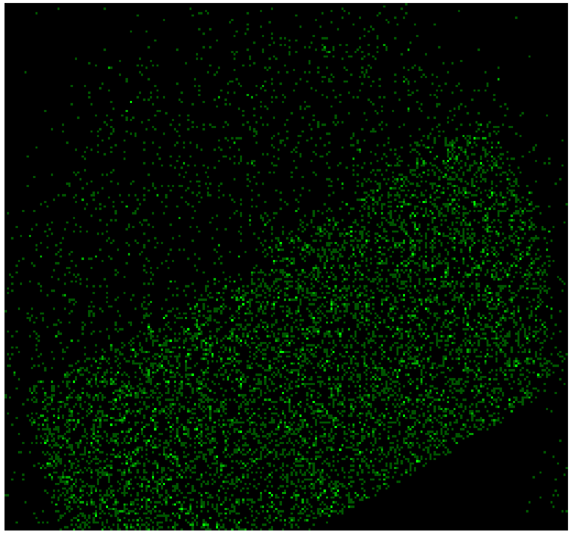

Ni Ka1

Figure 4.24. SEM image in BSE and X-ray maps showing element distributions through the interface of the sample treated for 100 minutes in inert conditions with agitation (continued). C: red, O: red, Si: red, Cr: red, Fe: blue, Cu: red, Ni: green.

.

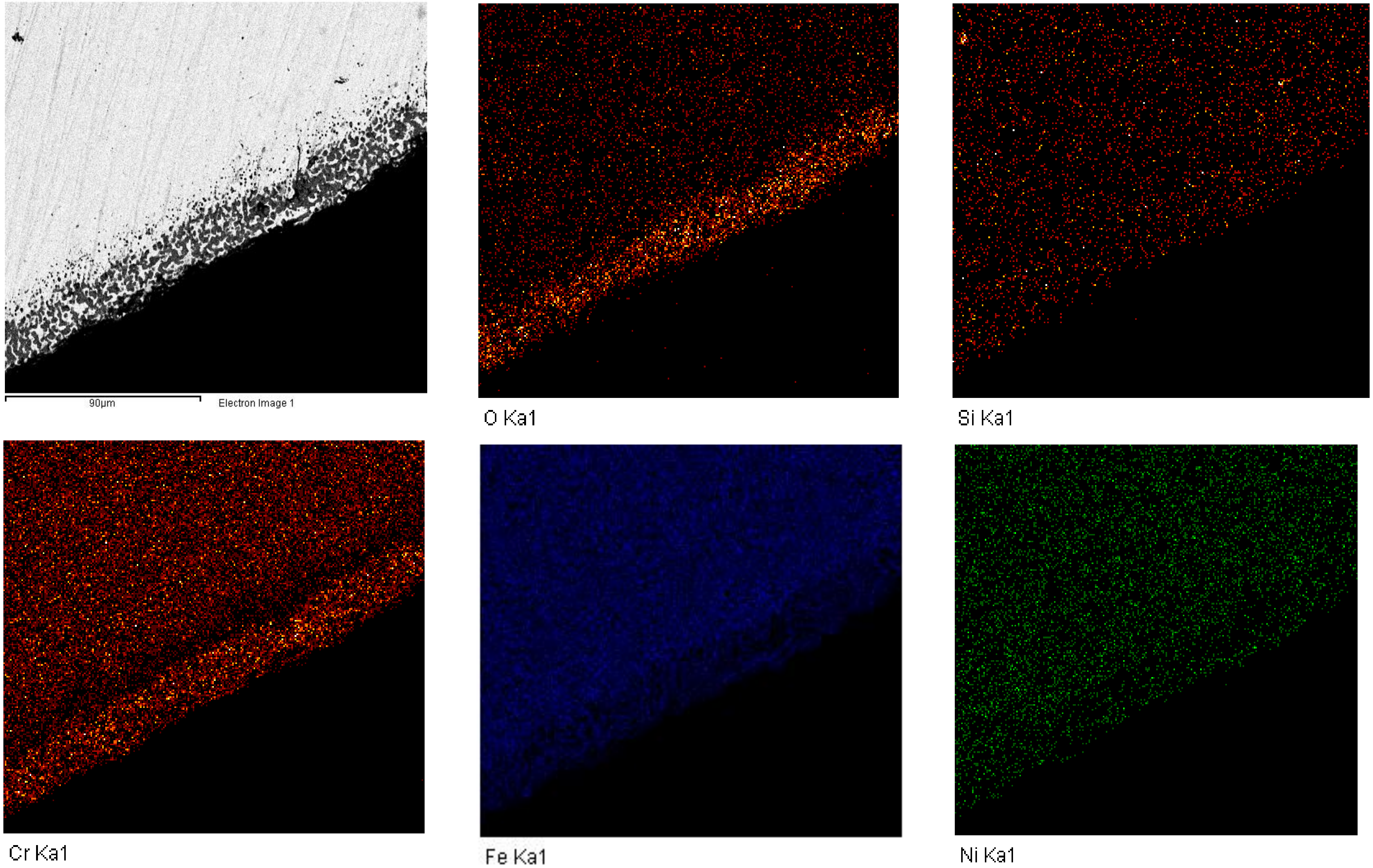

Figure 4.25. **SEM image in BSE and X-ray maps showing element distributions through the outside edge of the sample treated for 100 minutes in inert conditions with agitation O: red, Si: red, Cr: red, Fe: blue, Ni: green, N: red, Cu: red.**

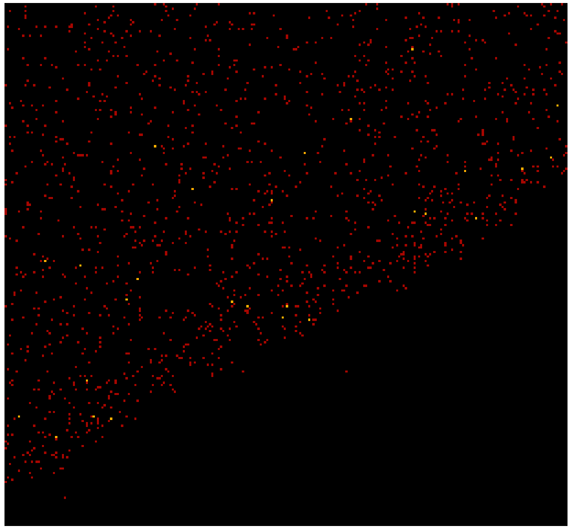

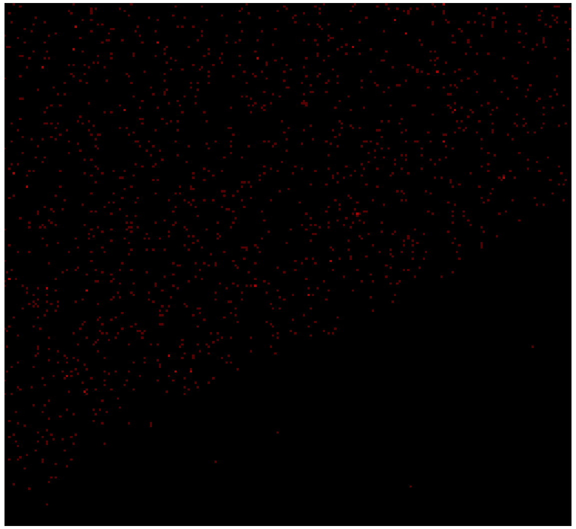

Figure 4.25. SEM image in BSE and X-ray maps showing element distributions through the outside edge of the sample treated for 100 minutes in inert conditions with agitation (continued) O: red, Si: red, Cr: red, Fe: blue, Ni: green, N: red, Cu: red.

Spot analyses were done on the different phases, as shown in Figure 4.26. The compositions in each spot are shown in Table 4.17. There were blisters left by gas blowing and slag phase within the copper-rich matrix.

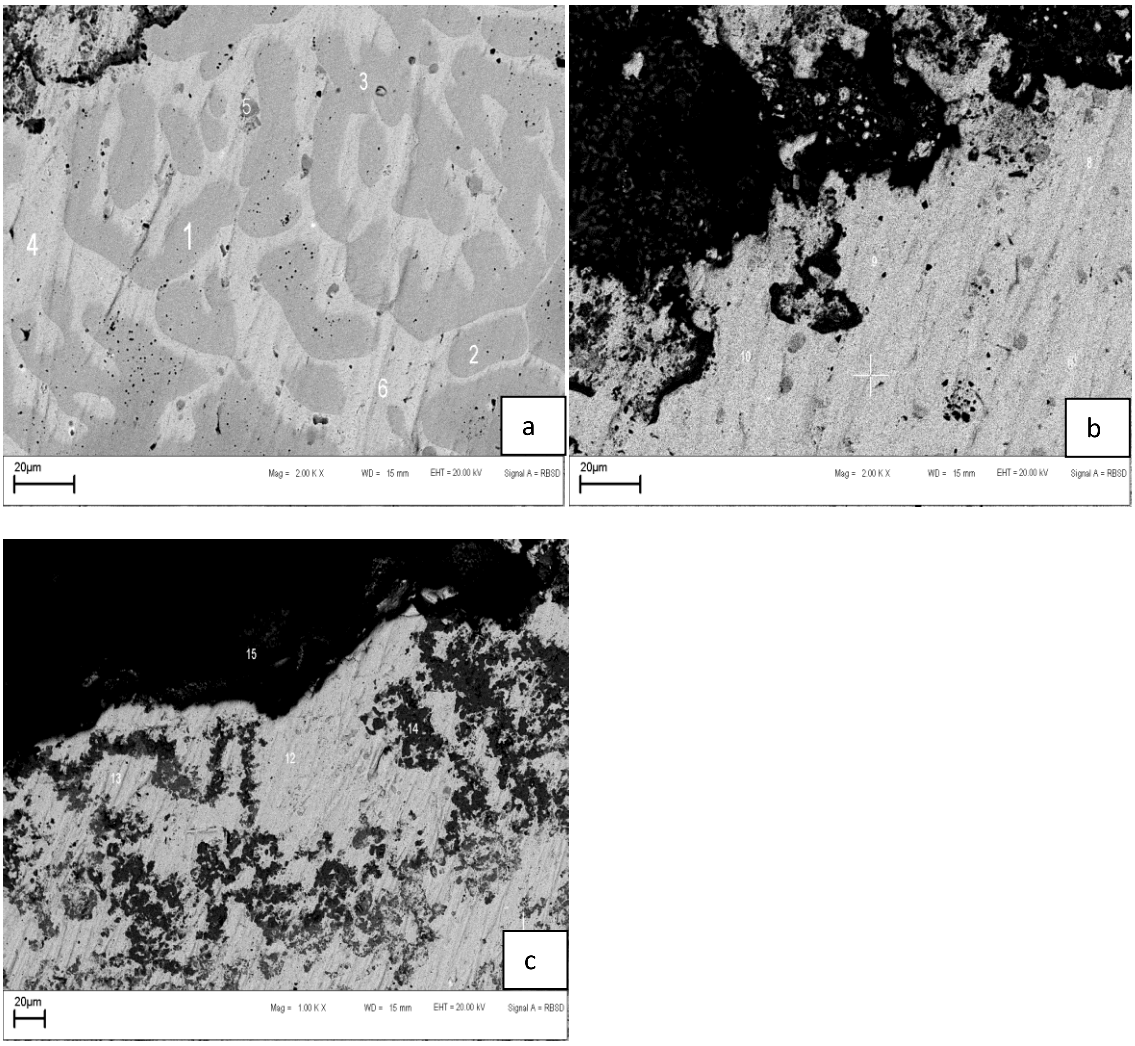

Figure 4.26. SEM-BSE micrographs showing where spot analyses were done for the sample treated 100 minutes in inert conditions with agitation.

Table 4.16. EDX Spot analyses (wt%) of the sample treated for 100 minutes in inert conditions with agitation.

Spot	Fe	Cu	Cr	Ni	C	O	S	Mn
1	67.8	12.3	4.1	10.8	2.7	0.7	1.6	0
2	65.9	14.3	2.7	11.6	2.6	0.8	0.2	0
3	66.7	13.7	2.7	11.7	2.2	0.8	2.2	0
4	3	87	0.3	1.4	6.6	1.7	0	0
5	65.8	14.9	2.7	11.6	2.5	0.6	2	0
6	4.4	84.8	2.4	1.5	3.9	0.5	2.2	0.2
8	5.2	86.1	0.2	2.5	4.1	1.9	0.1	0
10	64.5	16	2.7	11.3	2.8	0.8	1.9	0
11	2.9	89.8	0.7	1.5	4.5	0.6	0	0
12	19.2	59.5	5.3	1.7	4.5	9.2	0.2	0.3
14	80	7.2	9.8	0	1.6	0.9	0	0.5
15	19.3	59.1	5.3	1.6	4.8	9.4	0.2	0.4

Analyses were also performed on different spots across a line of the sample treated for 100 minutes in inert conditions with agitation as shown in Figure 4.27. The interface was ≈133 microns wide. The analyses results are summarised in Table 4.18 and plotted in Figure 5.10. EDX spectra are in Appendix E, Figure E.1 to Figure E.20.

Figure 4.27 shows the steel grains with diffusing iron-copper phases at the grain boundaries. The grains were larger after 100 minutes (43 μm) than after 60 minutes (38 μm) melting time.

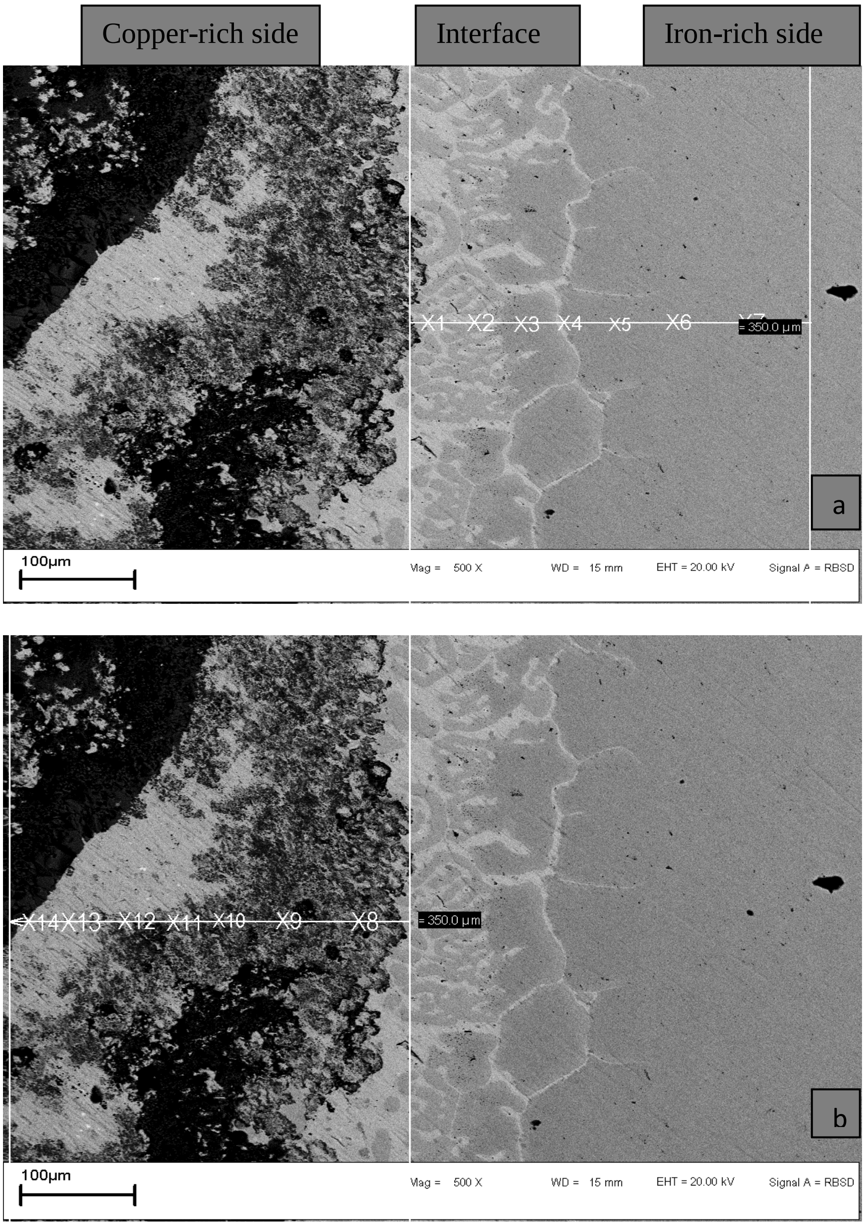

Figure 4.27. SEM-BSE image showing line scans from the copper-rich to the iron-rich sides for the sample treated 100 minutes in inert conditions with agitation.

Agitation had caused the reduction of the interface thickness. Metal concentrations at the copper-rich side of the sample treated 100 minutes in inert conditions with agitation were more irregular. Most of the blisters identified in the samples resulted from the reaction between sulphur and oxygen initially contained in the blister copper.

Table 4.17. EDX analyses (wt%) across a line spots of the sample treated for 100 in inert conditions with agitation.

Spot No.	Fe	Cu	Cr	Ni	C	O	S	Mn
1	13.1	78.0	1.5	2.6	2.9	1.2	0.8	0.0
2	67.3	6.5	11.8	10.2	2.1	0.7	0.9	0.5
3	66.0	1.7	16.6	10.0	2.0	2.4	0.6	1.0
4	66.6	1.3	17	10.0	2.0	1.4	0.7	1.1
5	62.6	3.9	16.5	9.0	2.0	4.2	0.7	1.2
6	67.0	0.0	17.3	10.0	3.4	3.3	0.2	0.0
7	13.0	76.4	2.0	1.8	3.4	3.3	0.2	0.0
8	66.9	14.5	2.6	11.5	2.1	0.4	2.0	0.0
9	6.8	66.1	11.9	0.8	3.1	10.9	0.2	0.2
10	22.0	35.2	15.4	1.0	6.3	18.8	0.1	1.2
11	6.8	63.8	12.0	0.3	3.0	13.9	0.0	0.2
12	13.1	52.2	10.9	0.4	3.3	19.6	0.0	0.6
13	11.5	47.5	14.3	0.3	4.7	20.6	0.9	0.3
14	7.5	72.7	3.7	0.2	3.4	12.3	0.0	0.2

4.2.2.5. Sample treated for 20 minutes in oxidizing conditions with agitation

The overall scanned area of the sample was analysed and the composition recorded in Table 4.19 and the EDX spectra are in Appendix B, Figures F.1 to F.13

Table 4.18. EDX analyses of metal distribution for sample treated 20 minutes in oxidizing conditions with agitation.

Elements	Concentration (wt%)
Fe	41.1
Cu	34.1
Cr	9.4
Ni	5.2
C	2.8
O	6.6
S	0.4
Mn	0.5

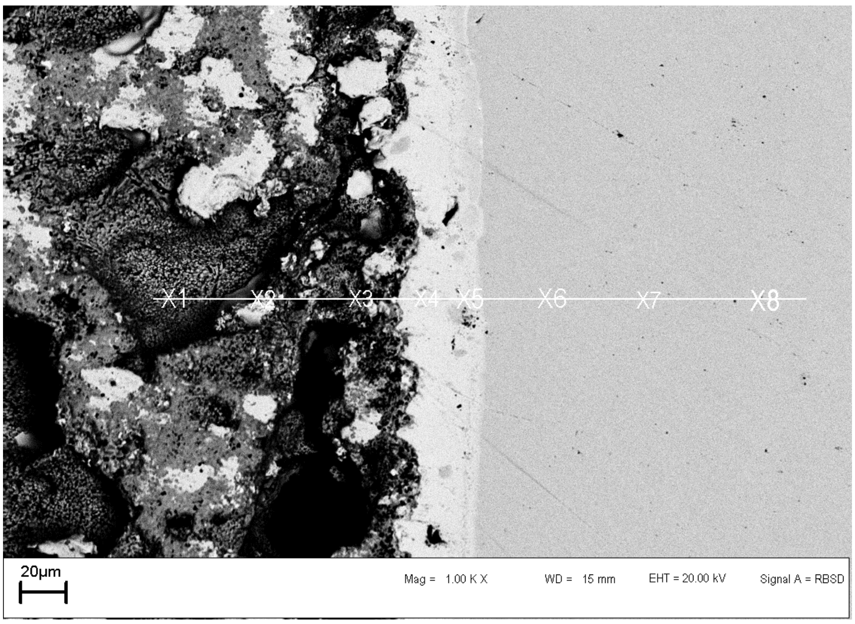

Figure 4.28. SEM-BSE image showing positions of spot analyses for sample treated 20 minutes in oxidizing conditions with agitation.

EDX spectra on different spots are in Appendix B. Figure 4.28 shows the different places across a line where spot analyses were obtained and values are shown in Table 4.19.

Table 4.19. EDX analyses (wt%) across a line on the sample treated for 20 minutes in oxidising conditions with agitation.

Spot No.	Fe	Cu	Cr	Ni	C	O	S	Mn
X1	53.7	44.6	5.8	1.8	4.1	7.8	0	0.8
X2	38.7	18.6	3.1	4.5	4.8	28.7	1.4	0.3
X3	20	31.5	3	6.4	4.4	34.2	0.5	0
X5	67.1	1.2	16.7	10.3	2.3	0.6	0.7	1.2
X6	67.3	1.3	17.4	9.6	1.7	0.9	0.6	1.2
X7	67.8	1	17.4	9.3	2.1	0.7	0.6	1.1
X8	31	44.6	7.2	5	3.2	8	0.5	0.5

The composition in the copper-rich zone was obtained from analyses in spots X1, X2 and X3 (Figure 4.28). Although quite different, both spots had fairly large oxygen peaks, showing oxides were present.

The composition in the interface was from analyses in spots X3 and X4. There was a mixture of the components from both sides of the interface, as both copper and iron were quite highly concentrated. The composition of the steel was from analyses in spots X6, X7 and X8.

Spot analyses were also done on the different phases in the sample to identify them, as shown in Figure 4.29. The secondary electron image (Figure 4.30) shows the blisters in the copper. Spot 9 EDX spectrum is shown in Figure 4.29 where higher iron concentration was observed, although the spot was located at the copper-rich zone. The spot was in the blisters caused by the flow of gas. Iron migrated to the interface (gas-liquid) due its affinity for oxygen and created a thin oxide film around blisters. Spot 4 had the EDX spectrum shown in Figure 4.32 and consisted mainly of oxides, while the matrix (white phase) composition is shown in the EDX spectrum of Figure 4.33.

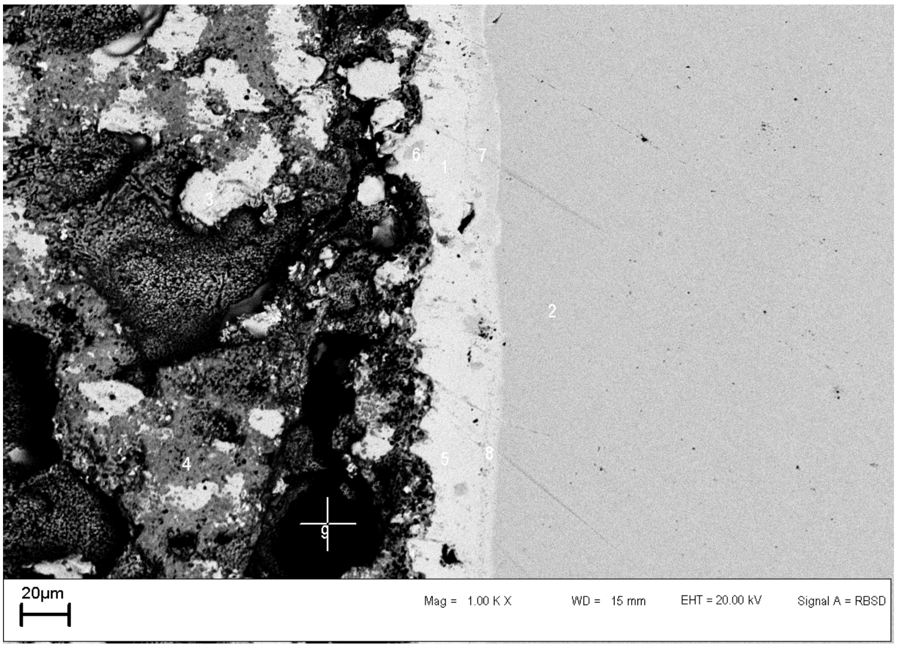

Figure 4.29. SEM-BSE image with spot analyses positions of the sample treated 20 minutes in oxidizing conditions with agitation.

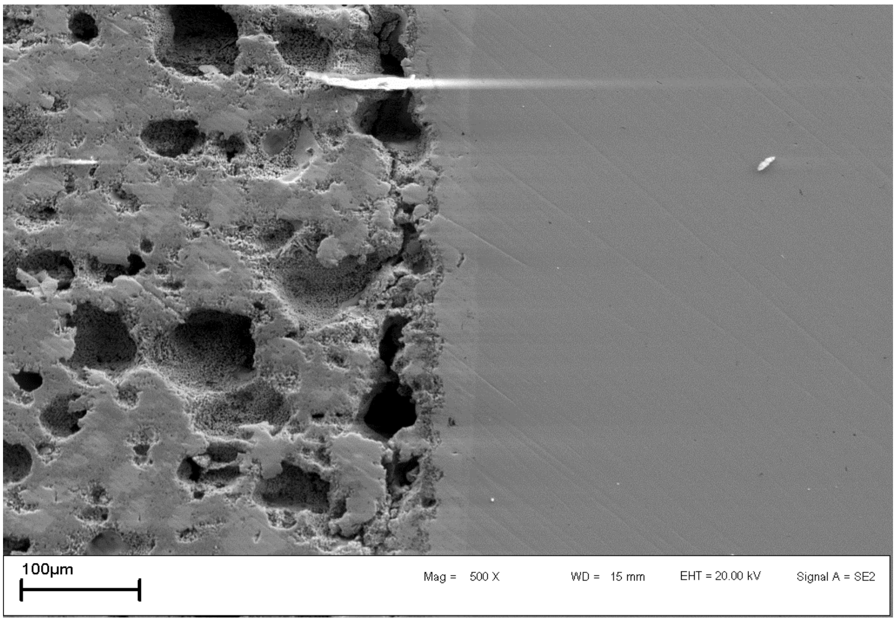

Figure 4.30. SEM-SE image of the sample treated 20 minutes in oxidizing conditions with agitation.

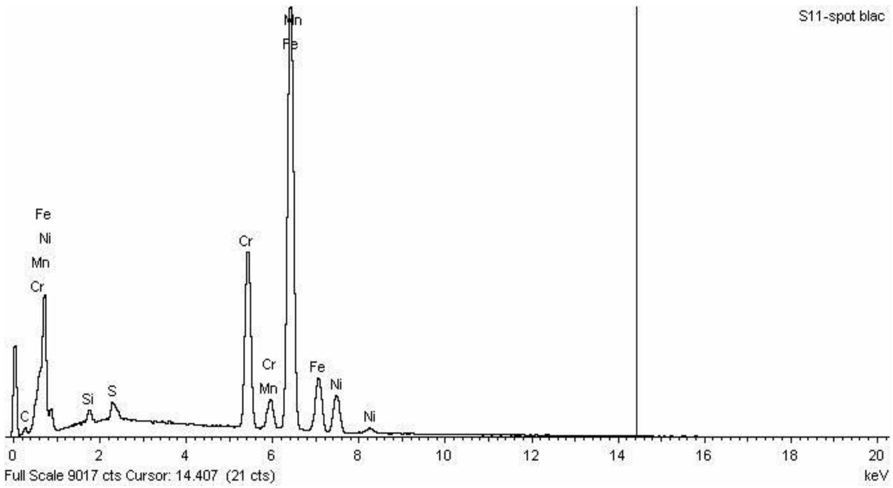

Figure 4.31. EDX spectrum of spot 9 (in black area) of the sample treated 20 minutes in oxidizing conditions with agitation.

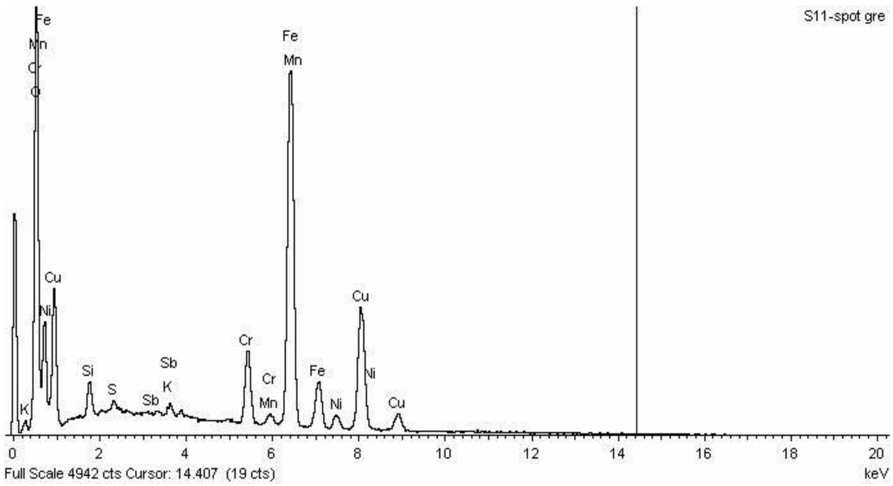

Figure 4.32. EDX spectrum grey region (spot 4) region of the sample treated 20 minutes in oxidizing conditions with agitation.

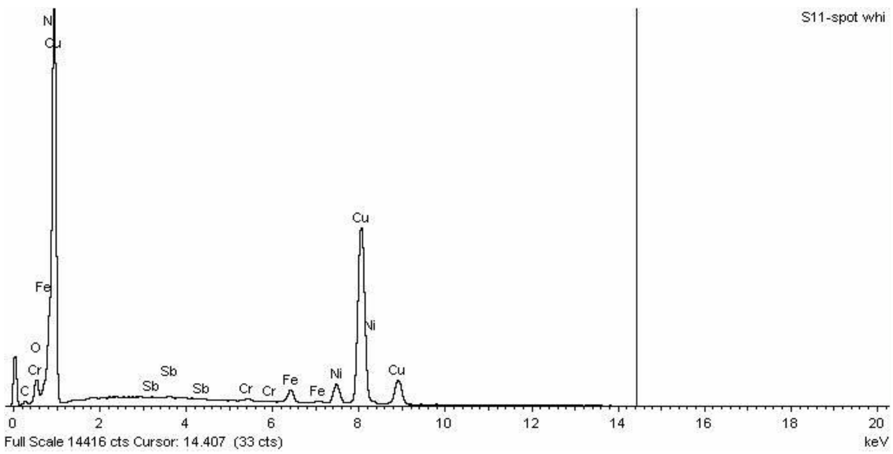

Figure 4.33. EDX spectrum of spot 1, on the white phase of sample treated 20 minutes in oxidizing conditions with agitation.

The distribution through the interface was identified by X-ray maps as shown in Figure 4.34. Figure 4.35 shows the morphology of a similar area with many blisters.

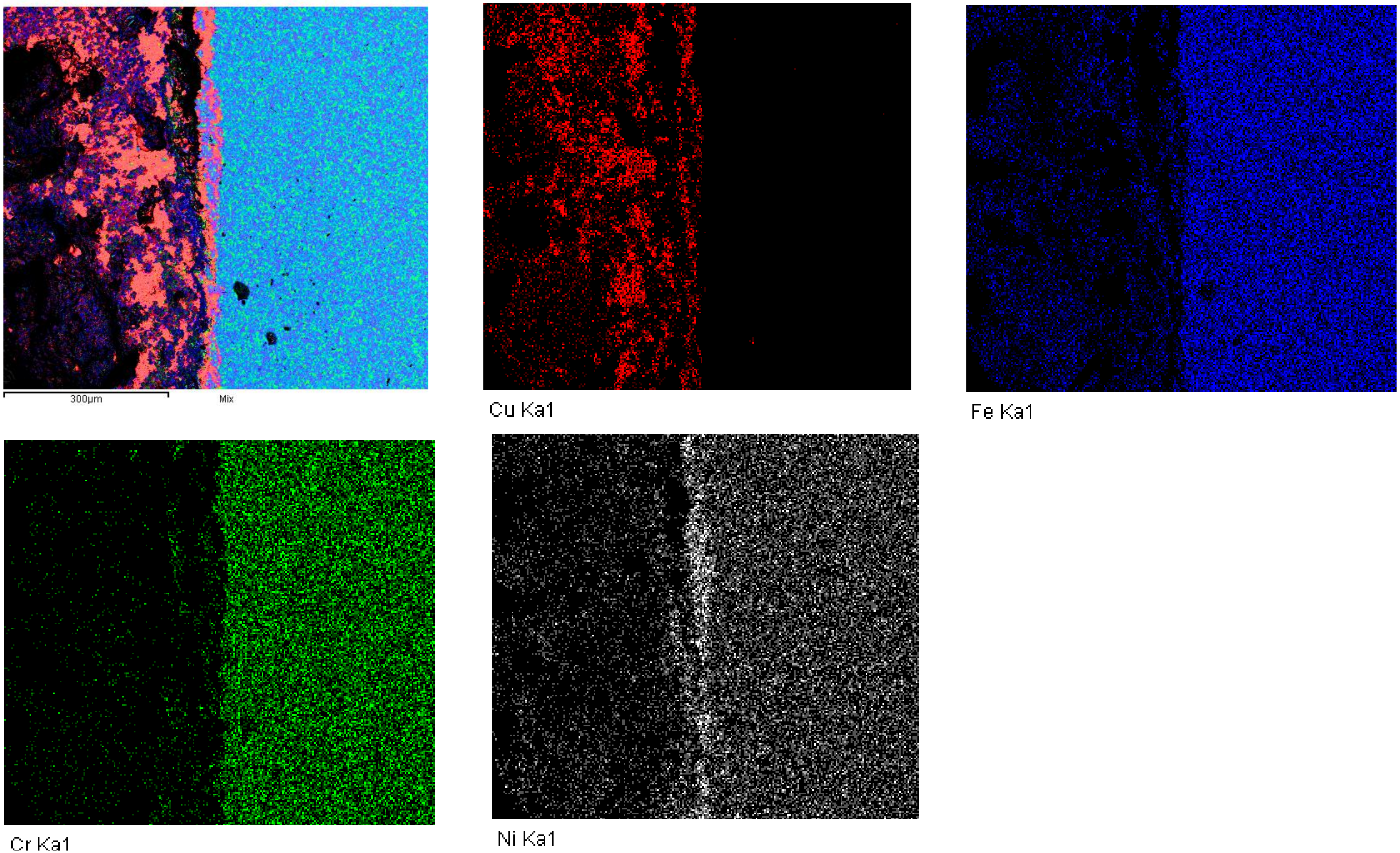

Figure 4.34. X-ray maps showing element distributions through the interface of the sample treated for 20 minutes in oxidizing conditions with agitations. Cu: red, Fe: blue, Cr: green, Ni: white.

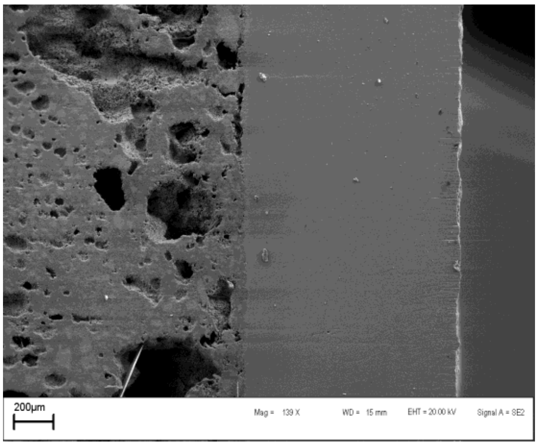

Figure 4.35. SEM-SE, image showing Blisters in the sample treated for 20 minutes in oxidizing conditions with agitation.

The sample contained blisters at the copper-rich side as large as 775 µm.

4.2.2.6. Sample treated for 40 minutes in oxidizing conditions with agitation

In order to determine the distribution through the interface of the sample treated for 40 minutes in oxidizing conditions with agitation, X-ray maps were taken as shown in Figure 4.36 and Figure 4.38 at two different magnifications.

The second showed more detailed element distribution through the interface than the first. Although irregularly distributed, iron was identified at the interface in a copper matrix. Nickel, copper, oxygen and sulphur showed peak concentrations values at the interface. Higher oxygen concentration was found at the copper-rich side, while smaller and evenly distributed amounts were found at the iron-rich side. Blisters occurred at the copper-rich side due to chemical reaction between oxygen and sulphur and also from the trapped amounts of oxygen and nitrogen. Carbon atoms quickly diffused in the interface and the copper-rich side during the cooling time. The carbon resulted from the coke used to prevent copper oxidation during the cooling cycle.

In addition to X-ray maps, line scans were also plotted for different metals as shown in Figure 4.38.

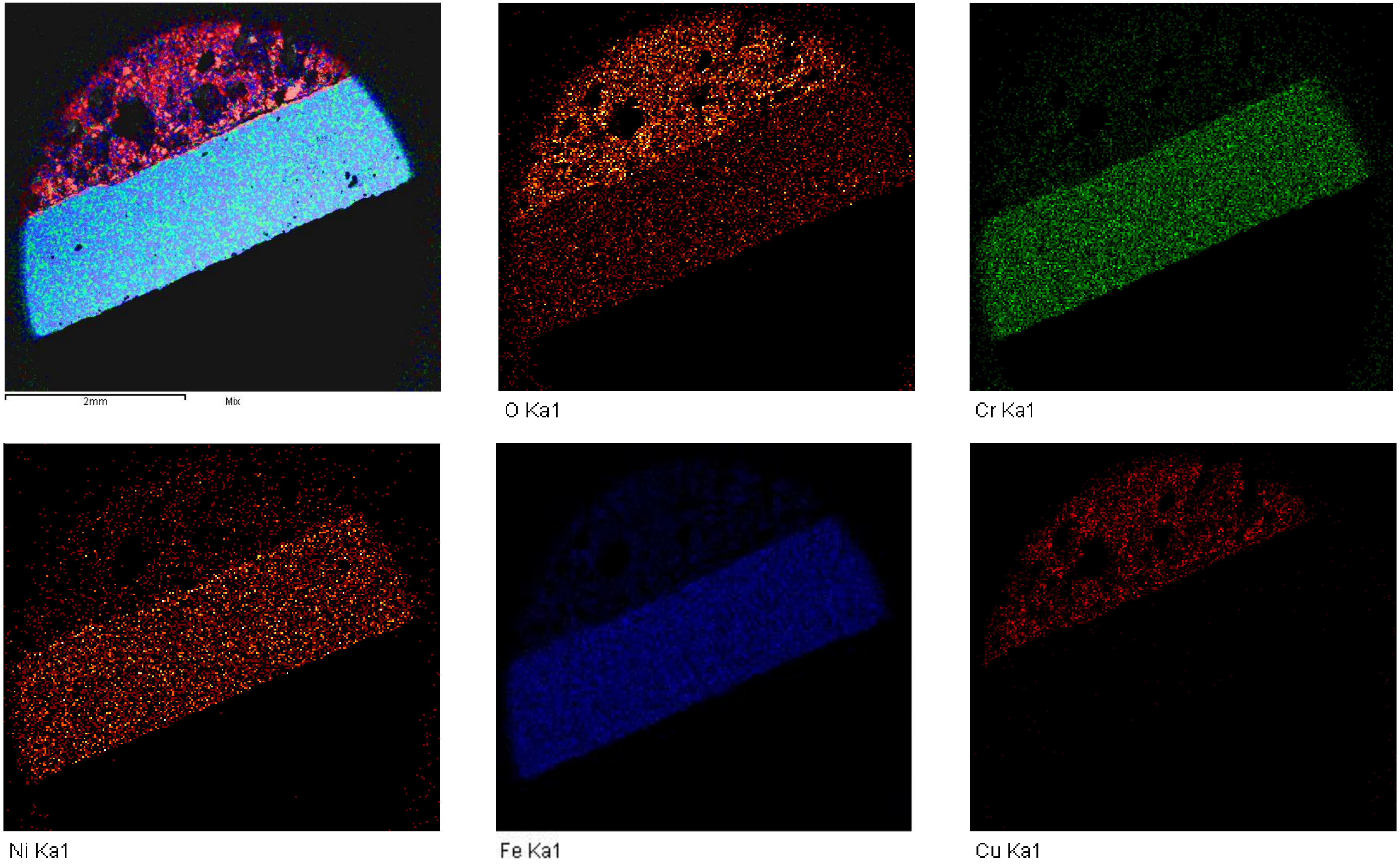

Figure 4.36. X-ray maps showing the distribution of the different elements through the interface of the sample treated for 40 minutes in oxidizing conditions with agitation. O: red, Cr: green, Ni: yellow, Fe: blue, Cu: red.

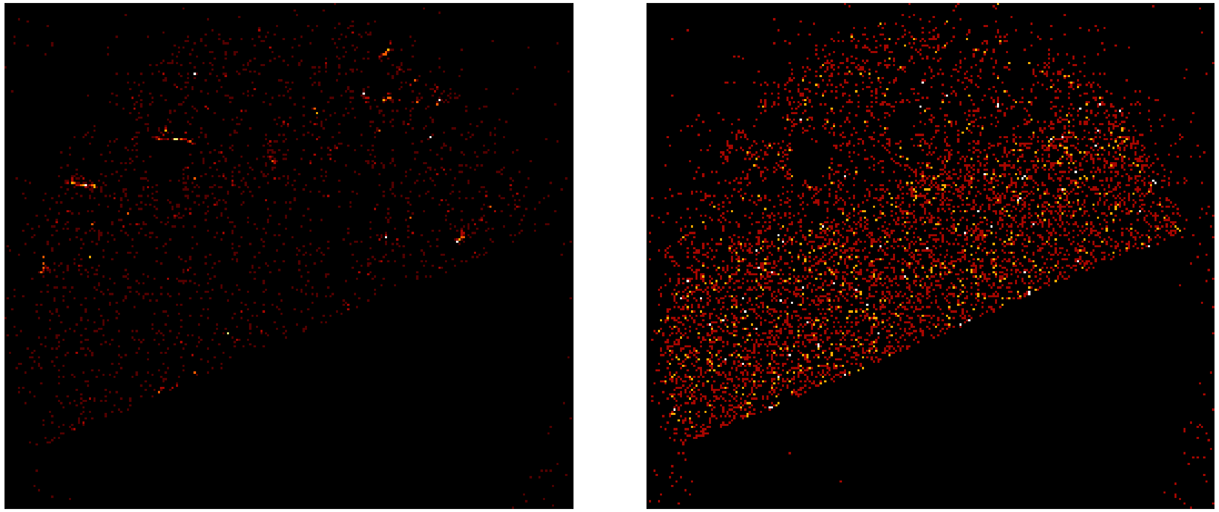

C Ka1_2   Mo La1

Figure 4.36. X-ray maps showing the distribution of the different elements through the interface of the sample treated for 40 minutes in oxidizing conditions with agitation (continued). O: red, Cr: green, Ni: yellow, Fe: blue, Cu: red, C: red, Mo: red.

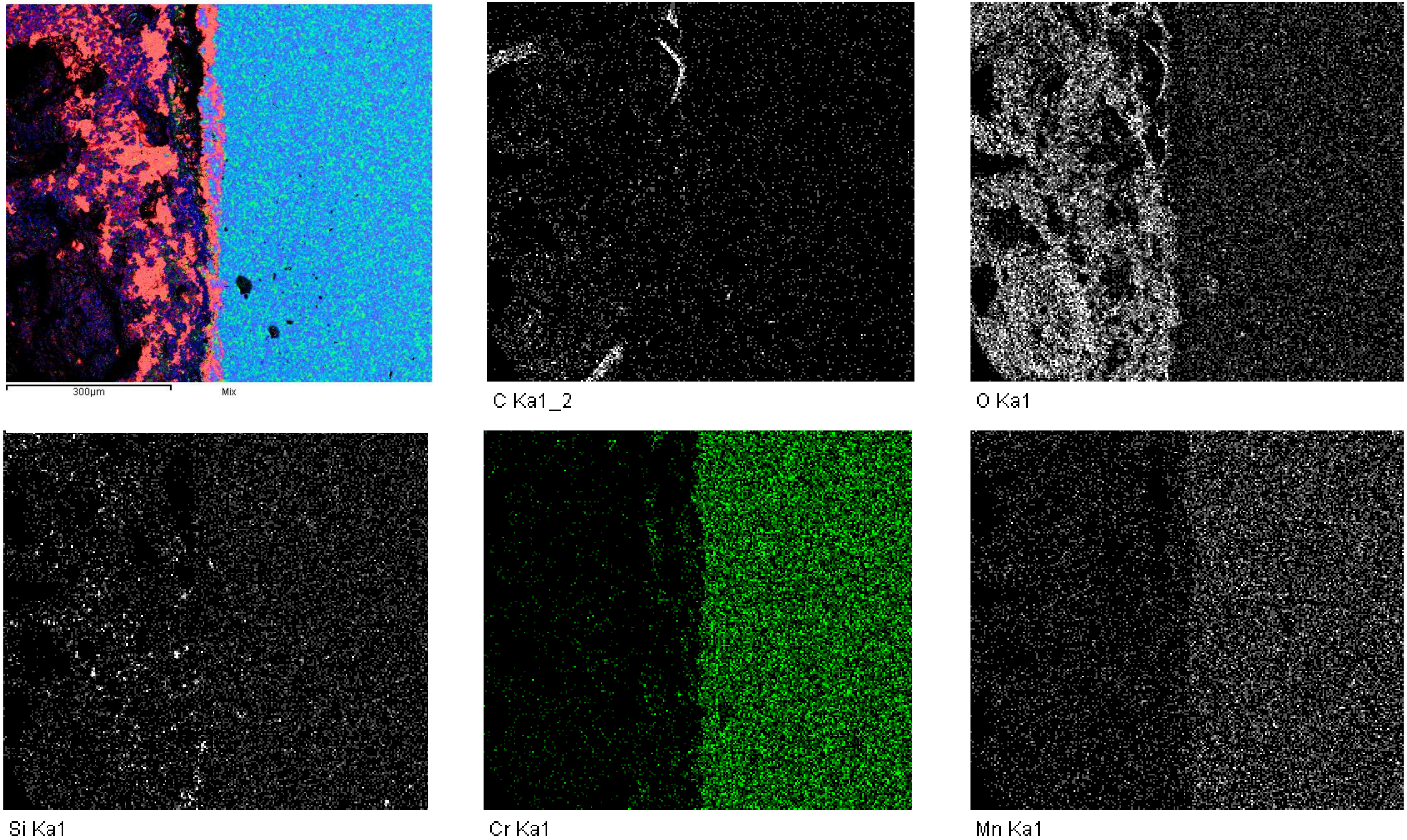

Figure 4.37. X-ray maps showing the distribution of the different elements through the interface of the sample treated 40 minutes in oxidizing conditions with agitation at different magnification. C: white, O: white, Si: white, Cr: green, Mn: white, Fe: blue, Ni: white, Cu: red, S: white.

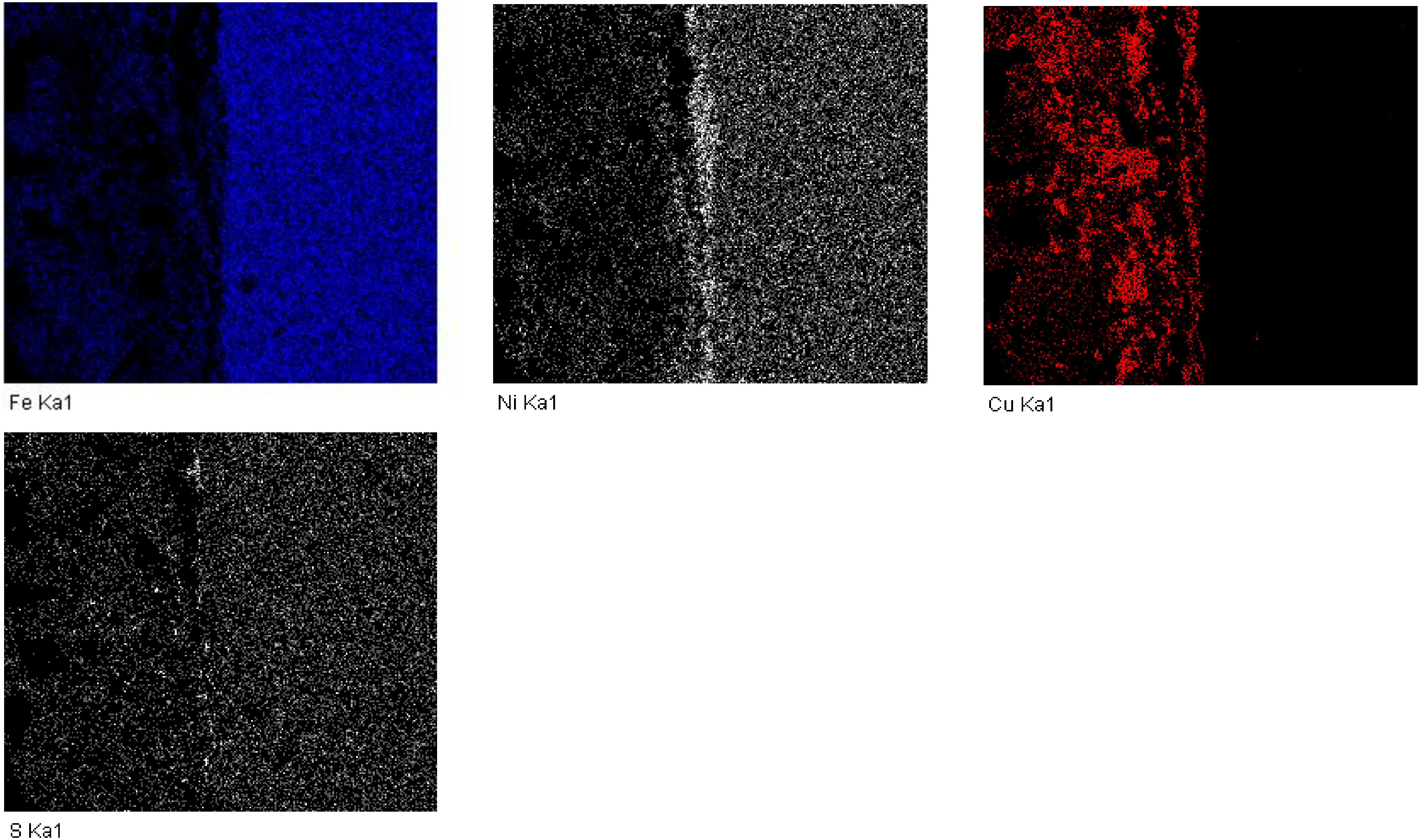

Figure 4.37. X-ray maps showing the distribution of the different elements through the interface of the sample treated 40 minutes in oxidizing conditions with agitation at different magnification (continued). C: white, O: white, Si: white, Cr: green, Mn: white, Fe: blue, Ni: white, Cu: red, S: white.

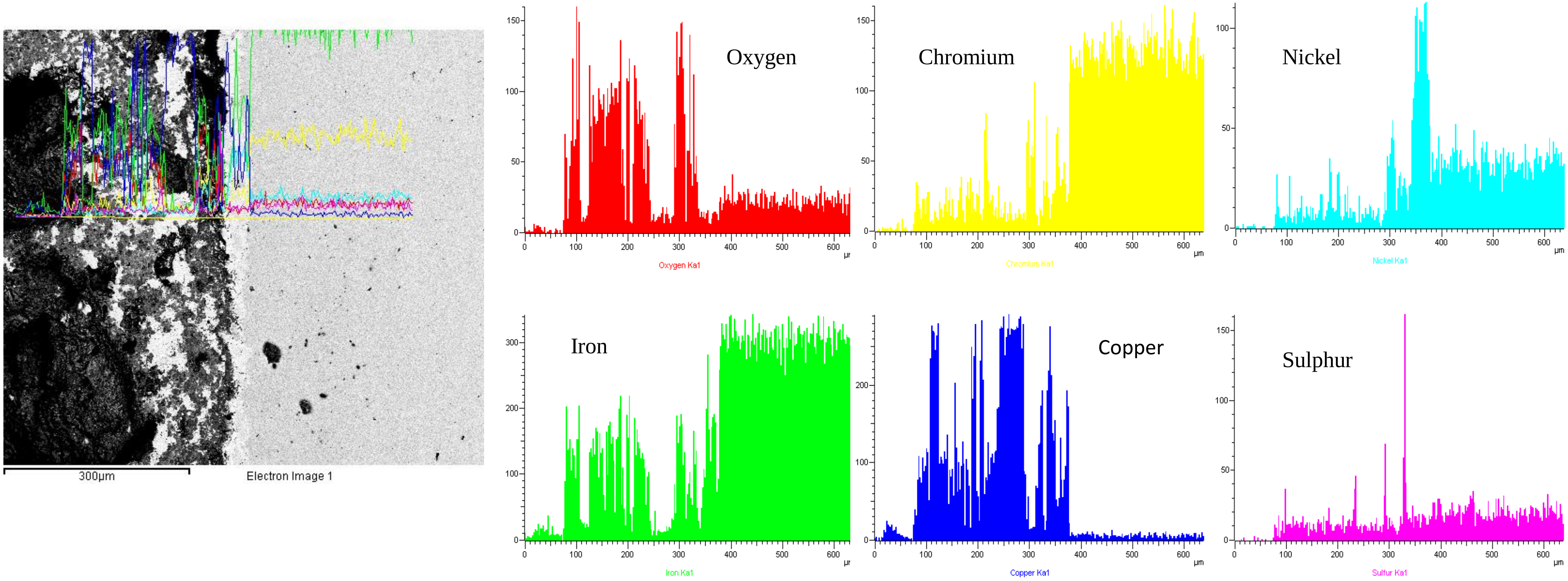

Figure 4.38. SEM image and spectra of the sample treated for 40 minutes in oxidizing conditions with agitation.

The interface of the sample treated 40 minutes in oxidized conditions with agitation was analysed across a line at different spots as shown in Figure 4.39. Each spot was analysed and the concentration determined with EDX as shown in Table 4.21. Copper remained still very low at the iron-rich side.

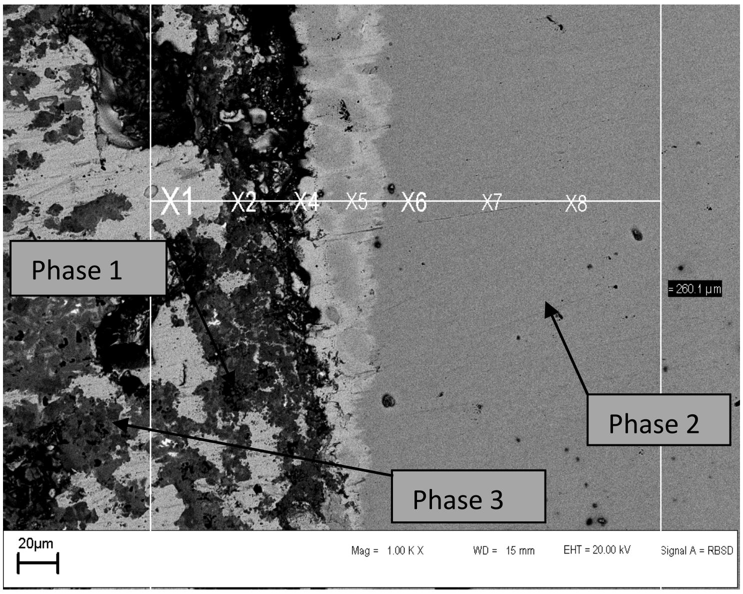

Figure 4.39. **SEM-BSE image showing a line scan across the interface of the sample treated 40 minutes in oxidizing conditions with agitation.**

Table 4.20. EDX analyses (wt%) in different spots on a line of the sample treated 40 minutes in oxidizing conditions with agitation.

Spot	Fe	Cu	C	Ni	C	O	S	Mn
X1	1.2	94.1	0	0	4.0	0.7	0	0
X2	28.2	28.8	4.2	17.3	4.0	16.9	0.4	0.2
X4	8.8	74.0	2.6	4.7	3.6	5.9	0.3	0
X5	16.8	59.2	2.2	17.9	3.0	0.8	0.2	0
X6	66.7	1.0	17.3	9.9	2.6	0.8	0.7	1.1
X7	67.8	0.0	17.4	10.0	2.2	0.8	0.7	1.1
X8	67.5	1.2	17.3	9.7	1.6	0.9	0.7	1.1

4.2.2.7. Analyses of the lab lance after 100 minutes in oxidizing conditions with agitation.

The lance used in the lab for the samples experiments at 100 minutes in oxidizing conditions with agitation was also analysed with EDX. The overall elemental composition was determined as shown in Table 4.21.

Table 4.21. Composition of the lab lance used to blow nitrogen in the sample treated 100 minutes in oxidizing conditions with agitation, wt%.

Element	Composition
Fe	81.3
Cu	4.8
Cr	0
Ni	0.2
C	8.4
S	0.3

X-ray maps were taken to identify the element distribution through the lance, as shown in Figure 4.41. Iron was the major component of the lance and its amount was less in interface. Copper was found in a small amount on the edge of the lance. Chromium was uniformly distributed in the steel, small amounts were seen at the edge. The chromium and nickel concentrations of Table 4.21 do not represent the contents of the original lance which was 17.2 wt% for chromium and 9.5 wt% for nickel. The portion of the lance cross-sectionned was submerged in the copper. Chromium precipitated through grain boundaries and diffused to the interface and copper-rich side, while nickel was oxidised and formed an oxide, or diffused to form solid solutions at the copper-rich side. This phenomenon caused a drop of their (chromium and nickel) in stainless steel. Most of the carbon was in the lance.

X-ray maps were also taken at a different positions on the same lance, to ascertain if the effect was the same at a different area (Figure 4.42).

4.2.2.8. Analysis of the lance from the Tsumeb Custom Smelter

An old lance from the Tsumeb Custom Smelter used for blowing oxygen in blister copper was sectioned as shown in Figure 4.40 and studied. The overall composition was determined by EDX as shown in Table 4.23.

X-ray maps were taken as shown in Figure 4.43. Iron was major element of the sample. Although the individual maps showed regular distribution of copper, chromium and nickel through the lance, the majority was found on the edge. Copper was so low that it could not be detected, Cr and Ni were detected by XRF.

Figure 4.40. Section of the original lance from Tsumeb smelter.

Table 4.22. EDX analyses for the Tsumeb Custom Smelter lance after four days operation.

Metal	Composition (wt%)
Fe	94.1
Cu	0
Cr	0
Ni	0.2
C	4.1
S	0.2

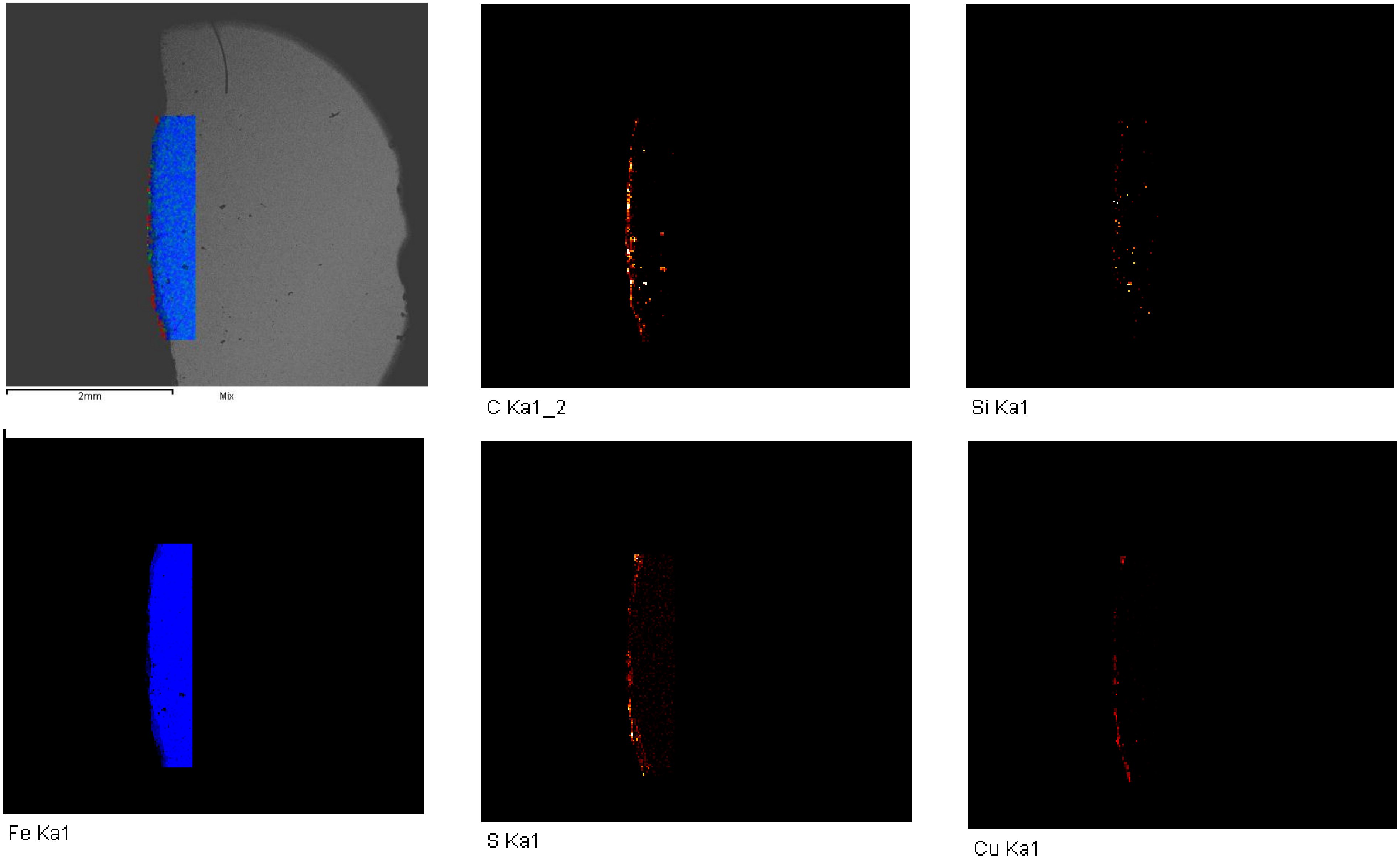

Figure 4.41. **X-ray maps showing elements distribution through the lance used in the lab for gas blowing in sample treated 100 minutes in oxidizing conditions with agitation. C: red, Si: red, Fe: blue, S: red, Cu: red, Cr: green.**

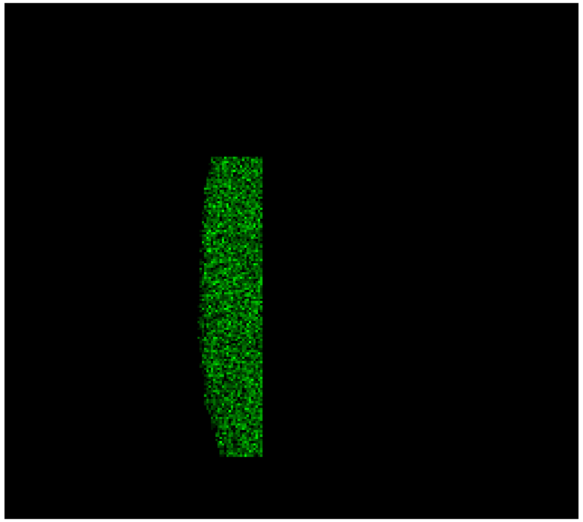

Figure 4.41. X-ray maps showing element distribution through the lance used in the lab for gas blowing in sample treated 100 minutes in oxidizing conditions with agitation (continued). C: red, Si: red, Fe: blue, S: red, Cu: red, Cr: green.

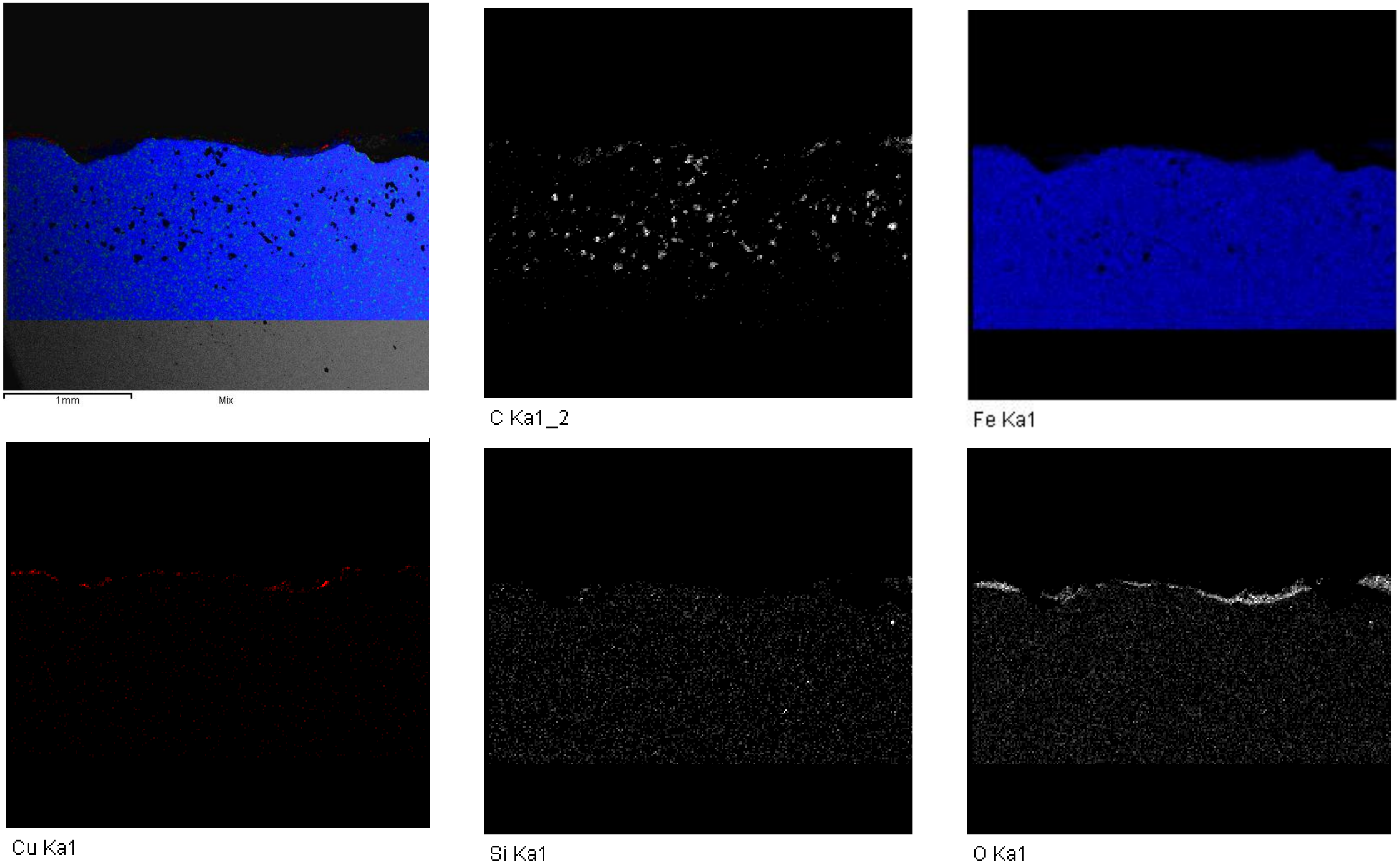

Figure 4.42. X-ray maps showing element distribution through the lance used in the lab for gas blowing in sample treated for 100 minutes in oxidizing conditions with agitation. (C: white, Fe: blue, Cu: red, Si: white, O: white, S: white, Cr: green.

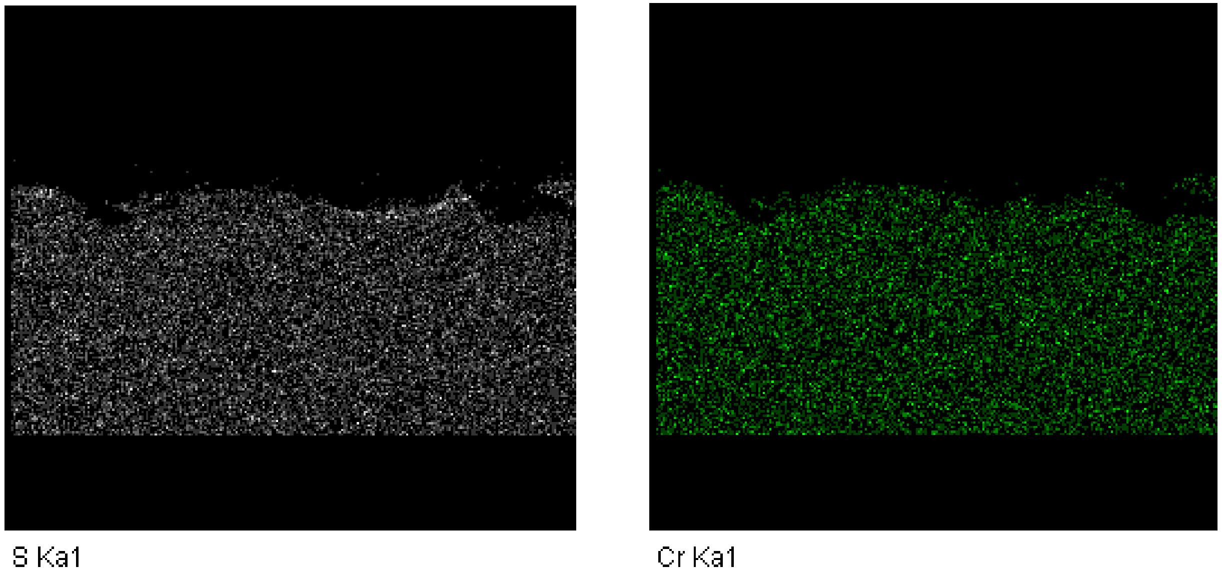

Figure 4.42. **X-ray maps showing element distribution through the lance used in the lab for gas blowing in sample treated for 100 minutes in oxidizing conditions with agitation (continued). C: white, Fe: blue, Cu: red, Si: white, O: white, S: white, Cr: green.**

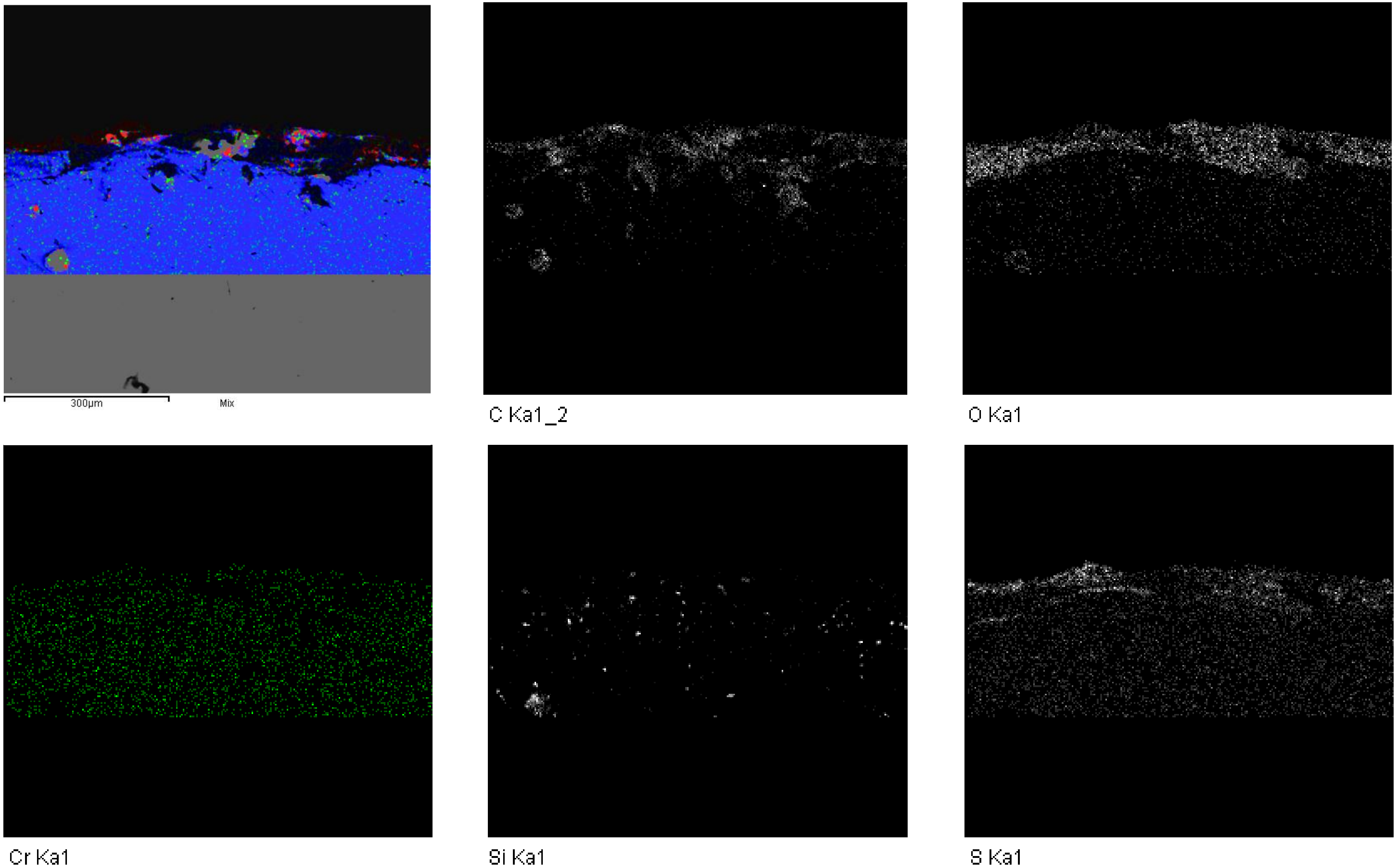

Figure 4.43. X-ray maps of the Tsumeb Custom lance after 4 days operation. C: white, O: white, Cr: green, Si: white, S: white, Fe: blue, Cu: red.

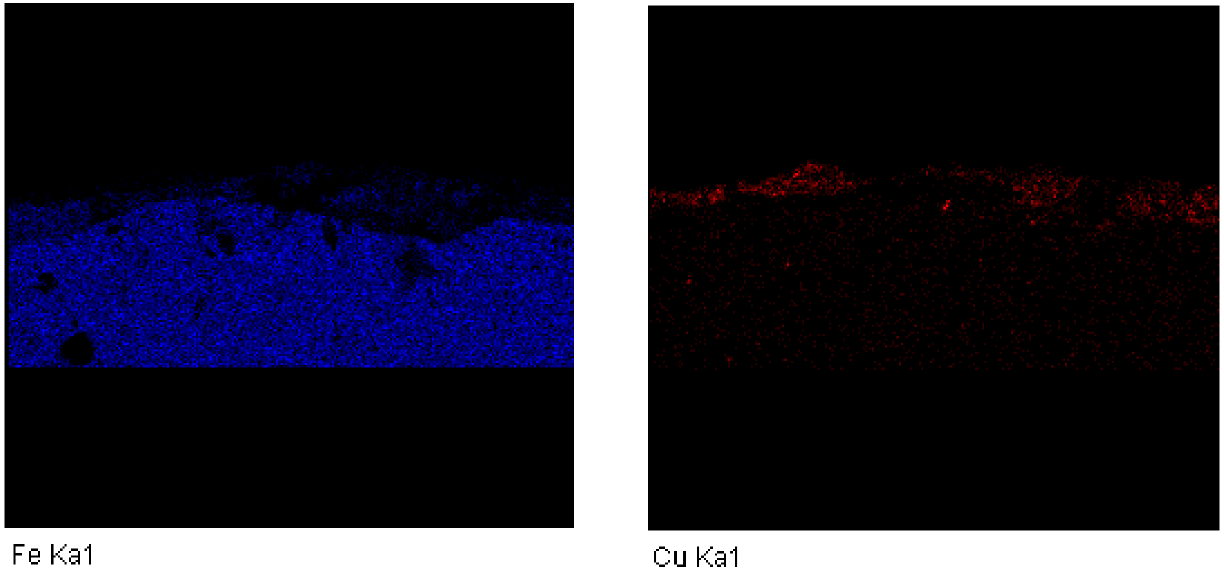

Figure 4.43. X-ray maps of the Tsumeb Custom lance after 4 days operation (continued). C: white, O: white, Cr: green, Si: white, S: white, Fe: blue, Cu: red.

CHAPTER 5: DISCUSSION

5.1. Cast blister copper

In the first set of experiments, the temperature was kept constant and the melting time was changed from 20 to 100 minutes with intervals of 20 minutes. The furnace environment was kept inert by a continuous nitrogen flow on top of blister copper.

After melting, blister copper was cast in ceramic moulds and the amount of metal that was poured out was expressed as percentage of the total weight of the sample.
No metal from stainless steel was found in the cast blister copper by XRF.

Conversely, after melting in inert conditions with agitation, iron and nickel were found in the cast blister copper as shown in Table 4.3 and Figure 5.1. Thus, agitation contributed to the transfer of nickel and iron from the interface to the cast blister. In the first 60 minutes of melting the nickel composition in the cast metal increased with time.

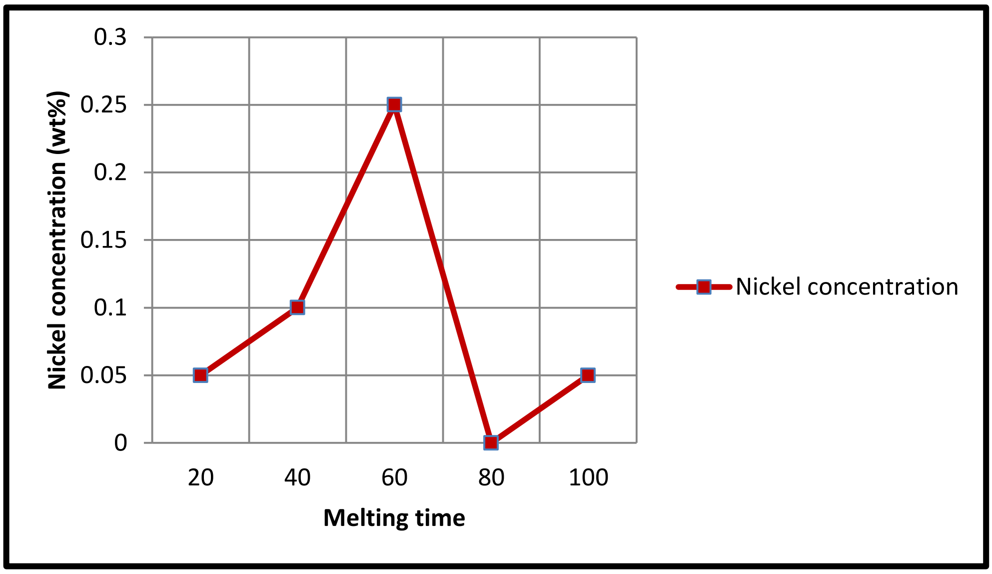

Figure 5.1. Nickel concentration in blister copper as a function of melting time in a inert melting environment with agitation.

At 60 minutes it has reached a maximum, then decreased again. This is thought to happen because the nickel diffused to the interface from the copper melt. This process involved two mechanisms: chemical reactions and mechanical agitation which led to composition changes of both blister copper and 316L stainless steel. A relative movement between corrosive fluid (copper-rich) and metal surface was thus established causing increase and decrease of concentration in the three coexisting different phases (copper-rich, interface, and iron-rich).

The oxidizing conditions gave slag near the interface and reduced the copper content of the blister copper to approximately 94 wt%. The slag formation stopped blister copper from being poured, and after 60 minutes, no copper could be poured. In the test conditions, the contact area between blister copper and stainless steel was higher than in the actual plant operating conditions, this was due to the melting being done in stainless steel crucibles. In plant conditions, 28 tuyeres were destroyed after 672 copper tons melted and could have resulted in impurities contamination of 4.49 ppm, therefore the copper contamination was negligible. The corrosive effect of the copper against stainless steel was the most important factors to be considered.

316L stainless steel should not be considered as substitute to mild steel, be it for lances manufacture or copper furnace sides when the gas supply to the furnace contains oxygen. In oxidizing environments, it is recommended to use lance made of silicon carbide for its established resistance to corrosion, abrasion at higher temperatures.

The iron composition of the cast blister copper was also determined for all five samples treated in inert conditions with agitation as shown in Table 4.3 and Figure 5.2. During the first 40 minutes, iron composition was not discernable. At 60 minutes, it had reached the maximum before starting to drop, but the decrease was less rapid, and there was no further increase for iron. Once again, the iron was thought to become part of the interface.

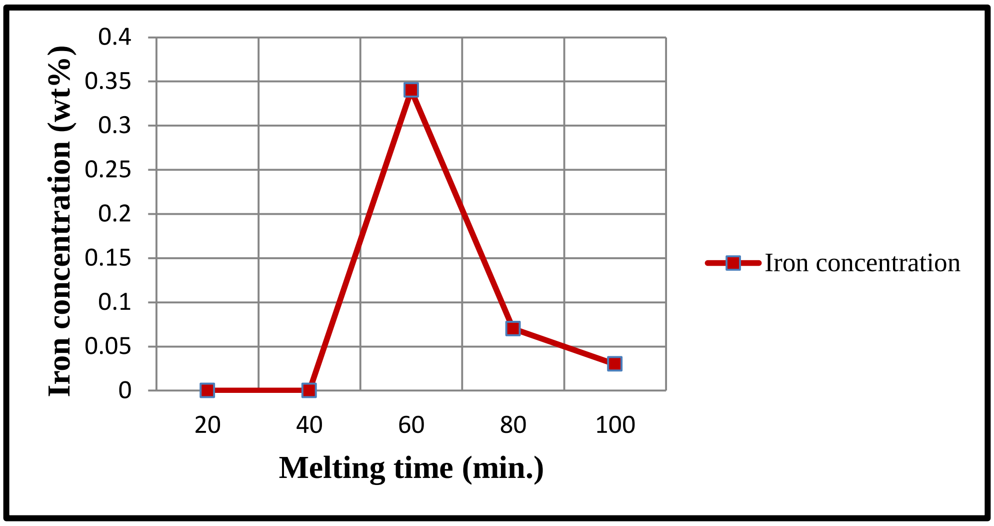

Figure 5.2. Iron concentration in blister copper as a function of melting time for the sample treated in inert conditions with agitation.

There was no chromium found in the copper melt by XRF.

The graphs have quite different trends in oxidising conditions with agitation. The maximum nickel content was over ten times higher, and it occurred at 100 minutes, rather than at 60 minutes of melting (Table 4.4).

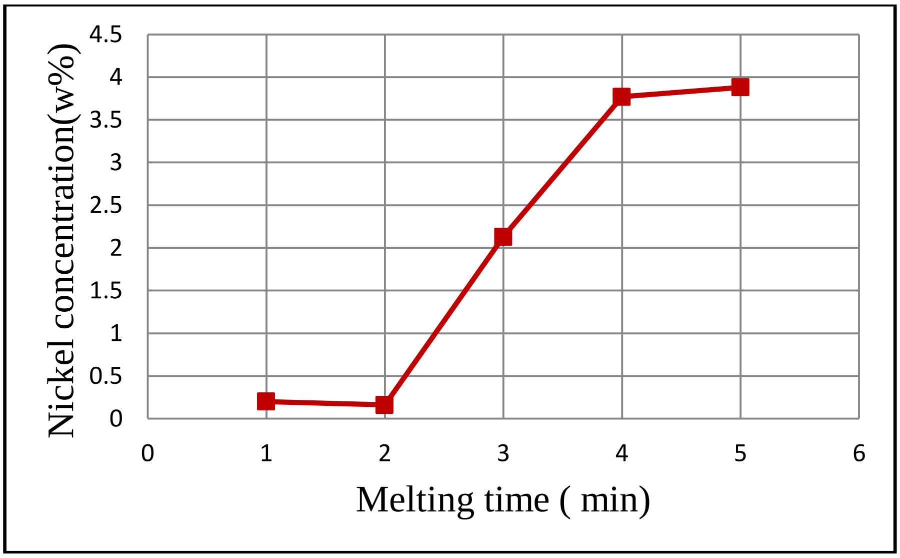

Figure 5.3. Nickel concentration in blister copper as a function of time in oxidizing conditions with agitation.

Nickel mixed with copper in all composition ranges while the other metals did not. This makes its behaviour different from the others.

The iron composition for the sample treated in oxidizing conditions with agitation was plotted as shown in Figure 5.4 (Table 4.4).

The iron content in the melt was negligible until 60 minutes, when it had reached approximatively 14 wt%. There after, it only increased by a small amount, but was still increasing, which showed that the iron did not go back to the interface, unlike nickel (Figure 5.3).

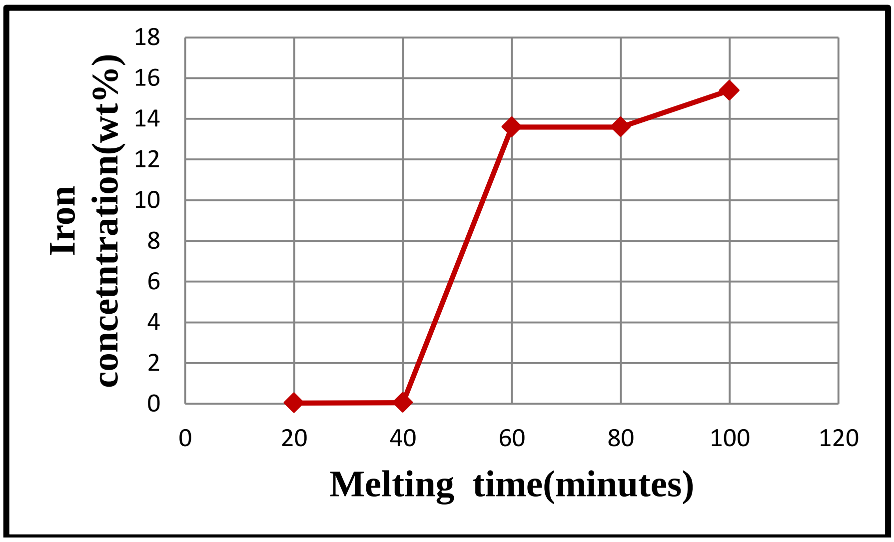

Figure 5.4. Iron concentration in blister copper as function of melting time in oxidizing conditions with agitation.

The chromium composition for the sample treated in oxidizing conditions with agitation is shown in Figure 5.5 (Table.4.4). Chromium was under the detection limit for the first 40 minutes of melting. The concentration started to increase, thereafter appeared to reach a maximum at 4.5wt% chromium. Similar to iron, this shows that the chromium did not return to the interface.

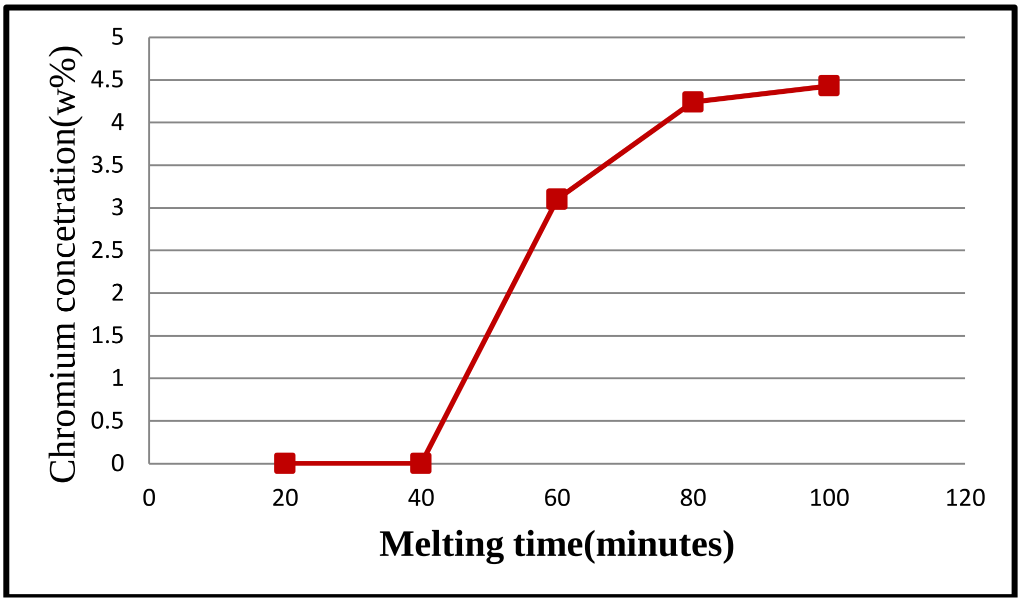

Figure 5.5. Chromium concentration in blister copper as a function of melting time in oxidizing conditions with agitation.

The relationship between melting time and the blister copper recovered from the crucible is shown in Figure 5.6 (Tables 4.2-4.4).

The amount of blister copper recovered after melting in inert conditions with agitation was after 20 minutes of melting higher than that recovered in inert conditions without agitation. Although the other conditions were kept constant, the amount of cast blister copper recovered was a minimum at 26.01 wt% copper. There was also a minimum amount of copper recovered at 60 minutes for the melt done in inert conditions without agitation. For the samples melted under oxidizing conditions, there was more slag with increased time, and after 60 minutes, the slag was stopping the copper from being poured out of the crucible. In industry, silica is added to make the slag flow better [2004Dav].

The interaction between blister copper and stainless steel resulted in formation of an interface, indicated in the microstructures shown by SEM figures in Chapter 4. Copper climbed the crucibles sides, thus, confirming its reactivity with iron as described by Presnyakov et al. [2002Pre] as superfluidity of copper.

The thickness of the interface as well as the copper penetration along the stainless steel grains boundaries was measured for different melting conditions and values are shown in Table 5.1. In inert conditions, the thickness increased with time, but in inert conditions and oxidizing with agitation, it decreased.

The penetration increased in both inert conditions without agitation and with agitation. However, in oxidizing conditions, the penetration was “Too small’’ to be identified by SEM.

Table 5.1. Interface thickness and copper penetration into stainless steel dependent of melting conditions.

Conditions	Melting time (minutes)	Interface width (µm)	Copper penetration (µm)
Inert without agitation	40	72	84
Inert without agitation	80	214	107
Inert with agitation	60	228	25
Inert with agitation	100	107	142
Oxidizing with agitation	20	32	Too small to read
Oxidizing with agitation	40	28	Too small to read

The interface width was dependent of type of gas supply, agitation duration and gas used. Longer melting times in non-agitated conditions increased the thickness of the interface, while longer agitation times decreased the thickness. Oxidation reduced the thickness and changed the morphology to give larger regions of the different phases. The copper also penetrated along the grain boundaries in all conditions, except for the oxidizing conditions with agitation.

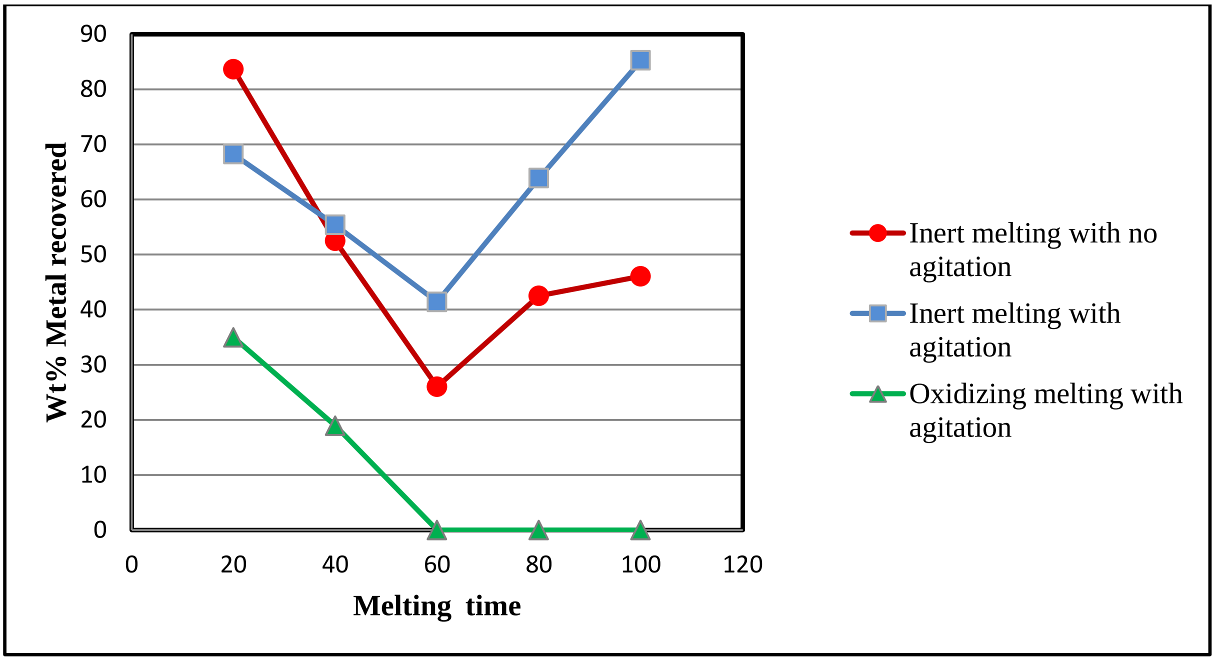

Figure 5.6. **Relationship between recovery of blister copper and melting time.**

The interaction between blister copper and stainless steel resulted in formation of an interface, characterised by different microstructures and compositions as shown by the different SEM analysis.

5.2. Interface between 316L stainless steel crucible and blister copper

5.2.1. Composition of iron, copper chromium and nickel across the interface of the sample treated for 40 minutes in inert conditions without agitation

The graphs representing Cu, Fe, Cr and Ni composition trends are shown in Figure 5.7. Iron, nickel, as well as chromium, curves have almost the same trend, while copper was different, because the former came from the steel, whereas the latter was from the copper melt. They all reached the minimum concentration between the interface and the copper-rich side.

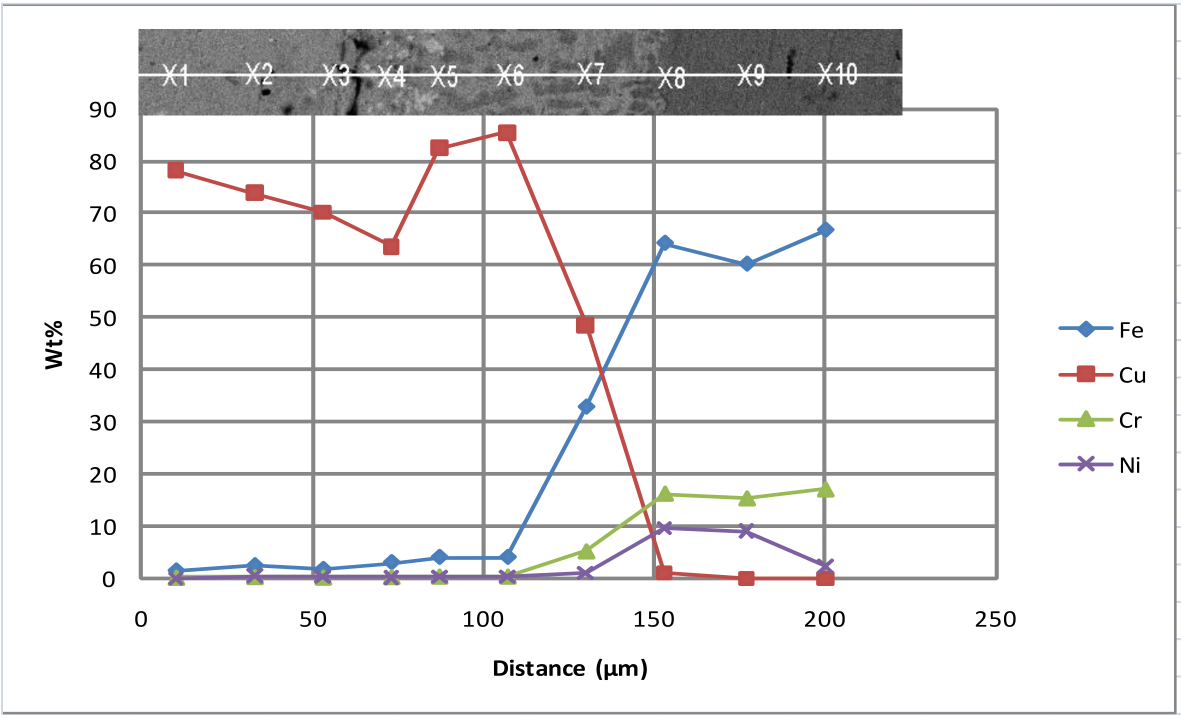

Figure 5.7. Compositions across the interface of the sample treated for 40 minutes in inert conditions without agitation.

The copper concentration varied and was irregular at the copper-rich side; the analyses at this side (copper-rich) included results for very light and dark phases. It decreased sharply across the interface, and penetrated the steel minimally.

The iron, nickel and chromium had very slight increases just before the interface, and sharply decreased over the interface, and were at a low level in the copper-rich side, being lower the further away from the interface. These results show some diffusion of iron, nickel and chromium into the copper, and negligible diffusion of the copper into the steel. The largest composition changes were at the interface. Although not on the line of plots, Figure 4.10 shows that there was some copper penetration along the grain boundaries into the steel.

Two mechanisms took place during melting: solubility of Fe and Ni from the stainless steel into the blister copper in one direction, and diffusion of copper into stainless steel along the grain boundaries in the other direction.

5.2.2. Compositions across the interface of the specimen treated for 80 minutes in inert conditions without agitation

At both sides of the interface, the compositions of copper, iron and nickel were constant, but in the interface the composition changed.

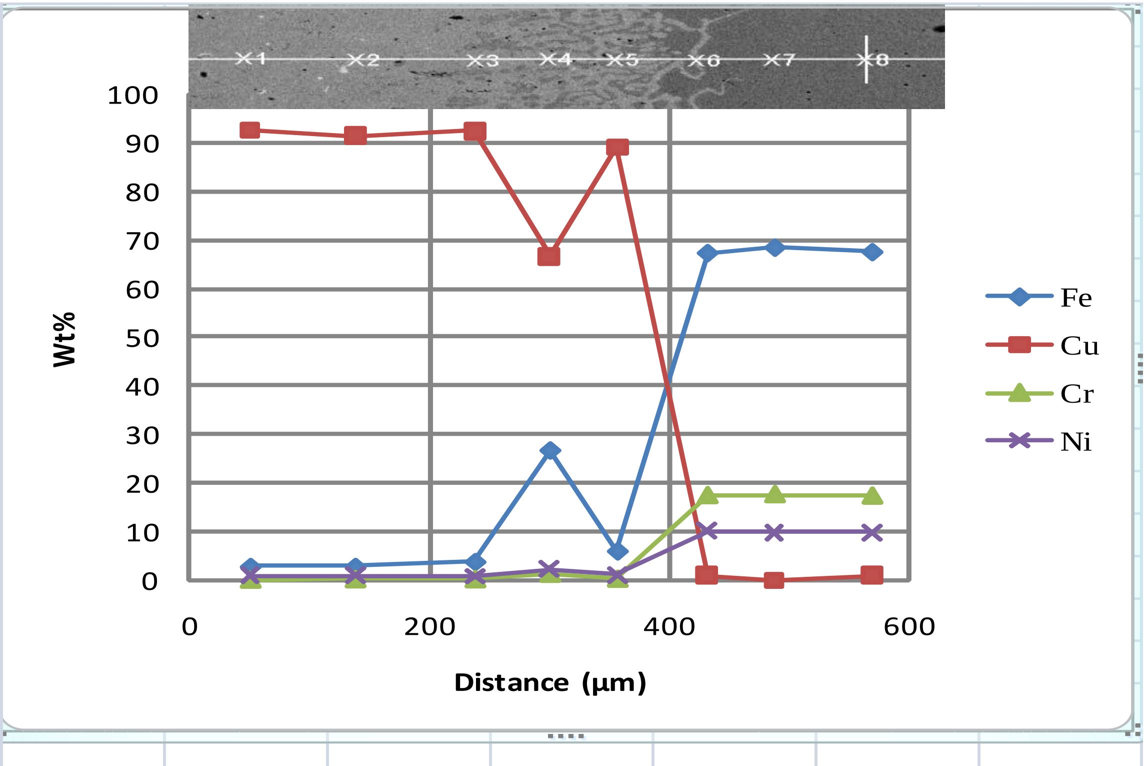

Figure 5.8. Compositions across the interface of the sample treated for 80 minutes in inert conditions without agitation.

The longer melting time allowed the dissolution of the light phase in the interface. The width of the interface increased from 72 microns in the 40 minutes sample to 214 microns in the 80 minutes sample (Figure 5.8).

5.2.3. Compositions across the line of the sample treated for 60 minutes in inert conditions with agitation

Figure 5.9 shows the compositions across the interface. Iron, chromium and nickel had the same trend in the interface, which is opposite of that of copper. Some of the analyses in the interface included the darker iron-rich phase, so making the results more iron-rich, and indicating that the copper content decreased further, and the iron content slower across the interface. This might not be true if the local overall compositions have been used. For these same points, chromium and nickel remained the same.

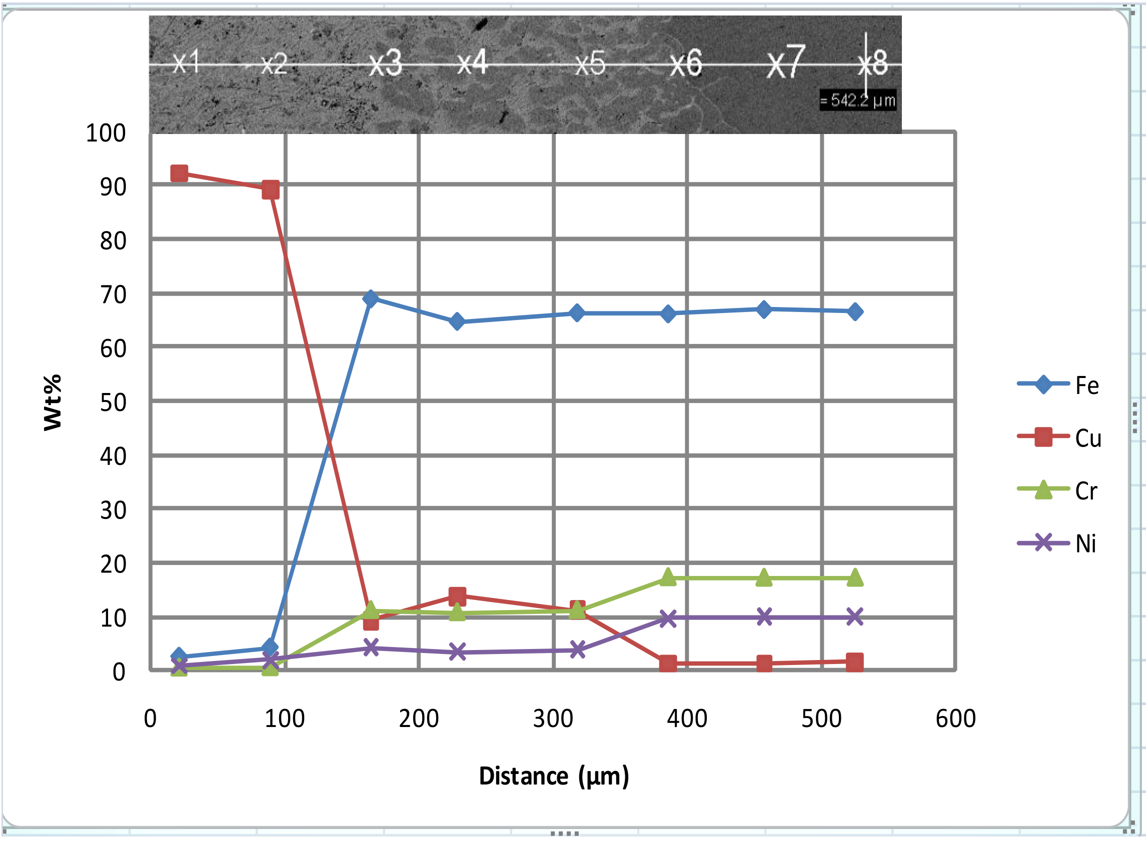

Figure 5.9. Compositions across the interface of the sample treated for 60 minutes in inert conditions with agitation.

5.2.4. Composition across a line of the sample treated for 100 minutes in inert condition with agitation

Iron, chromium and nickel had the same trend in the interface, which is opposite of that of copper. At the copper-rich side, copper and iron were irregularly distributed. The darker phase was replaced by lighter phases in several intervals. At the steel side, strange concentrations were found for all four metals (lower Fe, Cr, Ni, and higher Cu) as shown in Figure 5.10. This seems to be caused by the presence of liquid copper that was blown out of the crucible during agitation.

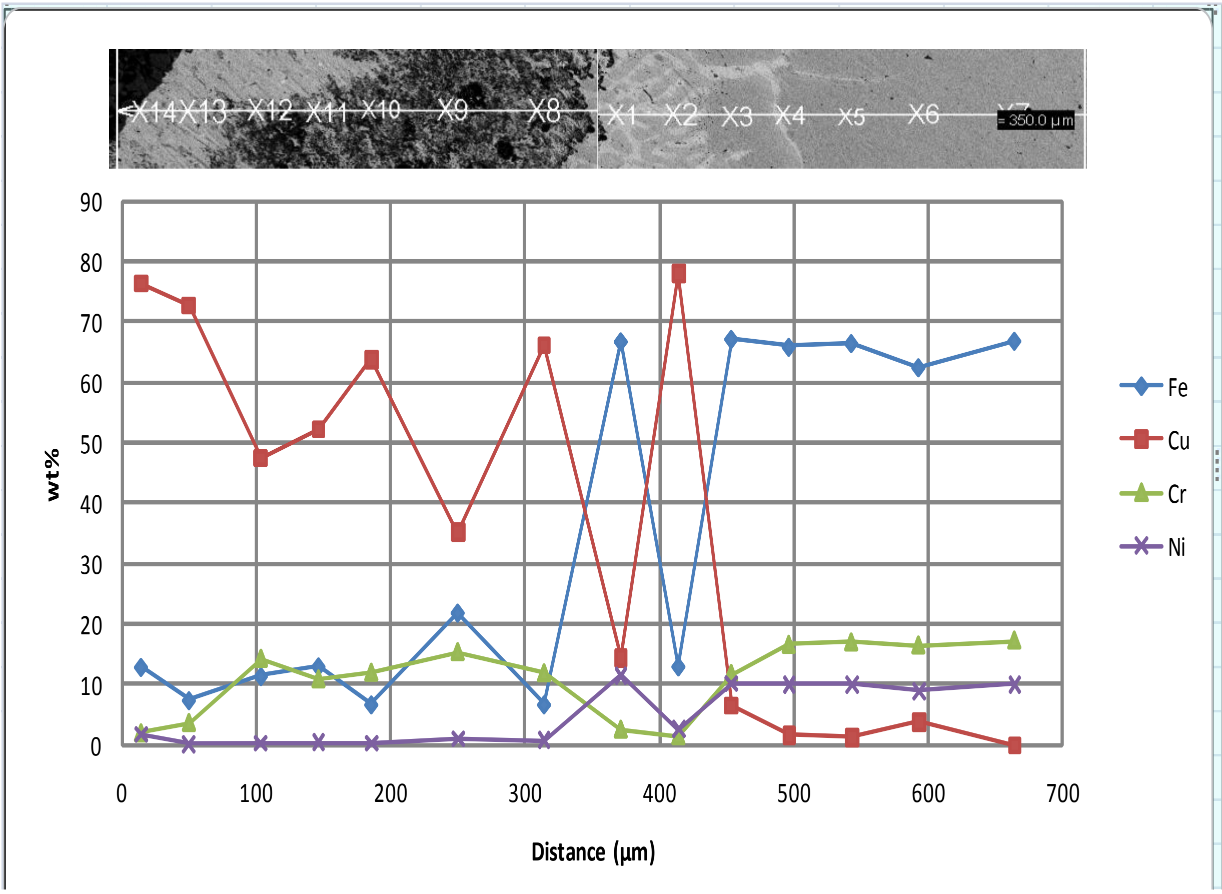

Figure 5.10. Compositions across the interface of the sample treated for 100 minutes in inert conditions with agitation.

5.2.5. Compositions across the line of the sample treated for 20 minutes in oxidizing conditions with agitation.

The amount of the darker phase increased at the copper-rich side and iron, copper, chromium and nickel concentrations were lower than in the previous samples as shown in Figure 5.11.

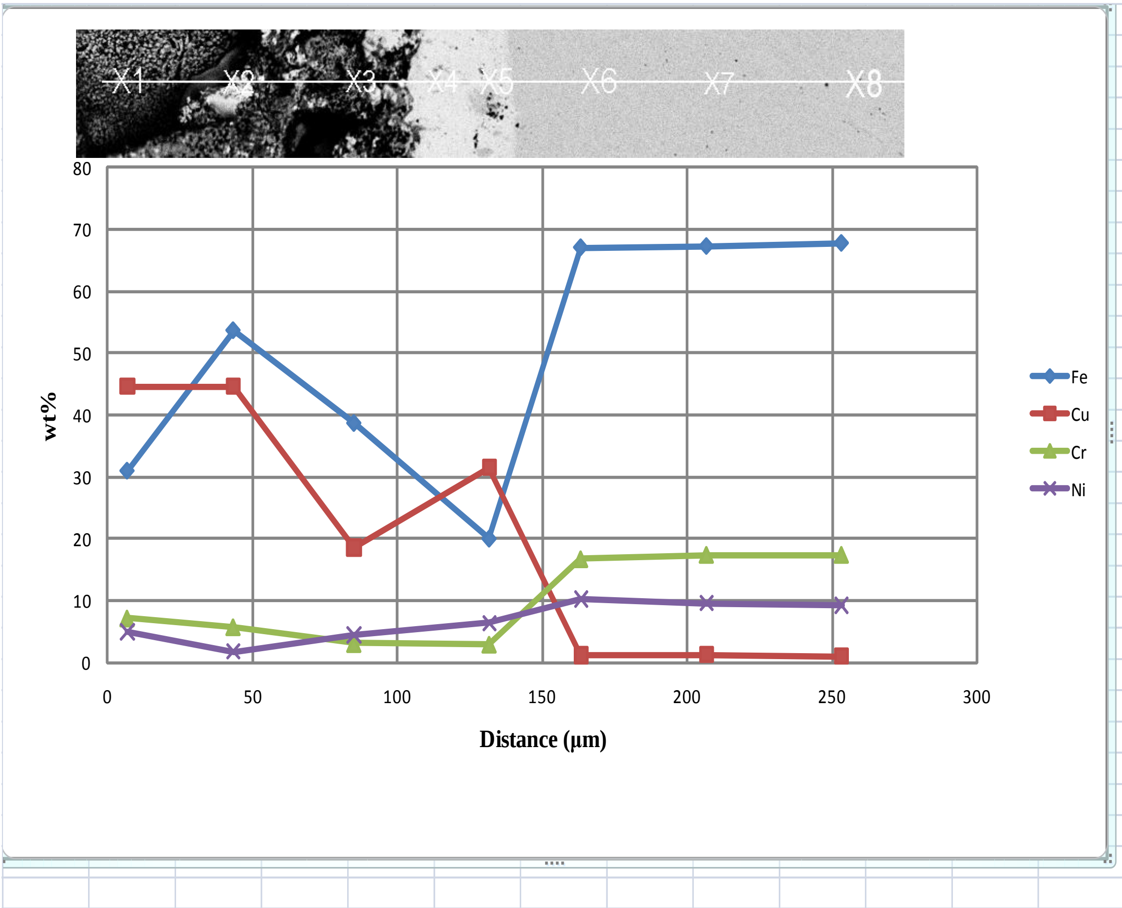

Figure 5.11. Composition across the interface as function of distance of the sample treated for 20 minutes in oxidizing conditions with agitation.

5.2.6. Compositions across the line of the sample treated for 40 minutes in oxidizing conditions with agitation.

The iron, chromium and nickel concentrations started changing at the interface, where they decreased (Figure 5.12). There were two phase contrasts in the interface, and the chromium content was higher in the darker phase (spot X5). The copper side was heavily oxidized to give “slag” which was nearly 17 wt% oxygen, together with areas of nearby affected blister copper. The concentration of iron, nickel and chromium were higher in the copper-rich side. The amount of oxide had seriously affected the copper concentration, which dropped to 94.1wt%.

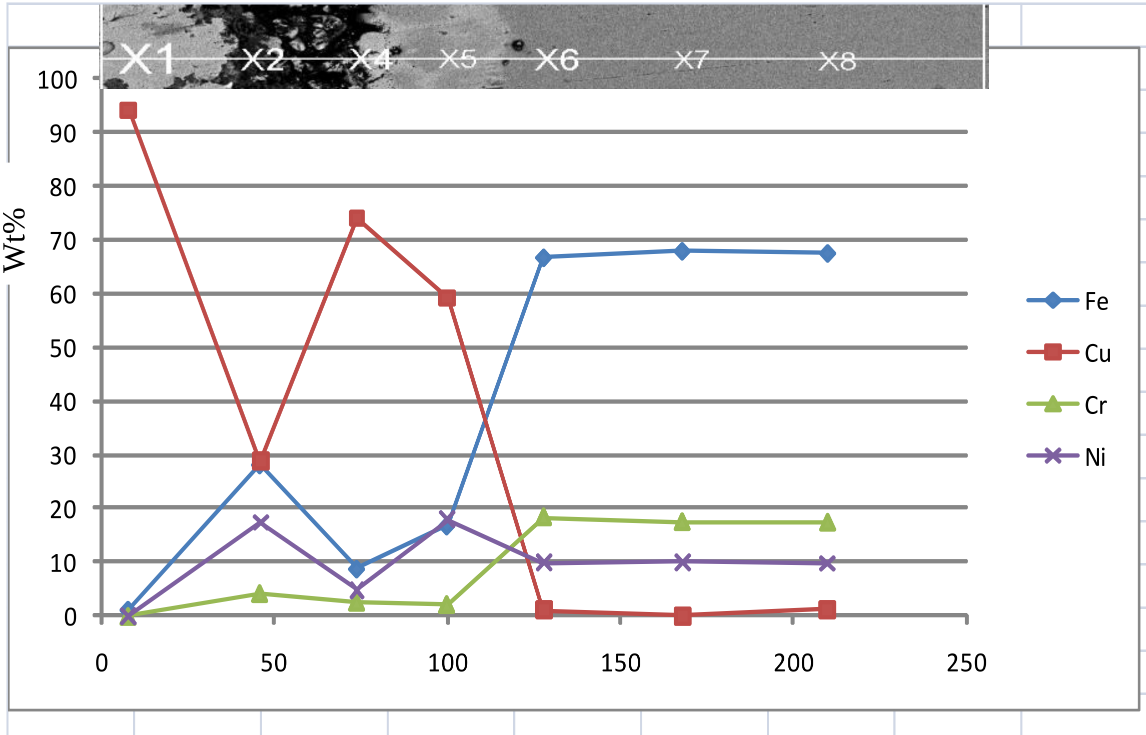

Figure 5.12. Compositions across the interface as function of distance of the sample treated for 40 minutes in oxidising conditions with agitation.

Ellingham diagrams determine the nature of oxides that could have been formed in operating conditions. The nature of these oxides was dependent of their respective free energies and the oxygen partial pressure. Based on thermodynamics, it was assumed that Cu, Ni, Fe, Cr oxides were formed as the oxygen partial was 0.3 atmosphere and free energies described at 1200°C [2004Shi]:

$4\mathrm{Cu} + \mathrm{O_2} = 2\mathrm{Cu_2O}$ ΔG = - 145 kJ/mole, $\mathrm{pO_2(equilibrium)} = 8.10^{-4}\mathrm{atm}$

$2\mathrm{Ni} + \mathrm{O_2} = 2\mathrm{NiO}$ ΔG = - 220 kJ/mole, $\mathrm{pO_2(equilibrium)} = 10^{-8}\mathrm{atm}$

$6\mathrm{Fe} + 2\mathrm{O_2} = 2\mathrm{Fe_3O_4}$ ΔG = - 251 kJ/mole, $\mathrm{pO_2(equilibrium)} = 2.10^{-10}\mathrm{atm}$

$\frac{4}{3}\mathrm{Cr} + \mathrm{O_2} = \frac{2}{3}\mathrm{Cr_2O_3}$ ΔG = - 495 kJ/mole, $\mathrm{pO_2(equilibrium)} = 10^{-18}\mathrm{atm}$

These are exothermic reactions and could have caused increase of temperature of the melt. However, the change in temperature was not noticeable given the size of the samples. Figures 5.7-5.12 show that Cu diffused from the copper-rich side to the iron-rich side and Ni, Cr, Fe diffused from the iron-rich side to the copper. Agitation contributed to more irregular distribution of different metals through the copper-rich side.

5.2.7. Phase composition

Five different phases appeared in the selected specimens with miscibility gap in fcc as shown in Tables 5.2-5.7. Metallics phases were dissolving in non-metallic phases (like oxides) which led to the slag formation. Table 5.2 shows the composition of two solid solutions (1 and 3) consisting of very high copper, low chromium and low iron contents. Table 5.3 shows that the richest phase (1) in copper has almost completely disappeared, and most of the copper had gone to phase 3, where copper had increased. The copper concentration in phase 3 remained almost the same for the two samples treated in inert conditions (80 minutes without agitation and 60 minutes with agitation) as shown in Tables 5.3 and 5.4. However, the copper concentration decreased in the sample treated at 100 minutes in inert conditions with agitation, probably due to the creation of the new phase (5), in Table 5.5. Iron had dissolved as well the new phase 5 as shown in Table 5.5, causing the diminishing of phase 4. Copper composition continued to decrease in phases 3 and 5, as shown in Tables 5.6 and 5.7. Nickel dissolved faster in phase 5 in the sample treated for 40 minutes in oxidizing conditions with agitation. Although the size of phase 4 reduced, the iron concentration remained almost the same.

Table 5.2. Phase composition (wt%) of the sample treated for 40 minutes in inert conditions without agitation.

Phase	Description	C	O	S	Cr	Mn	Fe	Ni	Cu
1	White metallised	10.0	0.8	0	0.2	0	2.3	0.2	86.6
2	dark grey in the interface	7.4	0.7	1.1	3.4	0	19.7	0.5	67.2
3	light grey in the interface and the copper-rich side	10.0	0.8	0	0.3	0	3.2	0.4	85.4
4	Dark grey at steel side	2.8	0	0.7	17.1	1.1	66.9	9.9	1.7

Table 5.3. Phase composition (wt%) of the sample treated for 80 minutes in inert condition without agitation.

Phase	Description	C	O	S	Cr	Mn	Fe	Ni	Cu
1	White (scattered in phase 3 matrix)	Too small to be characterized							
2	Dark grey in the interface	1.8	0	2.9	3.3	0	74.8	5.7	1.6
3	Light grey in the interface and the copper side	3.2	0.3	0	0	0	4.1	1.4	91.2
4	Dark grey at steel side	1.4	0.4	0.7	17.7	1.2	68.4	10.5	0

Table 5.4. Phase composition (wt%) of the sample treated for 60 minutes in inert conditions with agitation.

Phase	Description	C	O	S	Cr	Mn	Fe	Ni	Cu
1	White (occluded rare small spot) at copper-rich side	Too small to be characterized							
2	Dark grey in the interface	2.2	1.3	3.4	11.2	0	65.9	3.8	12.4
3	Light grey in the interface and the copper side	3.0	0.8	0	0.4	0	3.5	1.3	91.0
4	Dark grey at steel side	1.8	1.0	0.6	17.0	1.1	66.7	10.4	1.5

Table 5.5. Phase composition (wt%) of the sample treated for 100 minutes in inert conditions with agitation.

Phase	Description	C	O	S	Cr	Mn	Fe	Ni	Cu
1	White at copper-rich side	Too small to be characterized							
2	Dark grey in the interface	2.7	0.8	1.9	3.4	0	66.9	12.6	13.3
3	Light grey in the interface and the copper side	4.3	0.6	0.7	1.2	0.1	4.3	2.1	86.7
4	Dark grey at steel side	2.7	3.8	0.5	16.9	0.6	64.8	10.8	2
5	Black at copper-rich side	4.8	9.4	0.2	5.3	0.4	19.3	1.6	59.1

Table 5.6. Phase composition (wt%) of the sample treated for 20 minutes in oxidizing conditions with agitation.

Phase	Description	C	O	S	Cr	Mn	Fe	Ni	Cu
1	White at copper-rich side	Too small to be characterized							
2	Dark grey in the interface	2.3	5.4	0.5	7.7	0.5	33.6	8.7	41.3
3	Light grey in the interface and the copper side	3.6	2.6	0	0.6	0	3.6	6.2	83.6
4	Not clearly identified	1.1	0.5	0.7	18.2	1.4	68.6	9.6	0
5	Black at copper-rich	2.1	26.1	0.3	4.9	0.3	38.4	2.2	25.8

Table 5.7. Phase composition (wt%) of the sample treated for 40 minutes in oxidized conditions with agitation.

Phase	Description	C	O	S	Cr	Mn	Fe	Ni	Cu
1	White at copper-rich side	Too small to be characterized							
2	Dark grey in the interface	3.2	15.0	0.3	3.2	0.1	47.1	10.9	20.5
3	Light grey in the interface and the copper side	3.0	2.9	0.1	1.1	0.0	9.7	9.4	73.8
4	Not clearly identified	2.2	0.7	0.7	17.3	1.0	67.5	10.3	0.6
5	Black at copper-rich	4.5	22.0	0.3	2.9	0.1	36.3	14.6	19.5

As an austenitic material, 316L stainless steel is particularly resistant to different types of environments [1987Fon], including chemical and thermal, because of the presence of nickel which stabilises austenite and eliminates galvanic microcells, and chromium which protects the material from corrosion. It is recommended for more severe corrosion conditions such as those encountered in the process industries [1987Fon]. Based on these properties, this study was initiated to identify whether the steel could withstand the conditions encountered in copper melting. If so, it could be a substitute for mild steel, which was used at the Tsumeb smelter for copper converting. Although the cost of the lances was not high, their replacement involves time, and a different use of the well trained artisans and more skilled operators, thus, longer lasting lances would be advantageous.

A prototype of the lance taken from Tsumeb after four days operation was analysed and compared to the lab trial lance. Stainless steel lances and crucibles were subjected to molten copper at 1200°C in a variety of conditions in 15 experiments. Blister copper was melted at 1200°C in 316L stainless steel crucibles so that the interactions between copper and the stainless steel could be studied.

All the copper samples were immediately covered with metallurgical coke after melting, to protect them from oxidation. The crucible was also filled with coke immediately after casting and allowed to cool in air. Noticeable amounts of carbon and oxygen were detected in the samples, including those treated in inert conditions. Except for the fact that carbon from the coke might have diffused rapidly into the copper, from the copper-rich to the iron-rich side, carbon dioxide and oxygen from the air might have contributed to the amounts detected.

SEM-BSE and EDX were used to determine the microstructures and the compositions as well as element composition profiles. Five phases were identified in the interface with different compositions of elements. Comparison to the phase diagrams Fe-Cu [2001Tur], Cu-Ni [1991Nas], Cu-Cr [1997Oka] and Cu-Fe-Ni [2008Gal] showed that these apparent phases were not independently different, but just different compositions along the miscibility gap. The interface comprised three different zones, the copper-rich, the iron-rich and the interface itself between these two regions. Most of these phases were located at the copper-rich zone. This resulted from atomic diffusion from the iron-rich to the copper-rich zone. However, copper also penetrated stainless steel, thus degrading it. Carbon was also found in the interface as shown in the different phases in Tables 5.2-5.6, but its amount was too high to come from the stainless steel, and probably came from the coke. Carbon being a small atom would diffuse much quicker than all the other elements in this study. Being a strong reducer, carbon might have reduced some metal oxide from the slag and reverse the oxidation process between metallic and oxide phases. However future studies need to be done in order to identify the different phases by XRD.

Based on thermodynamic data [2004Shil], related to stability of different oxides, namely free energies, partial pressure, operating temperature, it was suggested that copper, nickel, chromium as well iron were selectively oxidised due to the oxygen presence.

The oxidizing conditions gave slag near the interface and reduced the copper content of the blister copper to approximately 94 wt%. The slag formation stopped blister copper from being poured, and after 60 minutes, no copper could be poured. In the test conditions, the contact area between blister copper and stainless steel was higher than in the actual plant operating conditions, this was due to the melting being done in stainless steel crucibles. In plant conditions, 28 tuyeres were destroyed after 672 copper tons melted and could have resulted in impurities contamination of 4.49 ppm, therefore the copper contamination was negligible.

The results of this study have shown the limitation of 316L stainless steel in these severe conditions. Copper was not detected at the iron-rich side and Ni, Cr, Fe were not detected at the copper-rich side, the inter-diffusion was limited to the interface for the samples melted in inert conditions without agitation. Nickel, iron and chromium were found in the copper-rich zone after melting in inert conditions with agitation, while copper penetrated the stainless steel along the grain boundaries. The concentration gradient from the iron-rich side to the copper-rich side showed that these elements (Ni, Fe, Cr) diffused from stainless steel to blister copper, while copper diffused in the opposite direction. The same metals, as well as copper, were found in the darker phase that contained most of the oxygen. It was found that oxygen selectively oxidized Ni, Fe, Cr, Cu and the resulting oxide phase was identified as slag. The 316L stainless steel was thus found not appropriate material to replace mild steel as used at the Tsumeb Custom Smelter. 316L stainless steel should not be considered as substitute to mild steel, be it for lances or the sides of the furnaces used to hold the molten copper when the gas supply to the furnace contains oxygen. In oxidizing environments, it is recommended to use lances made of silicon carbide for its established resistance to corrosion and abrasion at higher temperatures [1990For]. Copper melting can be done in inert conditions without agitation with lances made of 316L stainless steel. Copper penetration was the only mode of stainless steel reaction. However, where agitation is needed, stainless steel is not the recommended material, either for manufacturing the lances or the furnaces in temperatures as high as 1200°C. If used, direct contact with copper must be avoided by surrounding it with more corrosion-resistant materials like silicon carbide.

CHAPTER 6: CONCLUSIONS AND RECOMMENDATIONS

6.1. Blister copper contamination

Melting copper in 316L stainless steel at 1200°C in inert conditions without agitation did not have an effect on the original composition of the blister copper: none of the components of stainless steel was found in the cast blister copper.

The composition of the cast blister copper varied during melting in inert conditions with agitation. Nickel and iron were detected in the cast blister copper, but chromium was not. Nickel was identified after 20 minutes melting, the concentration increased and reached a maximum at 0.26 wt%. After 80 minutes it increased again. From 20 minutes of melting, nickel was diffusing from stainless steel to blister copper while the interface was forming at the same time. The interface growth resulted into formation of a diffusion barrier that retarded nickel diffusion. Interdiffusion of elements mainly occurred in the interface neighbourhood, as well as further away.

In addition, when the lance is attacked, copper is automatically contaminated, which is unacceptable for the product. International standards have limited the maximum level of contamination that, if exceeded, involves direct penalties on the overall market value.

Iron started appearing in the copper after 40 minutes melting, and reached a maximum of 0.34 wt% after 60 minutes.

After melting in oxidizing conditions with agitation, nickel, iron and chromium were found in cast blister copper. Nickel concentration increased to a maximum of 3.8 wt% at 80 minutes. The oxidizing conditions gave slag near the interface and reduced the copper content of the blister copper to approximately 94 wt%. The slag formation stopped blister copper from being poured, and after 60 minutes, no copper could be poured. In the test conditions, the contact area between blister copper and stainless steel was higher than in the actual plant operating conditions, this was due to the melting being done in stainless steel crucibles. In plant conditions, 28 tuyeres were destroyed after 672 copper tons melted and could have resulted in impurities contamination of 4.49 ppm, therefore the copper contamination was negligible. Copper corroded stainless steel causing its components diffusion in opposite direction.

Chromium increased to a maximum of 4.43wt% after 60 minutes of melting.

In the experiments, agitation contributed to higher concentrations of iron, chromium and nickel into the blister copper, and it speeded up the transfer of the stainless steel components to the copper, which then decreased the copper content of the blister copper to 75%.

6.2. Interface and phase characterisation

SEM and EDX analyses were done on different samples under different conditions have shown the existence of interfaces between the blister copper and stainless steel crucibles after melting. Different apparent phases with different morphologies were identified in the interfaces at different times as a result of interaction between blister copper and 316L stainless steel. Faster cooling rates (air cooling) might have prevented nucleation and growth of some phases. Most of newly-created phases which formed were within the copper-rich matrix, and when compared to the Cu-Fe-Ni phase diagrams were found to be different compositions in the miscibility gap between fcc(Cu) and fcc(Fe). Being a highly reductant element, carbon prevented further copper oxidation by oxidizing itself. Ni, Cr, as well as Fe have more affinity for oxygen than copper, therefore no interaction between copper and slag could be predicted.

6.3 Recommendations

Copper melting can be done in inert conditions without agitation with lances made of 316L stainless steel. Copper penetration was the only mode of stainless steel reaction. However, where agitation is needed, stainless steel is not the recommended material, either for manufacturing the lances or the furnaces in temperatures as high as 1200°C. If used, direct contact with copper must be avoided by surrounding it with more corrosion-resistant materials like silicon carbide.

316L stainless steel should not be considered as substitute to mild steel if the gas supply to the furnace contains oxygen. In oxidizing environments, silicon carbide is recommended for its established resistance to corrosion, abrasion at higher temperatures.

Further studies need to be done in order to identify the different phases by XRD.

REFERENCES

[1941Gla] S. Glasstone, K.J. Laidler and H. Eyring, The theory of rate processes, McGraw-Hill, New York, USA (1941).

[1953Hum] W. Hume-Rothery, J.W. Christian and W.B. Pearson, Metallurgical Equilibrium Diagrams, Institute of Physics, London, pp. 97-108 (1953).

[1956Mor] J.P. Morris and G.R. Zellers, Vapor pressure of liquid copper and activities in liquid iron – copper alloys, Met. Trans. AIME, vol. 8, pp. 1086-1091 (1956).

[1962Pal] E. Palmer, Structure and properties of binary metallic systems, Plenum publishing corporation, Moscow, vol. 2 (1962).

[1963Eva] U.R. Evans, An Introduction to Metallic Corrosion, 2nd Edn., Edward Arnold, London, UK (1963).

[1967Har] H. Schonhorn, Surface tention-viscosity relationship for liquids, Journal of Chemical Engineering Data, vol. 12, pp. 524-525 (1967).

[1973Uhl] H.H. Uhlig, Corrosion and Corrosion Control, 2nd Edn., Wiley, New York, USA (1971).

[1973Mie] A.R. Miedema, Electronegativity parameter for transition metals: Heat of formation and charge transfer in alloys, J. Less-Common Met., vol. 32, pp. 117-136 (1973).

[1976Che] N.Y. Chen, Bond parameter functions and their application, Science Press, Beijing, China (1976).

[1976Dav] W.G. Davenport and A.K. Biswas, Extractive Metallurgy of Copper, 1st Edn., Pergamon Press Ltd. Oxford (1976).

[1977Aus] Y.C. Austin, D. Goldeberg and J.P. Neumann, Phase Diagrams and Thermodynamic Properties of Ternary Copper-Silver Systems, Journal of Physical Chemistry, vol. 6, p. 3 (1977).

[1977Bar] R.G. Barton and J.K. Brimacombe, Influence of surface tension-driven flow on the kinetics of oxygen absorption in molten copper, Metallurgical Transactions B, vol. 8B, p. 417 (1977).

[1977Hil] J.H. Hildebrand, Viscosity and diffusivity, A predictive treatment, Wiley-Interscience, New York, USA (1977).

[1977Sal] G. Salje and M. Feller-Kniepment, The diffusion and solubility of copper in iron, Journal of Applied Physics, vol. 48, pp. 1833-1839 (1977).

[1980Bat] G.I. Batalin and V.S. Sudavtsova, Thermodynamic properties of liquid Fe-Cu alloys, Izv.Akad, Nauk SSSR, Metally, vol. 2, pp. 45-49 (1980).

[1982Alo] J.A. Alonso and N.H. March, Simple model for liquid metal alloys and relation to Miedema's variables, Elsevier B.V, Spain (1982).

[1984Cha] D.J. Chakrabarti and D. E. Laughlin, Bull. Alloy phase diagrams, vol. 5, pp. 59-68 (1984).

[1987Fon] Mars G. Fontana, Corrosion Engineering, McGrall-Hill, 3rd Edn., New York, USA (1986), pp. 78, 79, 90, 91, 226, 229, 231, 307.

[1987Hua] L.J. Huang, B.X. Liu and H.D. Li, Amorphization in Fe-Cu System by tracing its Microscopic Features, Applied Physics A, Springer-Verlag, vol. 44, pp. 269-272 (1987).

[1987Mun] A. Munitz, Liquid separation effects in Fe-Cu alloys solidified under different cooling rates, Metallurgical Transactions B, vol. 18B, pp. 565-575 (1987).

[1988Roy] A.K. Roy and R.P. Chhabra, Prediction of solute coefficient in liquid metals, Metallurgical Transactions A, vol. 19A, pp. 273-274 (1988).

[1989Par] Y.G. Park and D.R. Gaskell, The thermodynamic activities of copper and iron in the system copper-iron-platinum at 1300°C, Metallurgical Transactions B, 20B, No. 2, pp. 127-135 (1989).

[1990For] R. J. Fordham, High Temperature Corrosion of Technical Ceramics, Elsevier Science Publisher ltd, England (1990).

[1990Lew] M. Lewis and G. Waller, Advancing Chemistry, Oxford University Press, Oxford, UK, p. 117 (1982).

[1992Mie] A.R. Miedema, Energy effects and charge transfer in metal physics; modelling in real space, Physica B, vol. 182, pp. 1-17 (1992).

[1993Atz] E. Ma. M. Atzmon, E.E. Pinkerton, Thermodynamic and magnetic properties of metastable Fe_xCu_{100-x} solid solutions formed by mechanical alloying, Journal of Applied Physics, vol. 74, p. 955 (1993).

[1994Atk] P.W. Atkins, Physical Chemistry, Oxford University Press, Oxford (1990), pp. 230-231.

[1994Hig] R.A. Higgins, Properties of Engineering Materials, 2nd Edn., McGraw Hill, New York, USA (1994).

[1995Qin] Q. Chen and Z. Jin, The Fe-Cu system: A thermodynamic evaluation, Met. Trans. A, vol. 26A, pp. 417-426 (1995).

[1995Zen] K. Zeng and M. Hamalainnen, Thermodynamic analysis of stable and metastable equilibrium in the Cu-Cr system, vol. 19, pp. 93-104 (1995).

[1997Guo] Guo Jin, Li Chongonghe, Qin Pei and Chen Nianyi, Formability criterion of intermetallic compounds containing transition metal systems, Trans. Nonferrous Met. Soc, vol. 7, no. 3, pp. 135-138 (1996).

[1997Oka] H. Okamoto, Phase Equilibria, ASM International, vol. 18, p. 220 (1997).

[2000Lin] C.B. Lin and J.S. Ho, The effect of continuous cooling heat treatment on interface properties of SK3/copper compound casting, Journal of Materials Engineering and Performance, vol. 9, no. 1, pp. 81-87 (2000).

[2001Rag] V. Raghavan, Cr-Cu-Fe (Chromium-Copper-Iron), Journal of Phase Equilibra and Diffusion, ASM International, vol. 25, no. 6, p. 544 (2004).

[2001Tur] M.A. Turchanin and P.G. Agraval, Thermodynamics of liquid alloys, and stable and metastable phase equilibra in the copper – iron system, Poroshkovaya Metallutgiya, vol. 40, no. 7-8, pp. 34-53 (2001).

[2001Yao] L. Yao, J. Yang, C. Ye and N. Chen, Regularity of formation of binary intermetallic compounds between transition and non transition elements, Chinese Science Bulletin, vol. 46, no. 21, pp. 1845-1848 (2001).

[2002Gup] K.P. Gupta, The Cu-Ni-Ti system, Journal of Phase Equilibria, vol. 23, p. 541 (2002).

[2002Pre] A.A. Presnyakov, B.K. Kenzahaliev, S.M. Kozhakhmetov, A.V. Panichkin and S.V. Ponomareva, High Temperature “Superfluidity” of copper, Metal Science and Heat Treatment, Plenum Publishing Corporation, vol. 44, no 1-2, p. 79 (2002).

[2003Tru] Trudeau Zywice, the New Encyclopaedia Britannica, The River Publishing company, vol. 12, p. 395 (2003).

[2004Dav] W.G. Davenport, M. King, M. Schlesinger and A.K. Biswas, Extractive Metallurgy of Copper, 4th Edn., Elsevier Science Ltd., United Kingdom (2004).

[2012Rag] V. Raghavan, Cu-Fe-Ni (Copper-Iron-Nickel), Journal of Phase Equilibra and Diffusion, in press.

[2004Shi] S. Shigeru, T. Kimura, E. Masatoshi, M. Masazumi, Y. Waseda, Characteristic depth profiles of surface layers formed in Cu-based alloys by annealing in low partial pressure of oxygen, Materials Transactions, vol. 45, no 2, pp. 411-414 (2004).

[2004Wan] C.P. Wang, X.J. Liu, I. Ohnuma, R. Kainuma and K. Ishida, Thermodynamic database of the phase diagrams in Cu-Fe base ternary systems, Journal of Phase Equilibria and Diffusion, vol. 25, no 4, pp. 320-321 (2004).

[2005Ken] Kenneth G. Budinski and Michael K. Budinski, Engineering Materials: Properties and Selection, 8th Edn., Pearson Education, Inc. and Dorling Kindersley, India (2005).

[2005Mar] T. Main and T. Utigard, The kinetics and mechanism of molten copper oxidation by top blowing of oxygen, Journal of Materials, vol. 57, p.1 (2005).

[2006Ash] F. Michael Ashby and R.H. David Jones, Engineering Materials, 3rd Edn., Butterworth-Heinemann, United States of America, (2006).

[2006Cha] D. Charalambous, P.C. Henrdry, M. Holmes, G.G. Ihas, P.V.E. McClintock and L. Skrbek, Quantum turbulence in ^{4}He, oscillating grids, and where do we go next? Journal of Low Temperature Physics, vol. 145, no. 1-4, p. 109 (2006).

[2006He] J. He, J.Z. Zhao and L. Ratke, Solidification microstructure and dynamics of metastable phase transformation in undercooled liquid Cu-Fe alloys, Acta Materialia, vol. 54, pp. 1749-1757 (2006).

[2006Tak] N. Takeshi, A. Yokoyama and Y. Umakoshi, Formation of Nanocrystalline Globules and Metallic glass in $Fe_{70-x}Cu_xZr_{10}B_{20}(x = 0 - 70)$ alloys, vol. 47, pp. 1105 to 1114, (2006).

[2006Was] Y. Waseda, S. Suzuki, Characterization of corrosion products on steel surfaces, spinger, Berlin Heidelberg, p. 132, (2006).

[2007Wan] Y. Qing Wang, Y. Qin Wu and X.F. Bian, Composition dependence of viscosity for $Al_{(1-x)}Mg_x$, alloys, Chinese Science Bulletin, vol. 52, pp. 1441-1445 (2007).

[2007Zha] J. Zhang, Y.S. Shi, J.H. Liu, K.H. Chen and S.H. Huang, Investigation into manufacturing Fe-Cu-C alloy parts through indirect selective laser sintering, Materials Science and Technology, vol. 23, no. 3 (2007).

[2008Gal] I. Gallino, S. Curiotto, M. Baricco, E.M. Kassner and R. Busch, Homogenization of highly alloyed Cu–Fe–Ni: A phase diagram study, ASM International, vol. 29, no. 2, pp. 131-135 (2008).

[2008Vin] E. Vincent, C.S. Becquart, C.Pareige, P. Pareige and C. Domai, Precipitation of the FeCu system : A critical review of atomic kinetic Monte Carlo simulations, Journal of Nuclear Materials, vol. 373, pp. 387-401 [2008].

[2009Sil] G.I. Sil'man, About retrograde solidus and stratification of melt in the Fe–Cu and Fe–Cu–C systems, Metal Science and Heat Treatment, vol. 51, no. 1-2, pp. 19-24 (2009).

[2010Mic] G.B. Mi, P.J. Li, N. Yu. Konstantinova and L.J. He, Structure and properties of metal melt III-Relationship between kinematic viscosity and size of atomic clusters, Science China: Physics, Mechanics and Astronomy, vol. 53, no.11, pp. 2054-2058 (2010).

[2010Ole] B. Oleksiak, G. Siwiec, A. Blacha and J. Lipart, Influence of iron on the surface tension of copper, International Scientific Journal, vol. 44, pp. 39-42 (2010).

[2012Sal] G. Salje, M. Feller-Kniepment, The diffusion and solubility of copper, Journal of Applied Physics, vol. 49, pp. 229-232 (2012).

[2012Liu] N. Liu, Investigation on the phase separation in undercooled Cu-Fe melts, Journal of Non-Crystaliline solids, vol. 358, pp. 196-199 (2012).

APPENDICES

Appendix A

Table A.1. EDX Spot analyses (wt%) for the sample treated 40 minutes in inert conditions without agitation.

Element	C	O	S	Cr	Mn	Fe	Ni	Cu	Total
Sum spectrum sample 2	7.16	3.17	0.78	7.71	0.26	21.00	2.31	57.62	100.00
s2-SPTX1-1000X	19.26	0.93	0.00	0.16	0.00	1.40	0.00	78.24	100.00
s2-Sptx2	21.23	1.78	0.14	0.26	0.00	2.42	0.37	73.80	100.00
S2-sptx3	26.49	1.14	0.00	0.15	0.00	1.74	0.28	70.20	100.00
S2-sptx4	31.40	1.24	0.24	0.30	0.00	3.04	0.23	63.55	100.00
S2-sptx5	12.36	0.50	0.00	0.40	0.00	3.98	0.33	82.43	100.00
S2-sptx6	9.44	0.43	0.00	0.42	0.00	3.97	0.34	85.39	100.00
S2-sptx7	9.55	1.59	1.31	5.22	0.00	32.81	0.97	48.56	100.00
S2-sptx8	6.18	0.77	0.63	16.24	1.01	64.49	9.58	1.10	100.00
S2-sptx9	13.05	0.97	0.56	15.34	0.91	60.20	8.98	0.00	100.00
S2-spotx10	4.64	0.40	0.69	16.97	1.14	66.65	9.52	0.00	100.00
s2-spot1-2k	11.09	0.83	0.00	0.22	0.00	2.01	0.00	85.85	100.00
s2-spot2	8.93	0.72	0.10	0.20	0.00	2.55	0.37	87.15	100.00
s2 spot3	4.66	0.68	4.41	12.54	0.00	72.33	1.05	4.34	100.00
s-2 spot4	10.39	0.68	0.00	0.32	0.00	4.07	0.32	84.22	100.00
s2-spot5	9.64	0.93	0.00	0.23	0.00	2.35	0.37	86.49	100.00
s2-spot6	14.88	0.91	3.00	7.65	0.00	42.74	0.76	30.06	100.00
s2-spot7	4.69	0.70	3.70	10.99	0.00	63.26	0.76	15.89	100.00
s2-spot8	7.40	0.72	1.09	3.44	0.00	19.66	0.53	67.18	100.00
s2-spot9	20.84	3.70	0.53	3.35	0.00	18.41	0.40	52.75	100.00
s2-spot10	2.83	0.00	0.66	17.07	1.05	66.88	9.85	1.66	100.00
Mean	12.19	1.09	0.85	5.67	0.21	26.47	2.25	51.26	100.00
Std. deviation	7.64	0.88	1.27	6.52	0.41	27.72	3.63	34.01	
Max.	31.40	3.70	4.41	17.07	1.14	72.33	9.85	87.15	
Min.	2.83	0.00	0.00	0.15	0.00	1.40	0.00	0.00	

Table A.2. EDX Spot analyses (wt%) for the sample treated 80 minutes in inert conditions without agitation.

Spectrum	.	C	O	S	Cr	Mn	Fe	Ni	Cu	Total
Sum Spectrumsample4		3.49	2.02	0.31	7.36	0.38	26.56	3.60	56.29	
s4-spotx1		2.90	0.53	0.00	0.13	0.00	2.91	0.98	92.55	
S4-spotx2		4.12	0.38	0.00	0.17	0.00	2.92	1.02	91.38	
S4-spotx3		2.24	0.48	0.00	0.17	0.00	3.83	0.84	92.44	
S4-spotx4		1.54	0.41	0.93	1.30	0.00	26.82	2.32	66.68	
S4-spotx5		2.77	0.64	0.15	0.26	0.00	6.07	1.12	88.99	
S4-spotx6		1.80	0.41	0.65	17.43	1.22	67.32	10.17	1.00	
S4-spotx7		1.70	0.68	0.66	17.64	1.06	68.37	9.89	0.00	
S4-spotx8		1.91	0.70	0.69	17.25	1.05	67.45	9.92	1.02	
S4-spot1		3.62	0.00	0.00	0.00	0.00	2.98	1.02	92.38	
s4-spot2		2.57	0.47	0.00	0.00	0.00	5.20	1.78	89.98	
S4-spot3		2.02	0.49	0.85	15.80	0.99	68.20	10.14	1.52	
s4-spot4		3.62	0.00	0.17	0.27	0.00	8.51	1.93	85.50	
s4-spot5		1.82	0.00	2.90	3.25	0.00	74.76	5.72	11.55	
s4-spot6		1.91	0.56	1.16	7.12	0.19	73.26	7.56	8.24	
s4-spot7		1.30	0.00	0.63	17.71	1.18	68.80	10.39	0.00	
s4-spot8		1.45	0.77	0.66	17.52	1.18	67.97	10.45	0.00	

Table A.3. EDX Spot analyses (wt%) for the sample treated 60 minutes in inert conditions with agitation. Sample 8, line scan composition

Spectrum	C	O	S	Cr	Mn	Fe	Ni	Cu	
Line scan sample 8	2.48	1.67	0.53	5.97	0.23	23.79	2.99	62.34	
s-8-spot-1	3.44	1.41	0.00	0.46	0.00	4.31	1.57	88.81	
s-8-spot2	3.15	1.56	1.32	4.06	0.00	24.26	1.79	63.86	
s-8-spot3-1kx	1.95	0.77	3.53	11.87	0.00	72.72	4.62	4.52	
s-8-spot4-1kx	2.10	5.87	0.62	16.02	1.07	60.59	8.94	4.80	
s-8-spot5-1k	2.72	0.52	0.00	0.37	0.00	3.01	0.77	92.62	
s8-spot7-1k	3.64	0.77	5.08	12.12	1.11	49.05	3.13	25.10	
s-8-spot8-1k	2.29	1.72	3.30	10.54	0.00	59.08	2.91	20.16	
s8-spot6-1k	2.82	0.57	0.00	0.30	0.00	3.21	1.46	91.64	
s-8-spot10-1k	2.00	1.13	0.60	16.84	1.11	66.50	10.35	1.47	
s8-spot11-1k	1.69	0.89	0.64	17.05	1.13	66.92	10.28	1.41	
S8-spt x1	3.38	0.53	0.00	0.42	0.00	2.57	0.90	92.20	
S8-spt x2	2.81	1.22	0.00	0.45	0.00	4.29	1.77	89.46	
S8-sptx3	2.42	0.97	3.19	11.06	0.00	68.96	4.25	9.16	
S8-sptx4	2.66	0.90	3.82	10.73	0.00	64.78	3.37	13.73	
S8-sptx5	2.22	1.66	3.56	11.05	0.00	66.41	3.93	11.18	
S-8 sptx6	2.58	1.36	0.70	17.23	1.07	66.17	9.58	1.32	
S8-sptx7	1.90	0.92	0.68	17.18	1.14	66.97	9.92	1.29	
S8-sptx8	2.02	0.98	0.63	17.08	1.13	66.61	9.97	1.58	
Mean	2.54	1.35	1.44	9.34	0.41	43.20	4.77	36.95	100.00
Std. deviation	0.55	1.14	1.63	6.56	0.53	27.98	3.56	37.98	
Max.	3.64	5.87	5.08	17.23	1.14	72.72	10.35	92.62	
Min.	1.69	0.52	0.00	0.30	0.00	2.57	0.77	1.29	

Table A.4. EDX Spot analyses (wt%) for the sample treated 100 minutes in inert conditions with agitation.

Elements	C	O	S	Cr	Mn	Fe	Ni	Cu
S10 spotX 1	2.93	1.15	0.77	1.47	0.00	13.14	2.59	77.96
S10-spot x2	2.10	0.74	0.90	11.84	0.51	67.26	10.18	6.46
S10-potx3	1.96	2.37	0.60	16.63	1.03	66.05	9.68	1.68
S10-spot4	2.01	1.41	0.65	16.99	1.11	66.55	9.96	1.32
S10-spotx5	2.05	4.20	0.65	16.36	1.18	62.62	8.99	3.94
S10-spotx6	3.14	0.82	0.67	17.27	1.12	67.00	9.98	0.00
S10-spotx7	3.36	3.26	0.23	1.97	0.00	12.95	1.84	76.40
s-10-X8	2.08	0.40	2.03	2.60	0.00	66.86	11.52	14.52
S10-spotx9	3.10	10.93	0.18	11.90	0.19	6.80	0.77	66.13
S10-spotx10	6.30	18.76	0.10	15.42	1.22	22.00	0.99	35.20
S10-spotx11	2.98	13.86	0.00	12.02	0.20	6.82	0.31	63.82
S10-spotx12	3.30	19.62	0.00	10.90	0.55	13.13	0.35	52.15
S10-spotx13	4.65	20.62	0.94	14.27	0.26	11.52	0.25	47.49
S10-spotx14	3.43	12.26	0.00	3.66	0.22	7.52	0.21	72.70

Table A.5. EDX Spot analyses (wt%) for the sample treated 20 minutes in oxidizing conditions with agitation.

Spectrum	In stats.	C	O	S	Cr	Mn	Fe	Ni	Cu	Total
S11-X1		4.09	7.80	0.00	5.78	0.81	53.65	1.78	26.08	100.00
S11-X2		4.76	28.70	1.40	3.08	0.34	38.70	4.45	18.57	100.00
S11-X3		4.40	34.24	0.48	2.95	0.00	19.97	6.42	31.54	100.00
S11-X5		2.25	0.64	0.68	16.69	1.21	67.06	10.26	1.20	100.00
S11-X6		1.68	0.94	0.64	17.38	1.17	67.33	9.57	1.29	100.00
S11-X7		2.06	0.66	0.61	17.42	1.13	67.84	9.31	0.97	100.00
S11-X8		1.60	1.13	0.53	17.05	1.12	68.12	10.44	0.00	100.00
S11-spot iron rich		0.00	0.00	0.68	19.18	1.66	69.40	9.08	0.00	100.00
S11-spot iron rich		2.17	0.86	0.69	17.21	1.14	67.87	10.06	0.00	100.00
S11-spot grey		3.34	6.12	0.50	9.64	0.50	40.61	5.81	33.48	100.00
S11-spot whit		3.32	1.59	0.00	0.86	0.00	3.38	11.53	79.32	100.00
S11-spot blac		2.13	0.52	0.65	17.63	0.97	67.55	9.40	1.15	100.00
S11-spot white		4.73	2.83	0.00	0.67	0.00	6.36	0.83	84.59	100.00
S11-spot gre		2.11	26.06	0.31	4.93	0.27	38.37	2.15	25.79	100.00
S11-spot whi		2.85	4.89	0.00	0.47	0.00	3.13	7.07	81.59	100.00
S11-spot whitee		3.34	1.17	0.00	0.24	0.00	1.29	5.20	88.76	100.00
S-11-Spot8		2.28	5.38	0.48	7.72	0.54	33.61	8.69	41.30	100.00
S11-Spot 9		0.00	7.42	0.00	4.56	0.00	60.26	0.00	27.76	100.00

Table A.6 EDX Spot analyses (wt%) for the sample treated 40 minutes in oxidizing conditions with agitation.

Elements	C	O	S	Cr	Mn	Fe	Ni	Cu
Sum Spectrum	4.75	7.65	0.39	8.61	0.51	38.51	5.77	33.81
Spot 1	7.89	15.15	0.00	1.11	0.00	12.01	0.00	63.84
sample 12-spot8	3.49	6.41	0.00	3.26	0.00	5.59	8.10	73.15
S12-spot iron rich	2.17	0.87	0.56	17.29	0.91	67.37	10.83	0.00
S12-spot iron rich	2.00	0.51	0.68	17.17	1.08	67.60	9.70	1.25
S12-spot copper white	2.80	0.74	0.28	3.09	0.00	22.98	23.11	47.00
S12-spot 2	4.93	27.02	0.08	1.62	0.00	44.29	11.89	10.17
S12-spot white	2.91	7.40	0.00	0.29	0.00	4.39	4.91	80.11
S12-spot white	3.19	0.48	0.00	0.00	0.00	1.57	0.33	94.43
S12-spot grey interface	2.46	14.11	0.24	3.83	0.00	44.97	10.54	23.85
S12-spot grey interface	3.93	15.79	0.29	2.50	0.20	49.09	11.15	17.05
S-12 X1	4.00	0.71	0.00	0.00	0.00	1.18	0.00	94.11
S12-x2	3.98	16.93	0.39	4.21	0.20	28.17	17.31	28.81
S12-x4	3.60	5.94	0.26	2.62	0.00	8.84	4.74	73.99
S12-x5	3.00	0.78	0.16	2.18	0.00	16.79	17.94	59.15
S12-x6	2.61	0.75	0.73	17.25	1.09	66.73	9.87	0.98
S12-x7	2.17	0.79	0.66	17.39	1.11	67.85	10.02	0.00
S12-x8	1.63	0.90	0.68	17.33	1.11	67.48	9.72	1.15
Max.	7.89	27.02	0.73	17.39	1.11	67.85	23.11	94.43
Min.	1.63	0.48	0.00	0.00	0.00	1.18	0.00	0.00

Appendix B

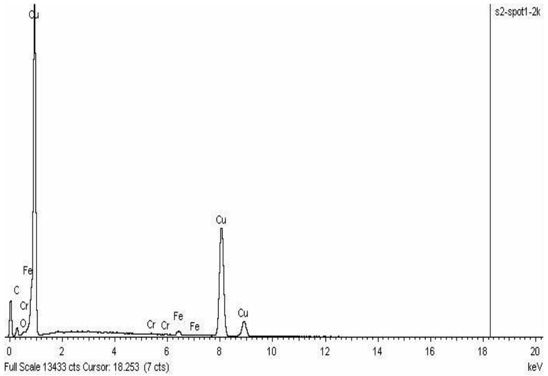

Figure B.1. EDX spectrum spot 1 of sample treated 40 minutes in inert conditions without agitation.

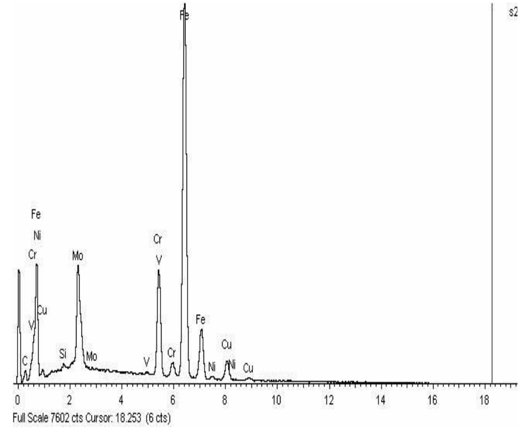

Figure B.2. EDX spectrum spot 3 of sample treated 40 minutes in inert conditions without agitation.

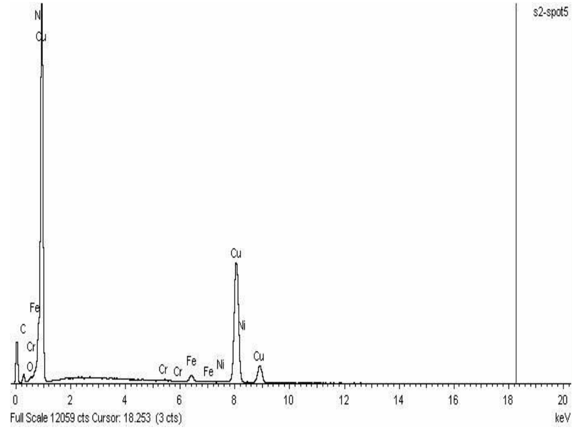

Figure B.3. EDX spectrum spot 5 of sample treated 40 minutes in inert conditions without agitation.

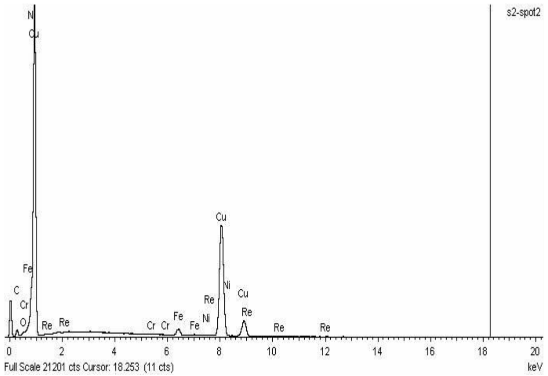

Figure B.4. EDX spectrum spot 2 of sample treated 40 minutes in inert conditions without agitation.

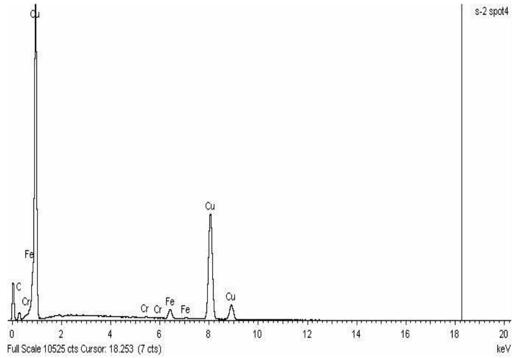

Figure B.5. EDX spectrum spot 3 of sample treated 40 minutes in inert conditions without agitation.

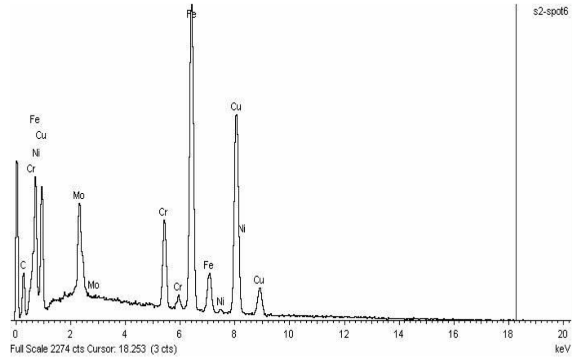

Figure B.6. EDX spectrum spot 6 of sample treated 40 minutes in inert conditions without agitation.

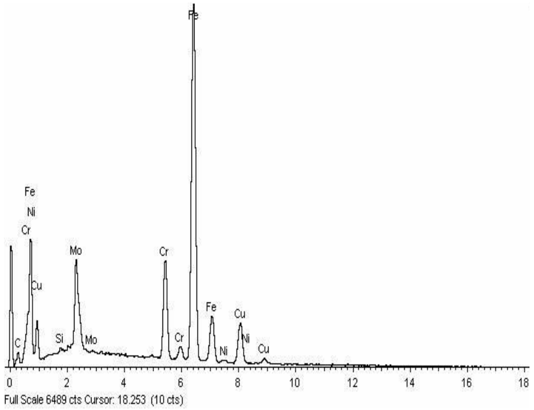

Figure B.7. EDX spectrum spot 7 of sample treated 40 minutes in inert conditions without agitation.

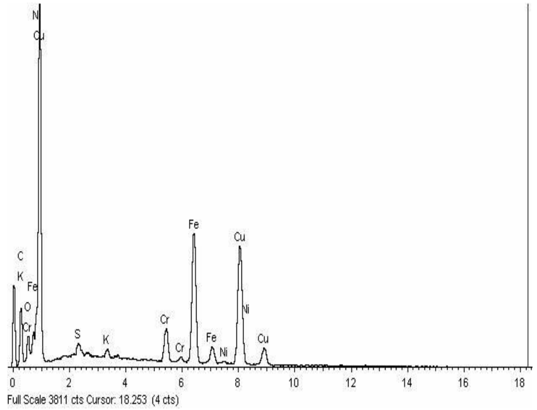

Figure B.8. EDX spectrum spot 9 of sample treated 40 minutes in inert conditions without agitation.

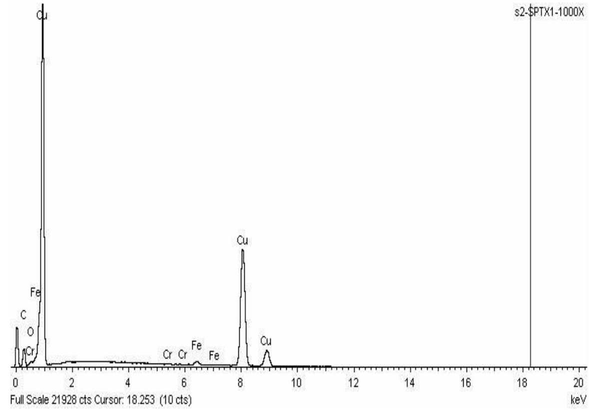

Figure B.9. EDX spectrum line can 1 of sample treated 40 minutes in inert conditions without agitation.

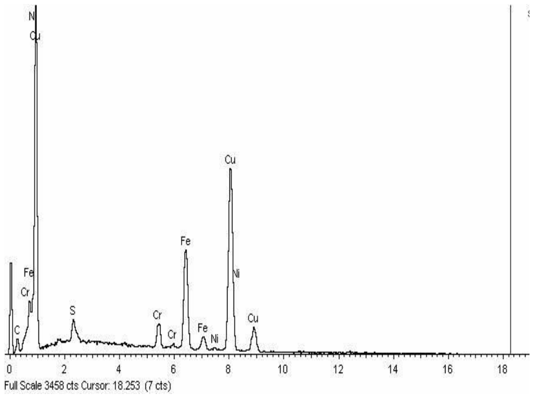

Figure B.10. EDX spectrum spot 8 of sample treated 40 minutes in inert conditions without agitation.

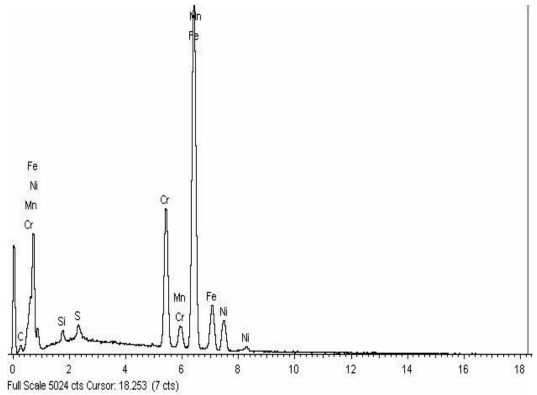

Figure B.11. EDX spectrum spot 10 of sample treated 40 minutes in inert conditions without agitation.

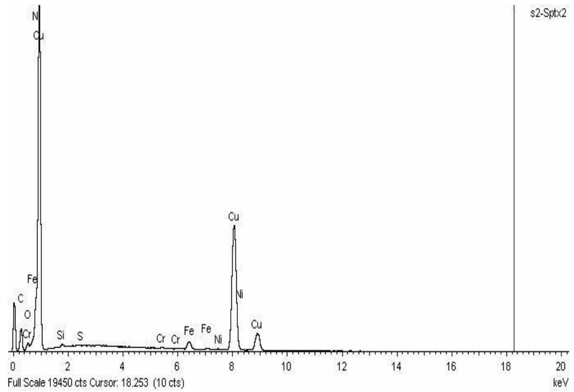

Figure B.12 EDX spectrum line scans 2 of sample treated 40 minutes in inert conditions without agitation.

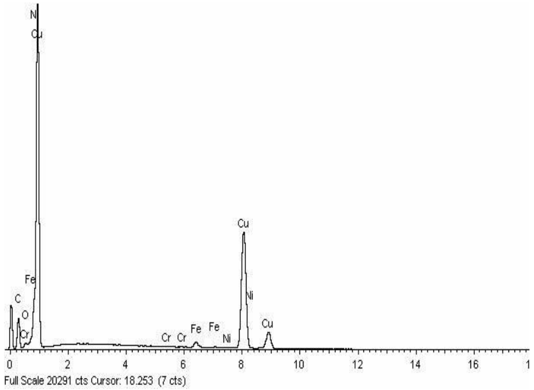

Figure B.13. EDX spectrum line scan 3 of sample treated 40 minutes in inert conditions

without agitation.

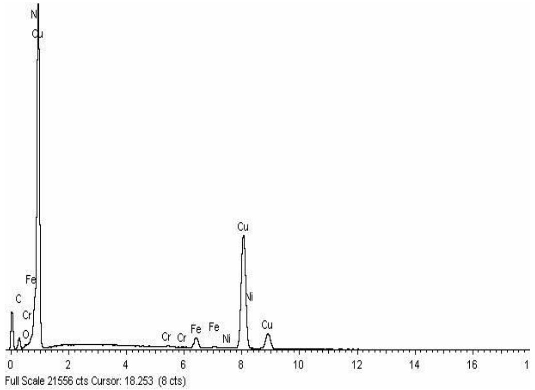

Figure B.14. EDX spectrum line scan 5 of sample treated 40 minutes in inert conditions without agitation.

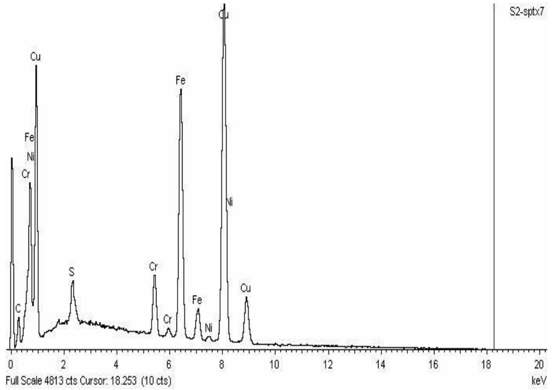

Figure B.15. EDX spectrum line scan 7 of sample treated 40 minutes in inert conditions without agitation.

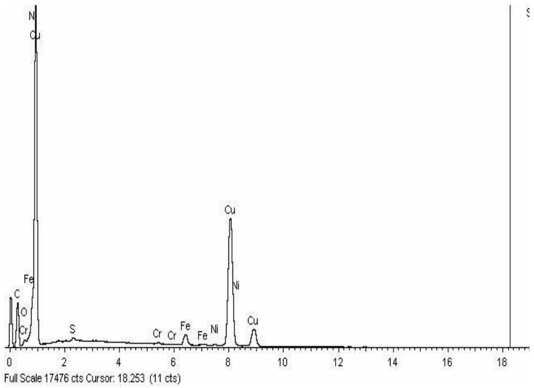

Figure B.16. EDX spectrum line scan 4 of sample treated 40 minutes in inert conditions without agitation.

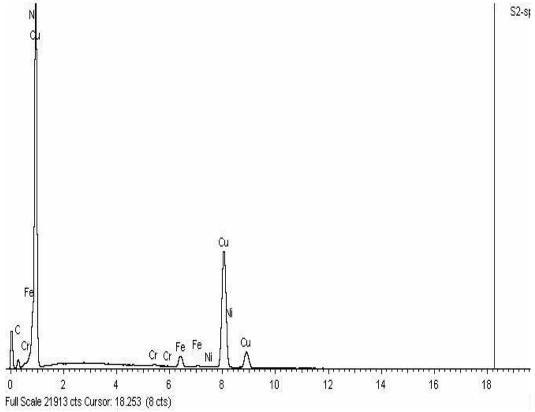

Figure B.17. EDX spectrum line scan 6 of sample treated 40 minutes in inert conditions without agitation.

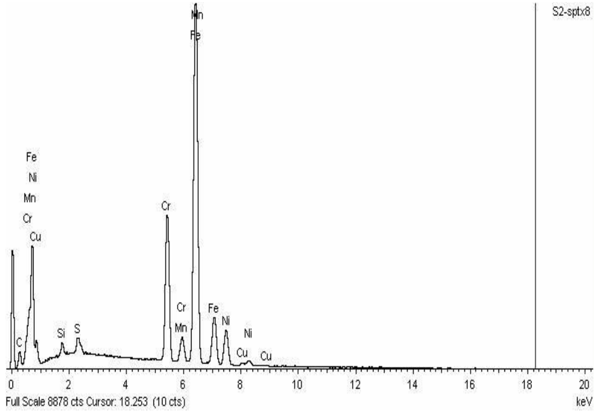

Figure B.18. EDX spectrum line scan 8 of sample treated 40 minutes in inert conditions without agitation.

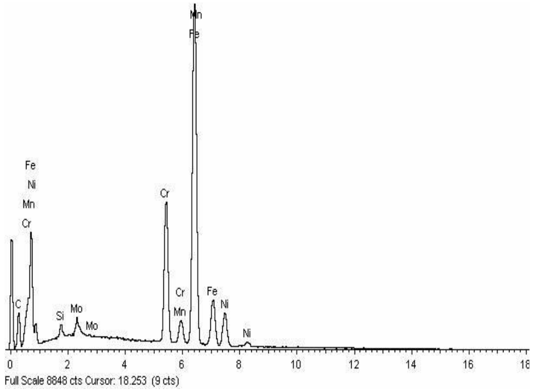

Figure B.19. EDX spectrum line scan 9 of sample treated 40 minutes in inert conditions without agitation.

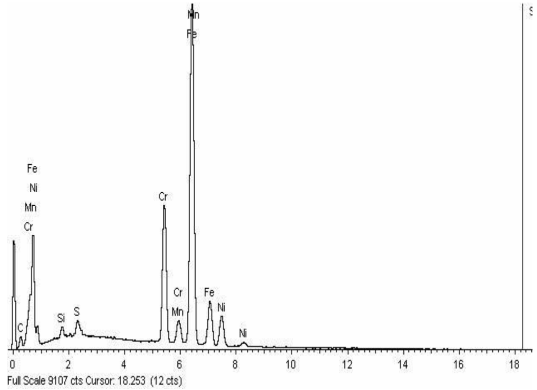

Figure B.20. EDX spectrum, line scan 10 of sample treated 40 minutes in inert conditions without agitation.

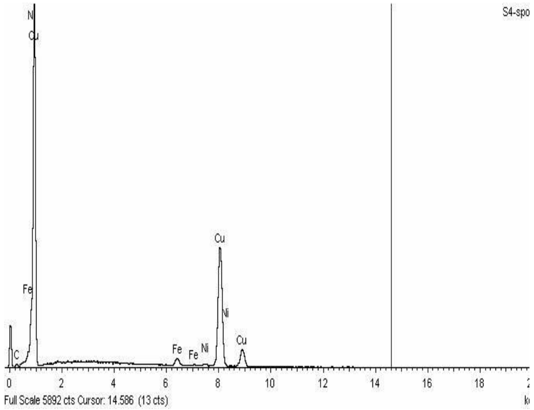

Figure C.1. EDX spectrum showing spot 1 analysis of sample treated 80 minutes in inert conditions without agitation.

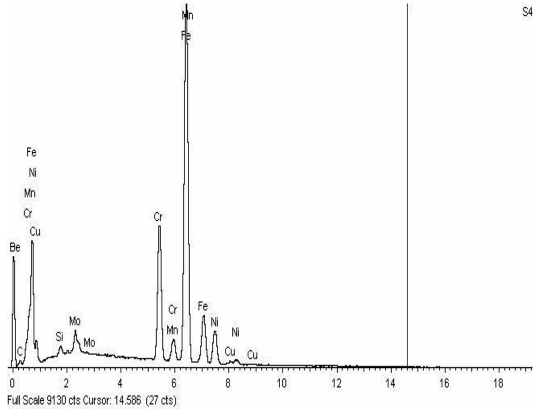

Figure C.2. EDX spectrum spot 1 of sample treated 80 minutes in inert conditions without agitation.

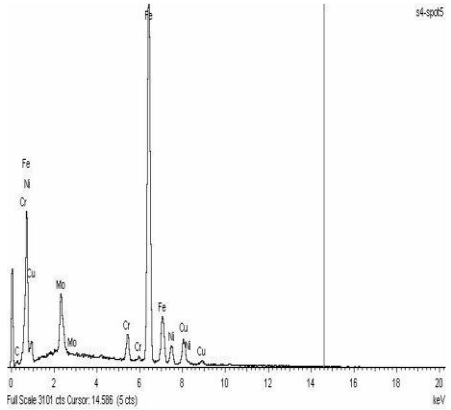

Figure C.3. EDX spectrum showing spot 1 analysis of sample treated 80 minutes in inert conditions without agitation.

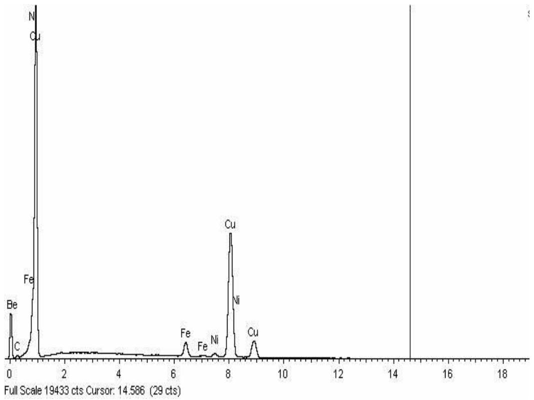

Figure C.4. EDX spectrum spot 1 of sample treated 80 minutes in inert conditions without agitation.

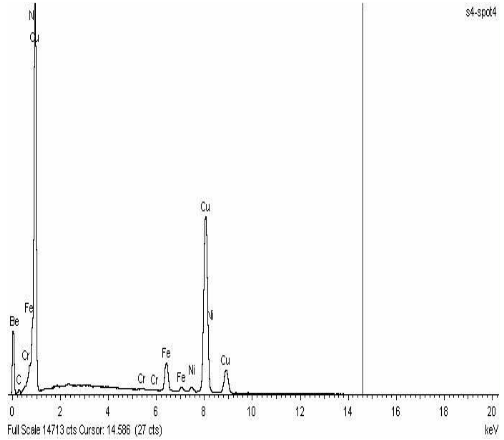

Figure C.5. EDX spectrum spot 1 of sample treated 80 minutes in inert condition without agitation.

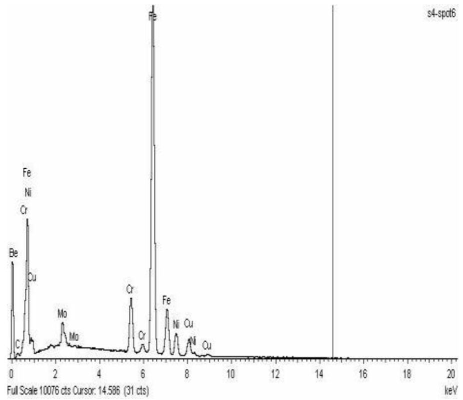

Figure C.6. EDX spectrum showing spot 6 analysis of sample treated 80 minutes in inert conditions without agitation.

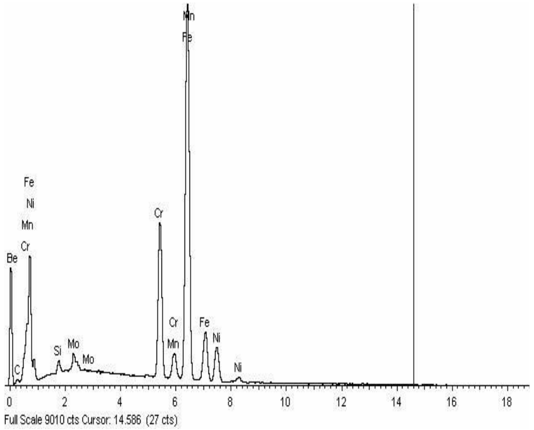

Figure C.7. EDX spectrum spot 1 of sample treated 80 minutes in inert conditions without agitation.

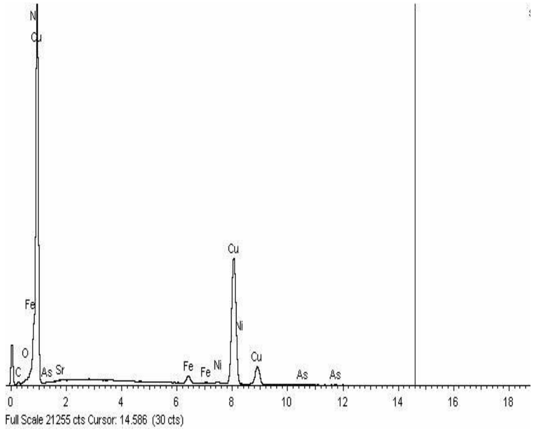

Figure C.8. EDX spectrum, line scan 1 of sample treated 80 minutes in inert conditions without agitation.

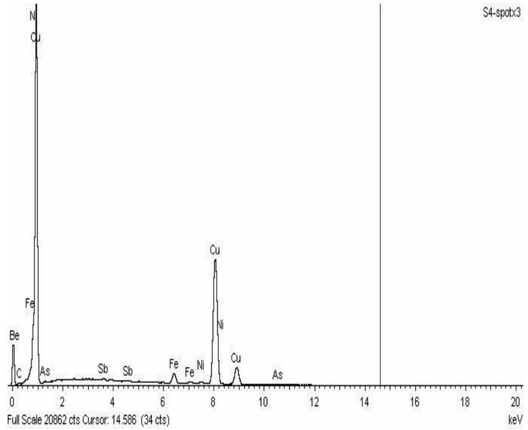

Figure C.9. EDX spectrum, line scan 3 of sample treated 80 minutes in inert conditions without agitation.

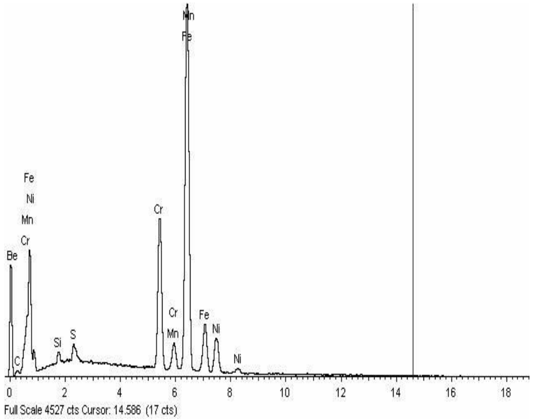

Figure C.10. EDX spectrum spot 1 of sample treated 80 minutes in inert conditions without agitation.

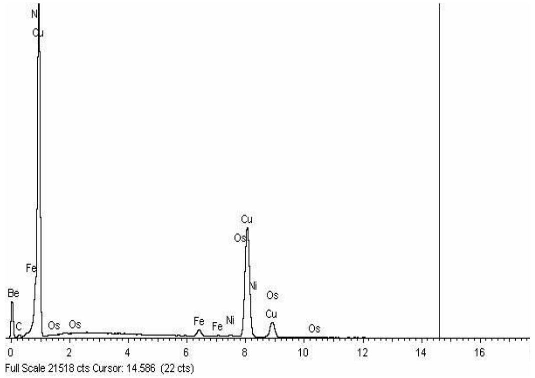

Figure C.11. EDX spectrum, line scan 2 of sample treated 80 minutes in inert conditions without agitation.

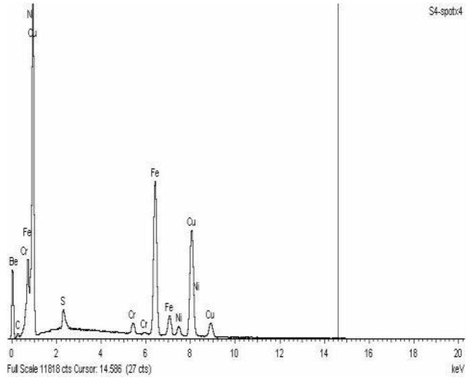

Figure C.12. EDX spectrum showing spots analysis of sample treated 80 minutes in inert conditions without agitation.

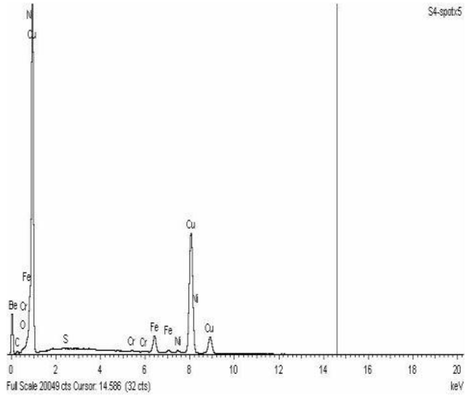

Figure C.13. EDX spectrum, line scan 5 of sample treated 80 minutes in inert conditions without agitation.

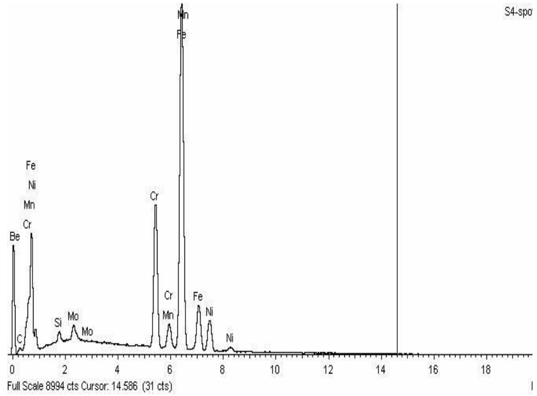

Figure C.14. EDX spectrum, line scan 7 of sample treated 80 minutes in inert conditions without agitation.

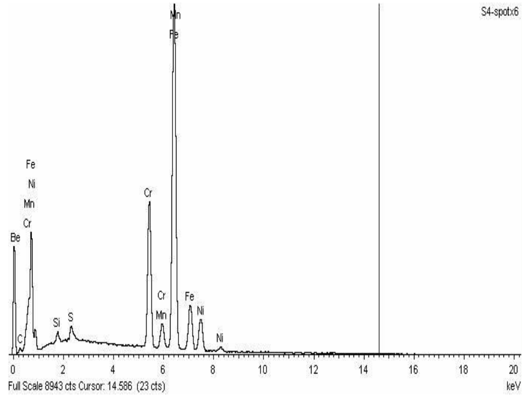

Figure C.15. EDX spectrum, line scan 6 of sample treated 80 minutes in inert conditions without agitation.

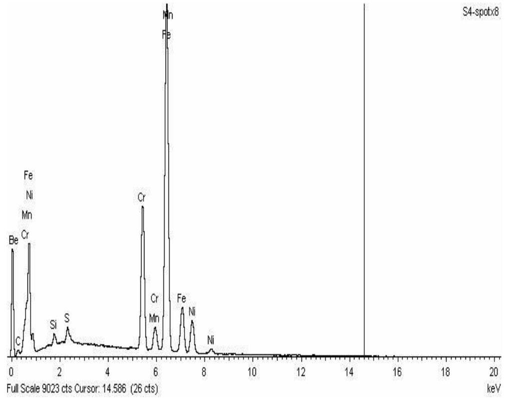

Figure C.16. EDX spectrum showing spots analysis of sample treated 80 minutes in inert conditions without agitation.

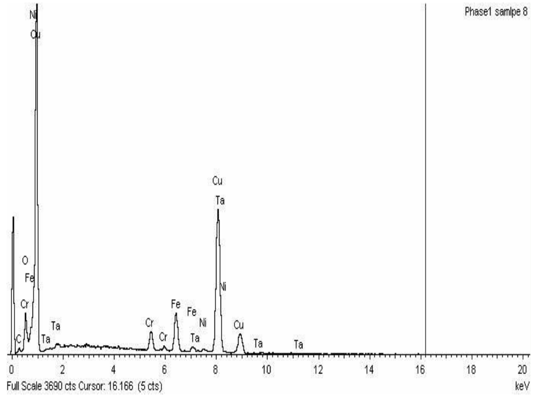

Figure D.1. Phase 1 EDX spectrum of sample treated 60 minutes in inert conditions with agitation.

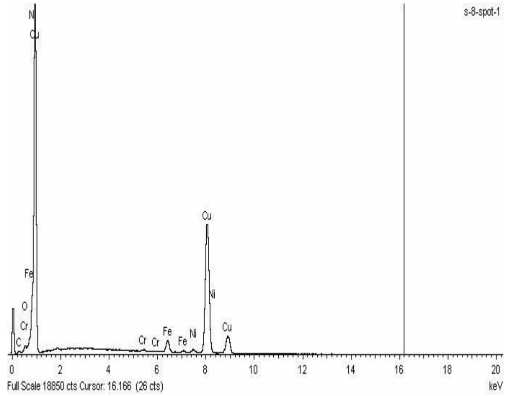

Figure D.2. EDX spectrum spot 1 of sample treated 60 minutes in inert conditions with agitation.

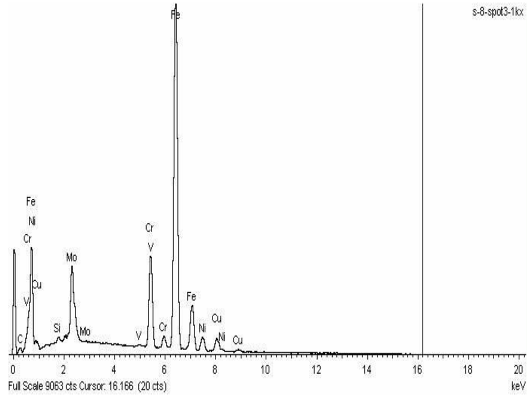

Figure D.3. EDX spectrum spot 3 of sample treated 60 minutes in inert conditions with agitation.

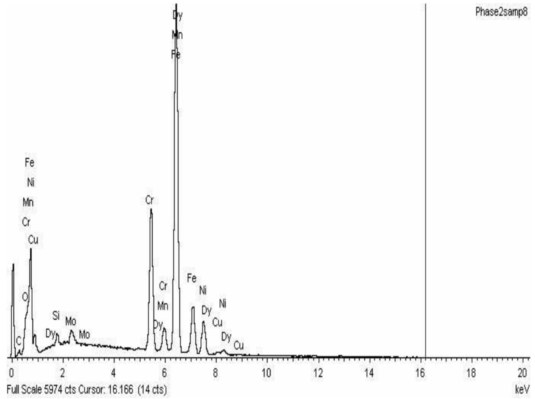

Figure D.4. Phase 2 EDX spectrum of sample treated 60 minutes in inert conditions with agitation.

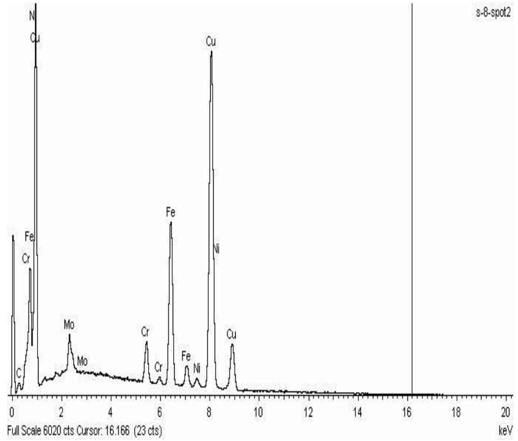

Figure D.5. EDX spectrum spot 2 of sample treated 60 minutes in inert conditions with agitation.

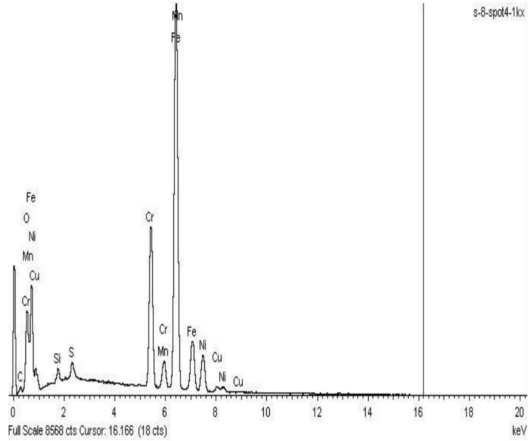

Figure D.6. EDX spectrum spot 4 of sample treated 60 minutes in inert conditions with agitation.

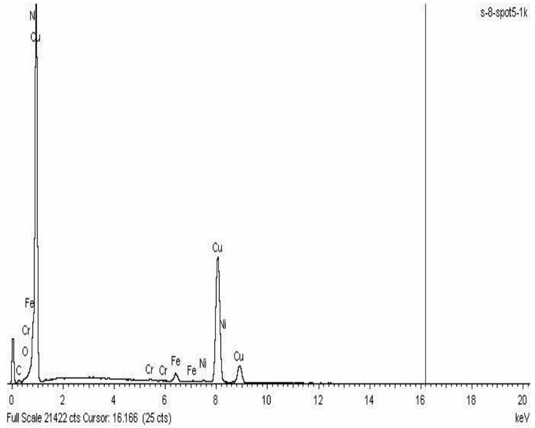

Figure D.7. EDX spectrum spot 5 of sample treated 60 minutes in inert conditions with agitation.

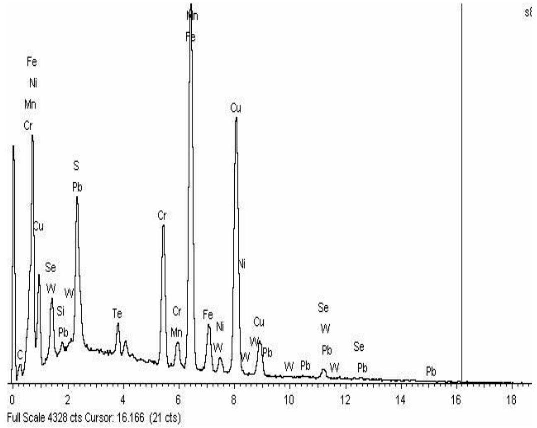

Figure D8. EDX spectrum spot 7 of sample treated 60 minutes in inert conditions with agitation.

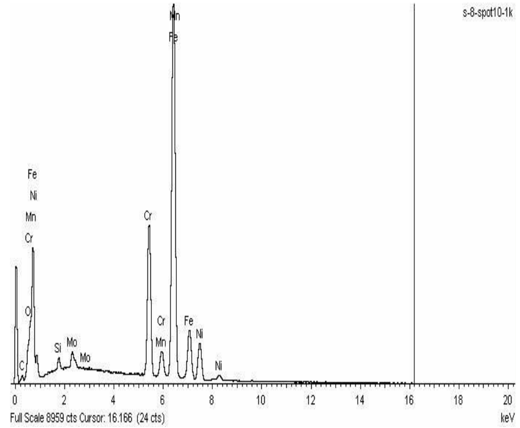

Figure D.9. EDX spectrum spot 10 of sample treated 60 minutes in inert conditions with agitation.

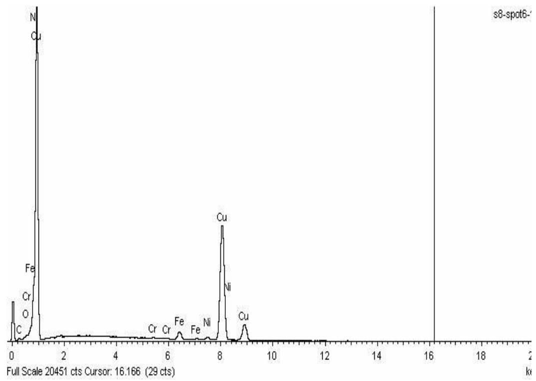

Figure D.10. EDX spectrum spot 6 of sample treated 60 minutes in inert conditions with agitation.

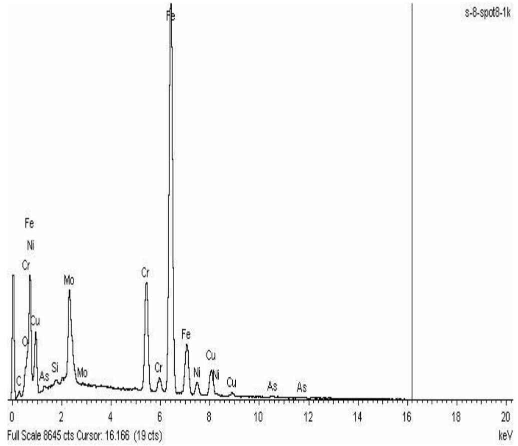

Figure D.11. EDX spectrum spot 8 of sample treated 60 minutes in inert conditions with agitation.

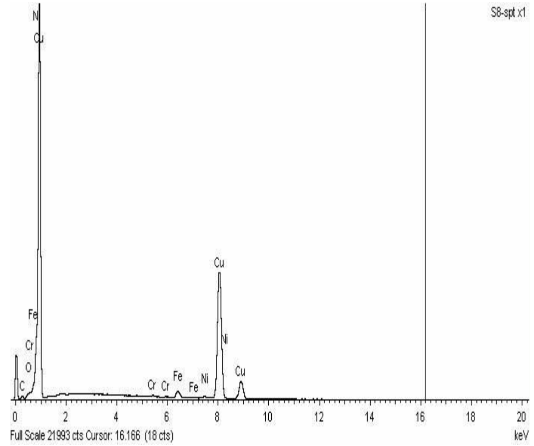

Figure D.12. EDX spectrum, line scan 1 of sample treated 60 minutes in inert conditions with agitation.

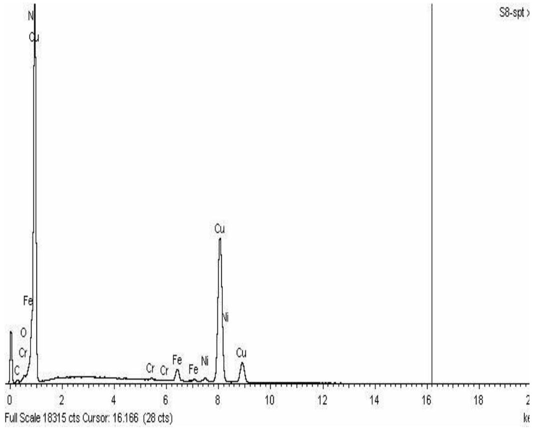

Figure D13. EDX spectrum, line scan 2 of sample treated 60 minutes in inert conditions with agitation.

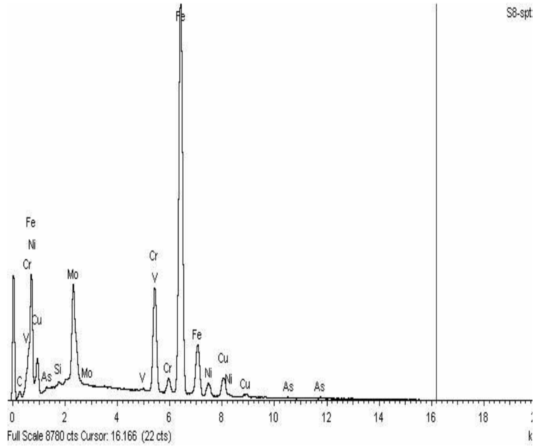

Figure D.14. EDX spectrum, line scan 4 of sample treated 60 minutes in inert conditions with agitation.

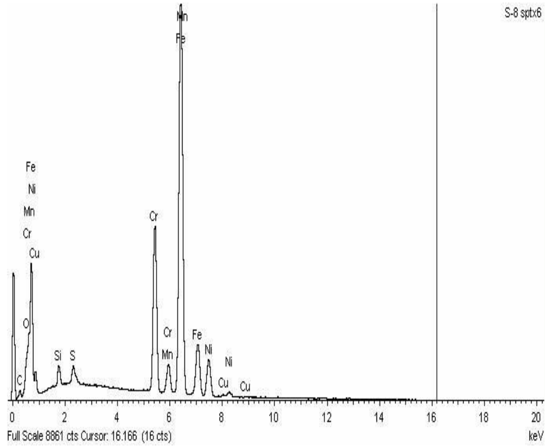

Figure D.15. EDX spectrum, line scan 6 of sample treated 60 minutes in inert conditions with agitation.

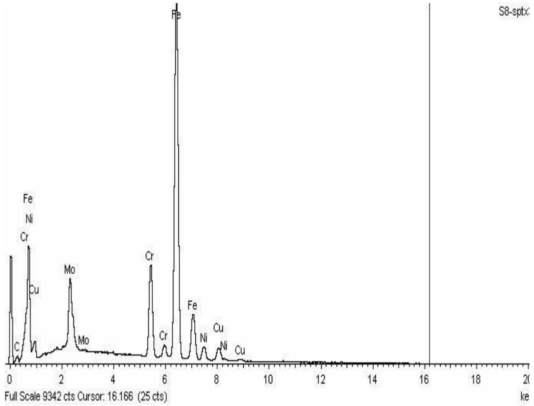

Figure D.16. EDX spectrum, line scan 3 of sample treated 60 minutes in inert conditions with agitation.

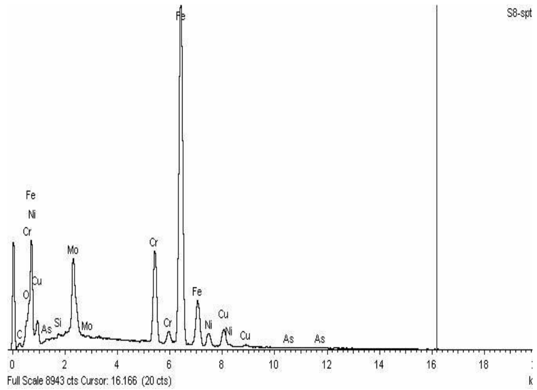

Figure D.17. EDX spectrum, line scan 5 of sample treated 60 minutes in inert conditions without agitation.

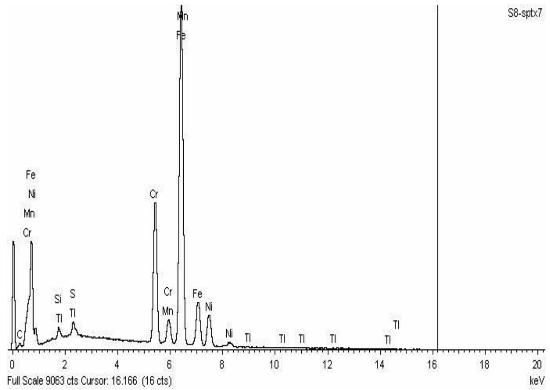

Figure D.18. EDX spectrum, line scan 7 of sample treated 60 minutes in inert conditions with agitation.

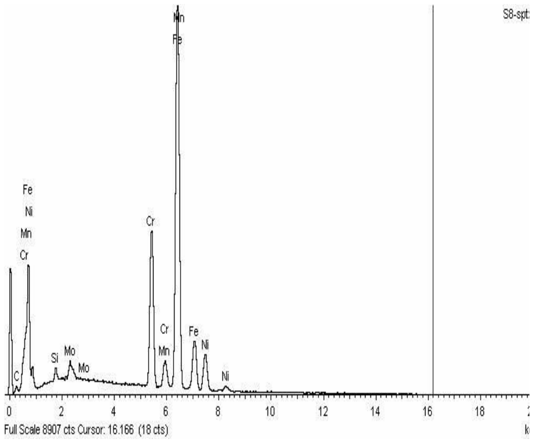

Figure D.19. EDX spectrum, line scan 8 of sample treated 60 minutes in inert conditions with agitation.

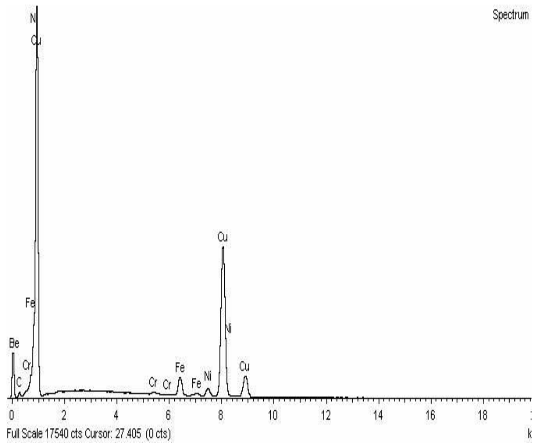

Figure E.1. EDX of the scanned area of sample treated at 100 minutes in inert conditions with agitation.

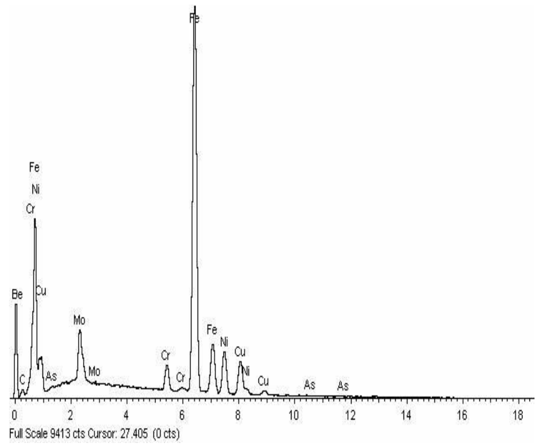

Figure E.2. EDX spectrum spot 2 of sample treated 100 minutes in inert conditions with agitation.

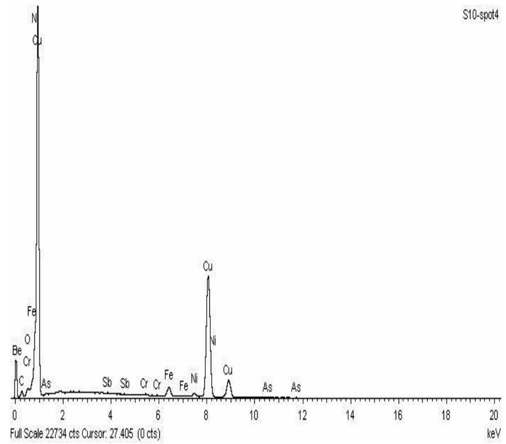

Figure E.3. EDX spectrum spot 4 of sample treated 100 minutes in inert conditions with agitation.

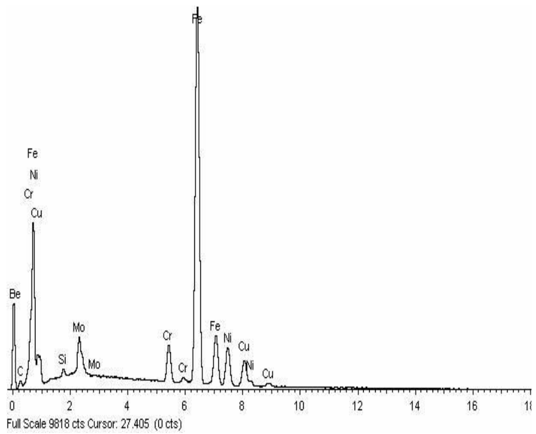

Figure E.4. EDX spectrum spot 1 of sample treated 100 minutes in inert conditions with agitation.

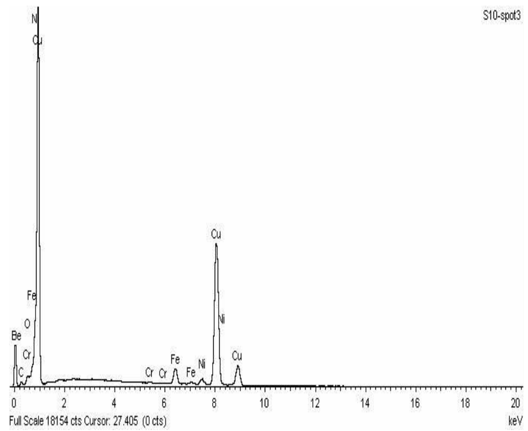

Figure E.5. EDX spectrum spot 3 of sample treated 100 minutes in inert conditions with agitation.

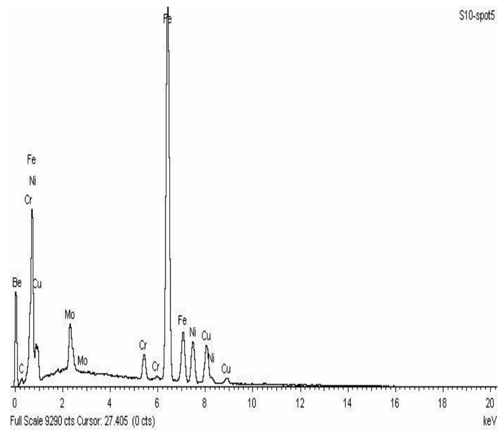

Figure E.6. EDX spectrum spot 5 of sample treated 100 minutes in inert conditions with agitation.

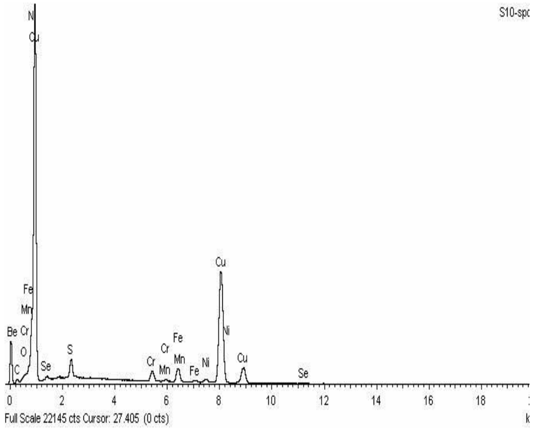

Figure E.7. EDX spectrum spot 6 of sample treated 100 minutes in inert conditions with agitation.

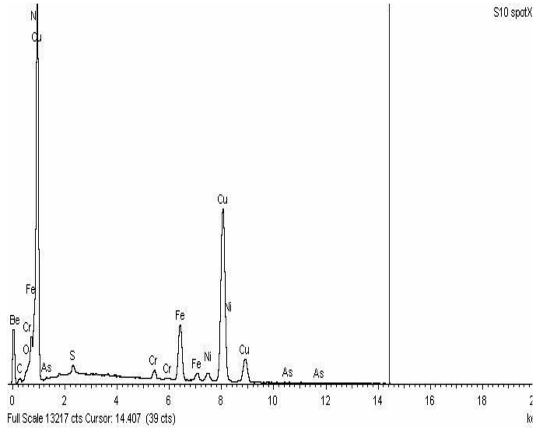

Figure E.8. EDX spectrum line scan 1 of sample treated 100 minutes in inert conditions with agitation.

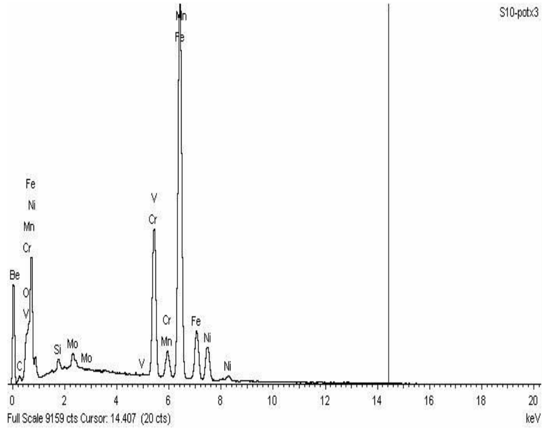

Figure E.9. EDX spectrum line scan 3 of sample treated 100 minutes in inert conditions with agitation.

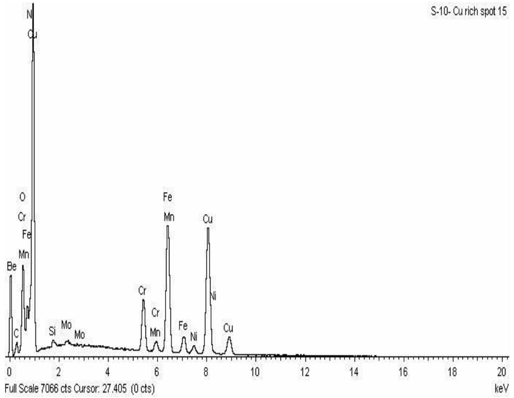

Figure E.10. EDX spectrum line scan 15 of sample treated 100 minutes in inert conditions with agitation.

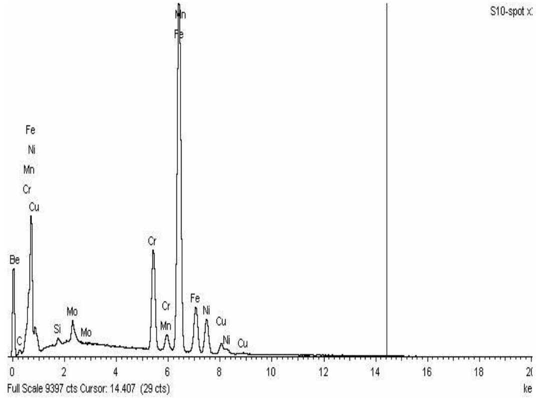

Figure E.11. EDX spectrum line scan 2 of sample treated 100 minutes in inert conditions with agitation.

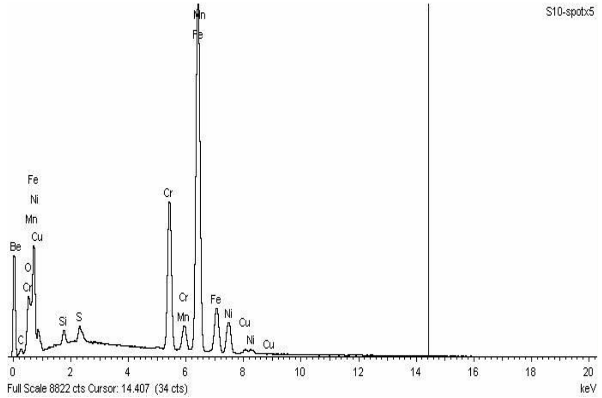

Figure E.12. EDX spectrum line scan 5 of sample treated 100 minutes in inert conditions with agitation.

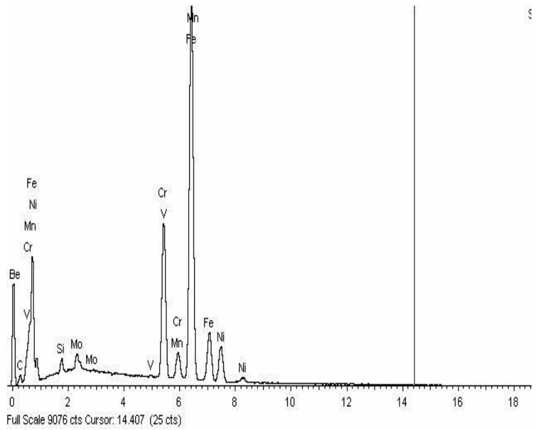

Figure E.13. EDX spectrum line scan 6 of sample treated 100 minutes in inert conditions with agitation.

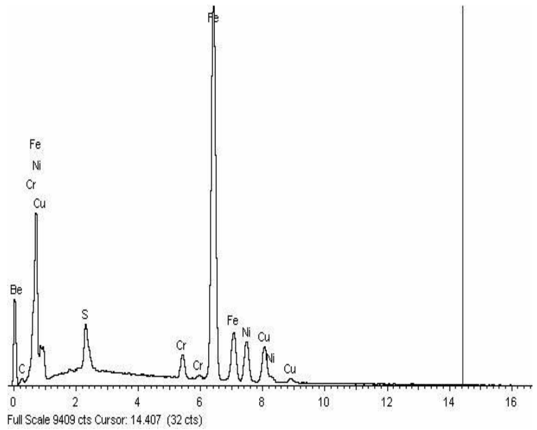

Figure E.14. EDX spectrum line scan 8 of sample treated 100 minutes in inert conditions with agitation.

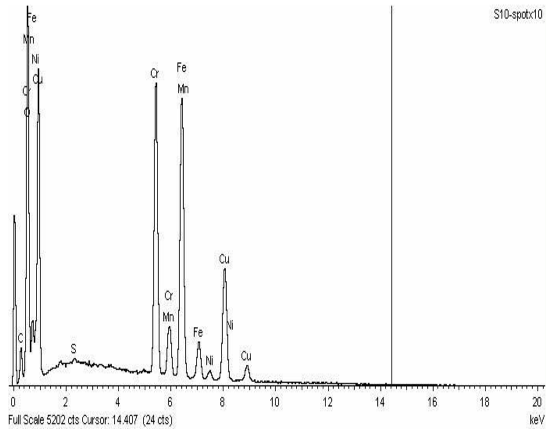

Figure E.15. EDX spectrum 10 of sample treated 100 minutes in inert conditions with agitation.

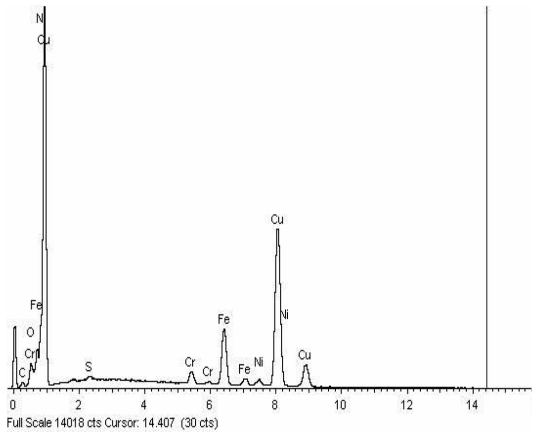

Figure E.16. EDX spectrum on spot 7 of sample treated 100 minutes in inert conditions with agitation.

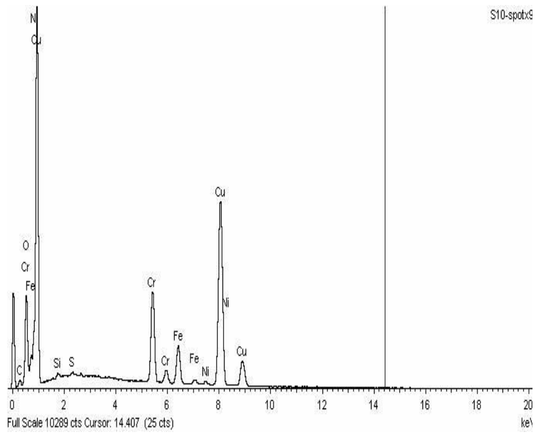

Figure E.17. EDX spectrum line scan 9 of sample treated 100 minutes in inert conditions with agitation.

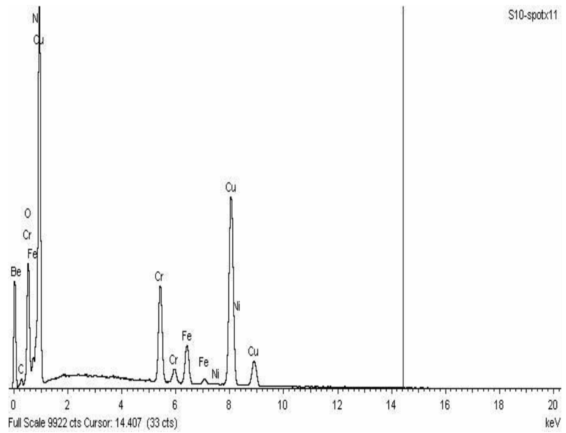

Figure E.18. EDX spectrum line scan 11 of sample treated 100 minutes in inert conditions with agitation.

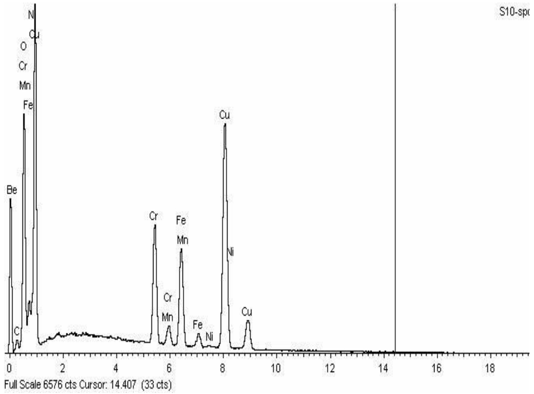

Figure E.19. EDX spectrum line scan 12 of sample treated 100 minutes in inert conditions with agitation.

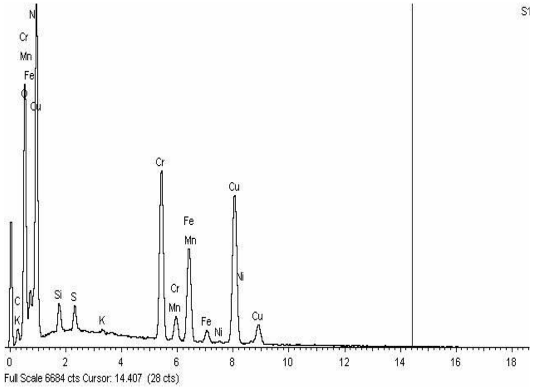

Figure E.20. EDX spectrum line scan 13 of sample treated 100 minutes in inert conditions with agitation.

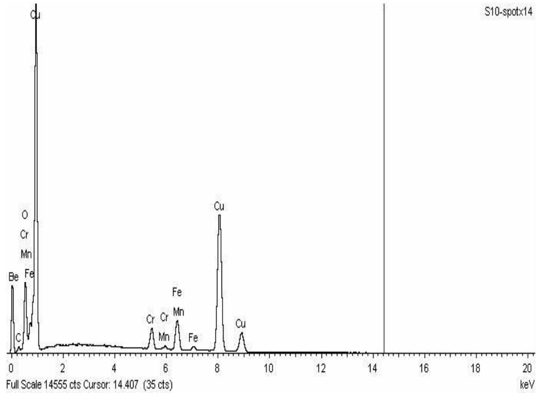

Figure E.21. EDX spectrum line scan 14 of sample treated 100 minutes in inert conditions with agitation.

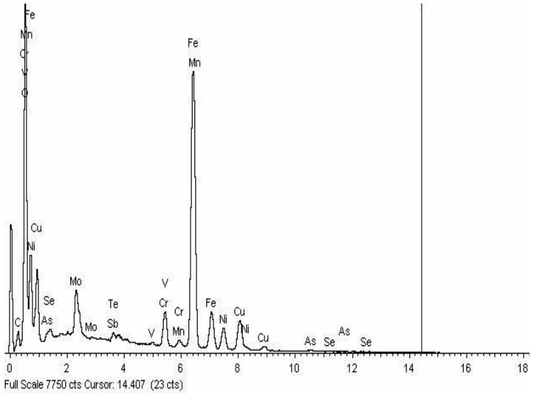

Figure F.1. EDX spectrum line scan 2 of sample treated 20 minutes in oxidizing conditions with agitation.

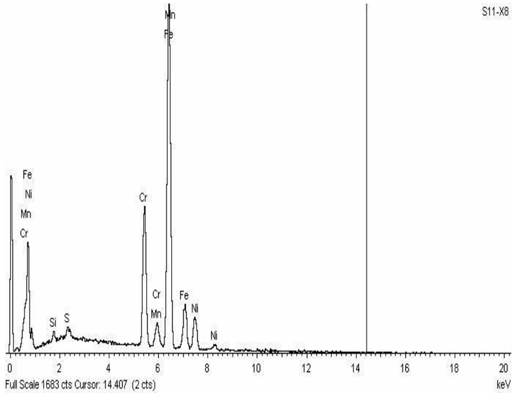

Figure F.2. EDX spectrum line scan 8 of sample treated 20 minutes in oxidizing conditions with agitation.

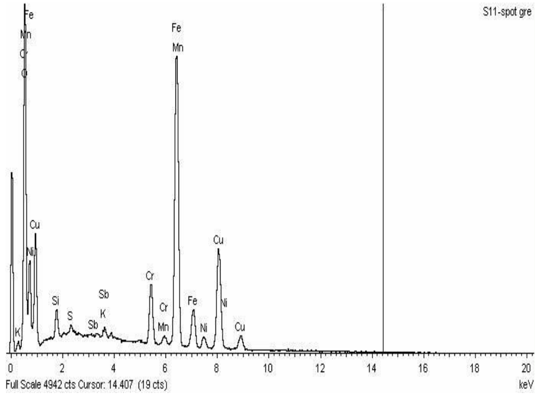

Figure F.3. EDX spectrum grey region of the sample treated 20 minutes in oxidizing conditions with agitation.

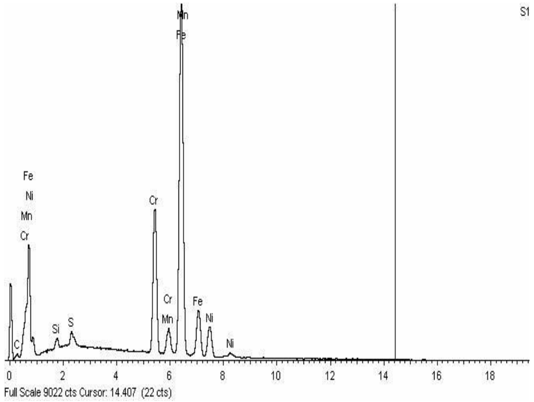

Figure F.4. EDX spectrum line scan 7 of sample treated 20 minutes in oxidizing conditions with agitation.

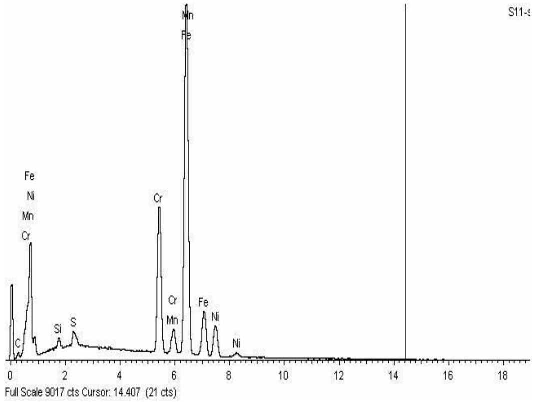

Figure F.5. EDX spectrum, of spot 9 (in black) of the sample treated 20 minutes in oxidizing conditions with agitation.

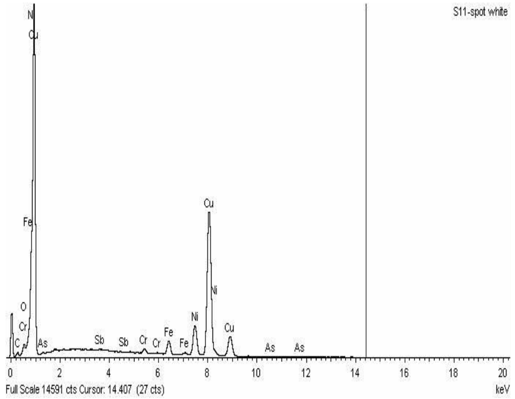

Figure F.6. EDX spectrum showing the composition in spot 3 for the sample treated 20 minutes in oxidizing conditions with agitation.

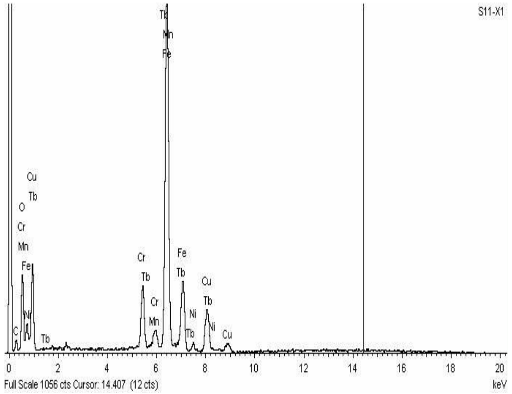

Figure F.7. EDX spectrum line scan 1of sample treated 20 minutes in oxidizing conditions with agitation.

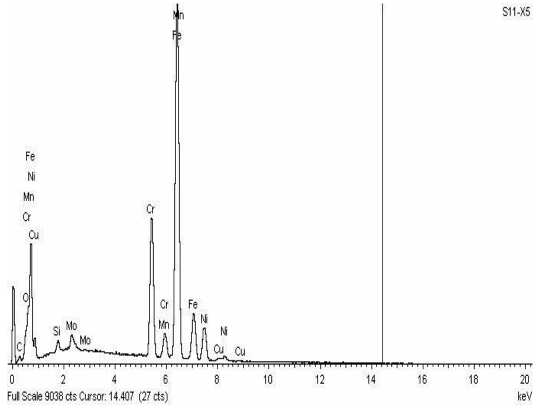

Figure F.8. EDX spectrum line scan 5 of sample treated 100 minutes in oxidizing conditions with agitation.

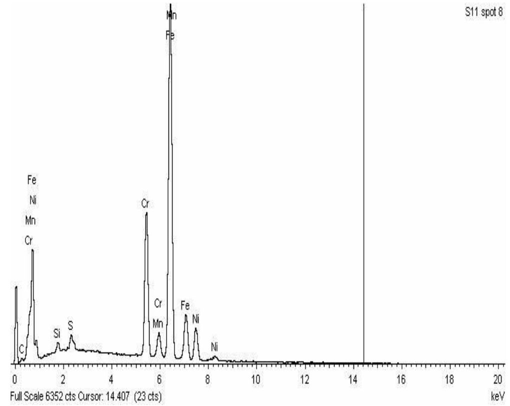

Figure F.9. EDX spectrum spot 8 of sample treated 20 minutes in oxidizing conditions with agitation.

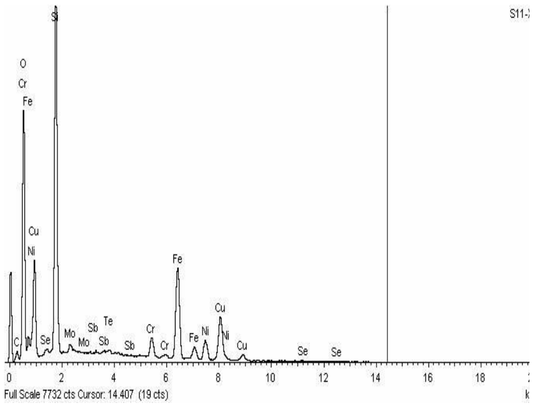

Figure F.10. EDX spectrum line scan 3 of sample treated 20 minutes in oxidizing conditions with agitation.

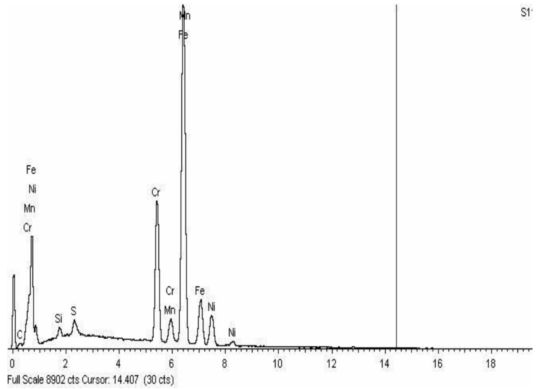

Figure F.11. EDX spectrum line scan 6 of sample treated 20 minutes in oxidizing conditions with agitation.

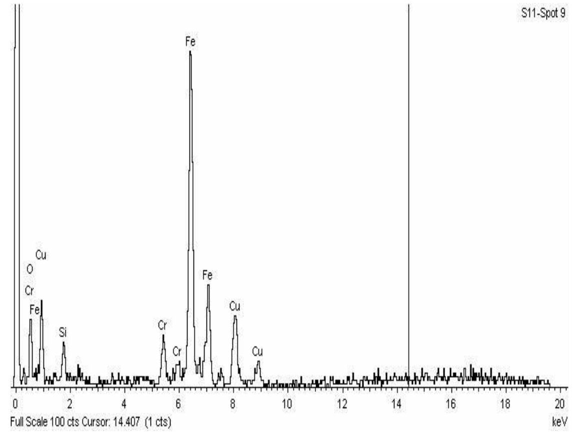

Figure F.12. EDX spectrum spot 9 of sample treated 20 minutes in oxidizing conditions with agitation.

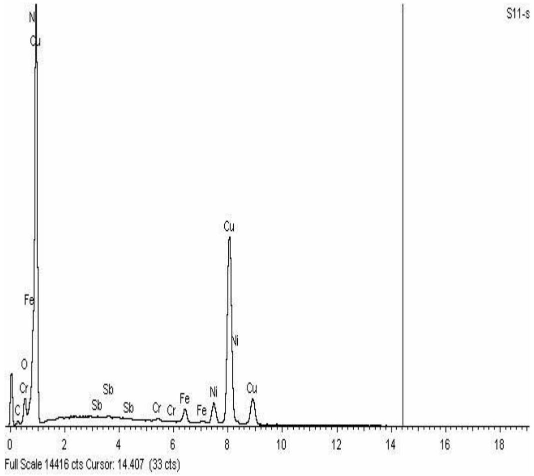

Figure F.13. EDX spectrum white spot of sample treated 20 minutes in oxidizing conditions with agitation.

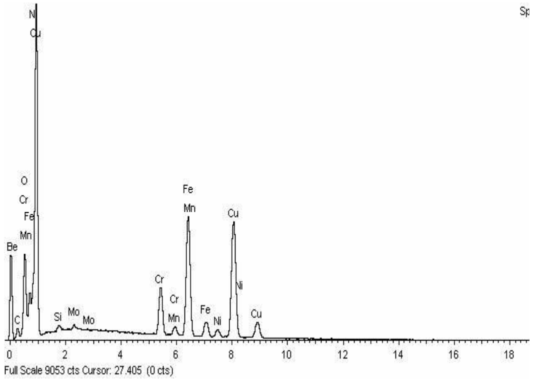

Figure G.1. EDX spectrum of the overall map of sample treated 40 minutes in oxidizing conditions with agitation.

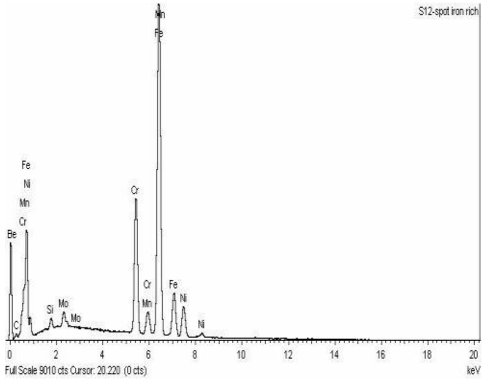

Figure G.2. EDX spectrum Interface iron rich spot of sample treated 40 minutes in oxidizing conditions with agitation.

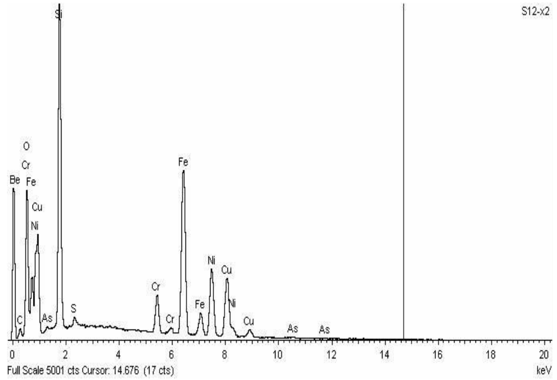

Figure G.3. EDX line scan 1 of sample treated 40 minutes in oxidizing conditions with agitation.

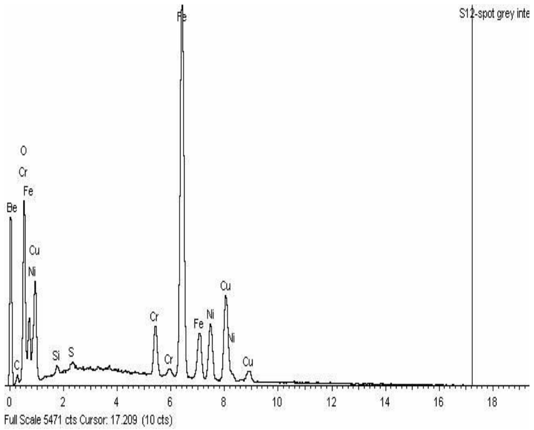

Figure G.4. EDX spectrum grey spot interface of sample treated 40 minutes in oxidizing conditions with agitation.

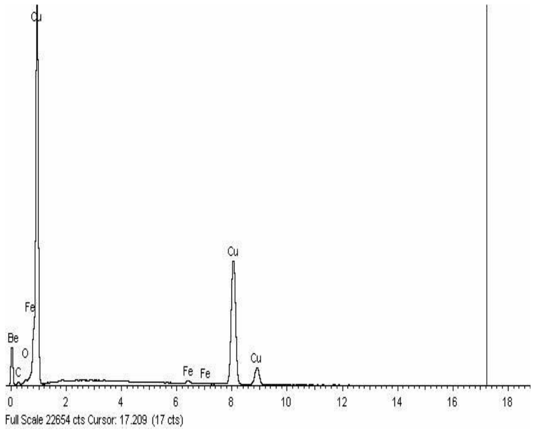

Figure G.5. EDX line scan 1 of sample treated 40 minutes in oxidizing conditions with agitation.

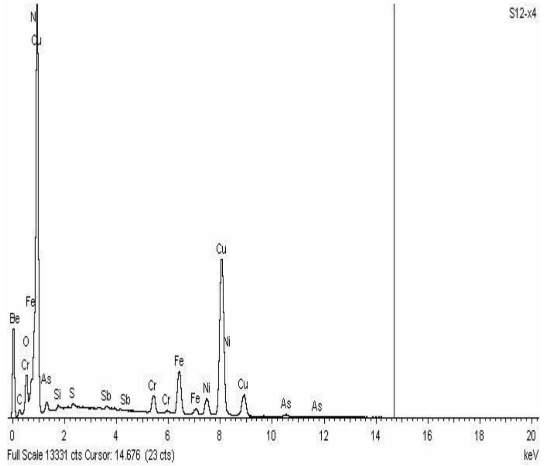

Figure G.6. EDX line scan 4 of sample treated 40 minutes in oxidizing conditions with agitation.

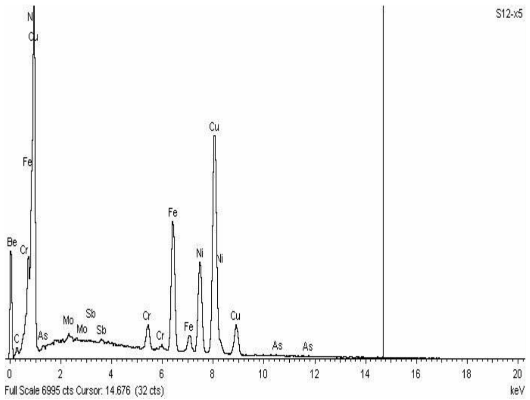

Figure G.7. EDX line scan 5 of sample treated 40 minutes in oxidizing conditions with agitation.

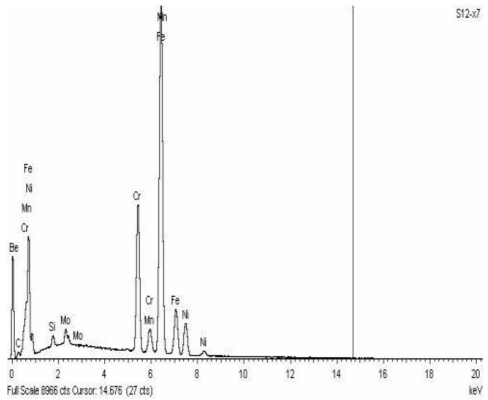

Figure G.8. EDX line scan 7 of sample treated 40 minutes in oxidizing conditions with agitation.

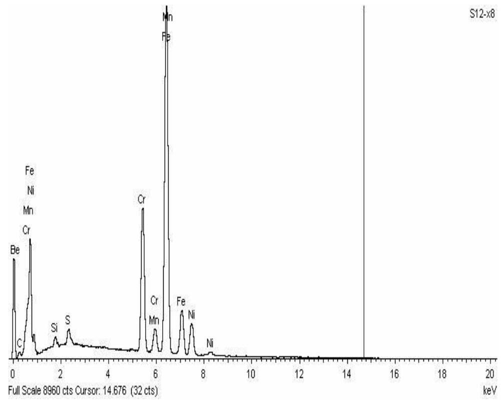

Figure G.9. EDX line scan 8 of sample treated 40 minutes in oxidizing conditions with agitation.

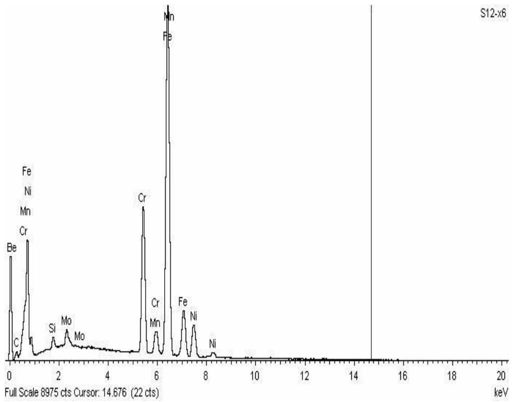

Figure G.10. EDX line scan 6 of sample treated 40 minutes in oxidizing conditions with agitation.